



The Arctic Fox

Final Report

Executive Summary

A team of 30 multidisciplinary engineering students was given a request for proposals demanding an unmanned aerial vehicle (UAV) with vertical take-off and landing (VTOL) capabilities as well as a 2000 NM range for operation in Northern Canada. Through market analysis of that region, it is determined that Nunavik and Nunavut are prime locations to establish a hub-to-point operation. The aircraft is found to be able to compete with the aging fleet of ATR-42 in the North and be of interest for the operators given the governmental subsidies on food in the region.

The ethical aspects of an autonomous aircraft are studied and a remotely managed operation is chosen to minimize the impacts on society. Such an operation requires changes in the current state of the law as the aircraft would be operating autonomously beyond visual line-of-sight (BVLOS). The impact on Northern communities is assessed and positive returns to the local population is found on a social, environmental and economical level.

The aircraft is conceptually designed with a gross take-off weight of 37,600 lb and a payload of 10,800 lb. An unpressurized rectangular fuselage is selected, with a total length of 70 ft and a wingspan of 87.7 ft. A T-tail configuration is chosen with a vertical stabilizer having a span of 12.5 ft and a horizontal stabilizer with a span of 30 ft. Both the horizontal and vertical stabilizer's airfoils are selected as NACA 0012.

The gross take-off weight is initially sized through iteration. A constraint diagram analysis leads to the selection of a wing area of 768 ft^2 and a thrust of 11,500 lbf. Triple redundant flight computers and standard antennae are equipped on the aircraft to provide it with the necessary hardware to be autonomous by avoiding other aircraft and maintaining proper aircraft control during regular and emergency operations.

By looking at the takeoff and average weights of the aircraft, maximum and ideal lift coefficients were obtained which allowed the selection of the NACA 653-418 airfoil. A MATLAB tool was used to verify that the three-dimensional wing would have enough lift and select

Fowler flaps for the aircraft. The static margin of the aircraft is calculated to be between 26% and 61% of the mean aerodynamic chord (MAC).

A twin turboprop configuration is selected, with the PW127N engine and Hamilton Standard 568F propeller being chosen for the aircraft. This combination produces 6,240 lbf of thrust per engine, resulting in a balanced field length (BFL) of 2,442 feet for takeoff, a factored landing distance (FLD) of 2,323 feet and a cruise velocity of 225 kt.

Through trade studies, 230 VAC generation is selected for the electrical system and the primary flight controls are chosen to be electrically actuated. The flight control surfaces are to be split to prevent single point failure in the event of a jammed actuator. A fuel system capable of transporting 6,600 lb of fuel is designed using a wet symmetrical wing with a total volume of the fuel tanks of 135 ft³.

The landing gear configuration is selected using a trade study and the tricycle configuration is chosen. The placement of the landing gear was driven by the position of the center of gravity (CG). This was calculated using weight estimates on most of the important components of the aircraft. The CG is found to be between 36.8% and 63.5% of MAC from the leading edge of the wing depending on the loading of the aircraft.

During the preliminary design phase, the aircraft design is furthered and validation & verification is done. The weights and performance are recalculated to reflect the redesigns of important systems and components during the preliminary design phase. The performance changes do not affect the capacity of the Arctic Fox to land and takeoff at the targeted runways, and the cruise velocity increases to 236 kt.

From a V-n diagram, the aircraft load limits are calculated which allows for the design and analysis of the aircraft structure. The fuselage stringers, transverse beams, and skin are sized as per the highest bending moments. The wing structure is also designed and includes two main spars running from root to tip and an auxiliary spar. The wing-fuselage attachment points are sized and analyzed using finite element analysis, and so are the lugs in the centre wing box. The wing ribs, stringers, and skin are also sized.

The engine mount is sized and analyzed using finite element analysis for the worst loading case. The main landing gear kinematics are determined through a kinematics study, and finite element analysis is performed for the landing gear attachment points.

The T-tail empennage is sized to allow for the required performance and aircraft stability. A kinematics study is done for the actuator linkages, and the hinges are sized and analyzed using finite element analysis. The hinge moments are estimated using a 2D computational fluid dynamics method, and the actuator envelope is determined using historical correlations.

To validate the aerodynamic modeling of the lifting surfaces, wind-tunnel testing is performed in an icing wing tunnel. This has the added advantage of validating the anti-icing model. Using the wind-tunnel data, the computational fluid dynamics analysis for the wing and horizontal stabilizer is validated. Computational fluid dynamics analyses are also done for the lift-reducing impact of the nacelle on the wing, resulting in a 1°wing incidence to allow for sufficient lift at cruise.

The anti-icing system of the Arctic Fox uses bleed air from the engines to heat up leading edges. The environmental control system regulates temperatures for different areas of the Arctic Fox. The electrical system was designed and validated on Amesim and there are two hydraulic systems to ensure redundancy.

The avionics system includes an icing avoidance system that ensures the Arctic Fox is equipped to fly in the North and the incorporation of progressive autonomy. Human factors tests are performed to evaluate the impact of autonomous systems on the human-machine interface and an identity access management system is designed to ensure the protection of the communication architecture of the Arctic Fox. The stability and handling qualities are evaluated with performance flight tests that include take-off, landing and stall performances.

Finally, the cost analysis of the Arctic Fox is evaluated to assess its profitability to the operator. Design recommendations are presented with regards to the dynamic stability of the Arctic Fox and future work involving defining the role of a remote manager in the progressive autonomy of the Arctic Fox.

The Arctic Fox

Final Report

*We certify that this submission is the original work of members of the group and meets the
Faculty's Expectations of Originality*

Submitted to Dr. Catharine Marsden

AERO 490 - Aerospace Engineering Design Project

April 29, 2019

CONTENTS

1	Introduction	1
1.1	Introduction to AERO 490	1
1.2	Problem Statement	1
2	Background	2
2.1	Market Analysis	2
2.2	Mission Analysis	3
2.3	Business Case	5
3	Impact of Technology on Society	7
3.1	Ethical	7
3.2	Legal	9
3.3	Social	9
3.4	Environmental	10
3.5	Economical	11
4	Conceptual Design	13
4.1	Overview	13
4.2	Aircraft Sizing	13
4.3	Autonomy Technology Review	15
4.4	Overall Performance	16
4.5	Systems	22
4.6	Weight and Balance	24
5	Preliminary Design and V&V	27
5.1	Overview and Dimensions	27
5.2	Weights and CG	28
5.3	Aircraft Performance	28
5.4	Loads and Structures	29
5.5	Aerodynamics	45
5.6	Systems	51
5.7	Stability - Cruise Condition	62
5.8	Performance Flight Testing	64
5.9	Autonomy	68
5.10	Cost	77
6	Conclusion	80
6.1	Future Work	80
Appendices		82
References		233

List of Figures

1	Current state of air transportation in Northern Canada	4
2	Rankin Inlet operator profit analysis	6
3	Overall market operator hourly revenue versus operating cost analysis	7
4	The Arctic Fox in the first semester	13
5	Payload-Range diagram of the aircraft	14
6	Constraint diagram of the aircraft	15
7	Lift distribution and wing parameters	17
8	The Arctic Fox wing and flaps	18
9	Static stability	19
10	Landing gear layout	24
11	Coordinate system	25
12	Orthographic and isometric views of the Arctic Fox	27
13	System architecture of the Arctic Fox	27
14	V-n diagram	29
15	Fuselage structure of the Artic Fox	31
16	The internal structure of the wing of the Arctic Fox	33
17	Wing-fuselage attachment of the Arctic Fox	34
18	Rib configuration of the Arctic Fox	36
19	Skin and stringer configuration of the Arctic Fox	37
20	Female lug attachment	38
21	Engine mount design iterations	40
22	Main landing gear options	40
23	Critical case landing	41
24	Empennage	42
25	Hinge and dogbone kinematics for the rudder	43
26	The wing section mounted once at the wind tunnel	46

27	Lift and drag coefficients obtained from MATLAB and the wind tunnel	47
28	Sprinkler rig provided by UOIT to simulate icing	48
29	Lift coefficients obtained from MATLAB and ANSYS	48
30	Induced drag coefficient obtained from MATLAB and ANSYS	49
31	CFD nacelle	50
32	Exhaust stagnation point	51
33	Final nacelle side view	51
34	Main components of the environmental control system	53
35	Electrical system architecture	55
36	Electrical system sizing results from the Amesim model	56
37	Hydraulic system configuration	58
38	Control panel	60
39	Installed antennas	60
40	Icing avoidance system decision making flowchart	61
41	Route revision process for one way point	62
42	O'hara Plot	64
43	Optimum Speed V1	66
44	Progression schemes	69
45	Requirements for trade study	70
46	Missions from Rankin Inlet airport	70
47	Experiment overview	71
48	Approach path deviation from ideal slope for participant 49004 for trial 1 . .	72
49	Heading deviation from ideal slope for participant 49004 for trial 1	72
50	Airspeed deviation from ideal slope for participant 49004 for trial 1	73
51	Average perceived workload	74
52	Excerpt from the checklist for engine fire in flight	74
53	Vital checklist items completed, non-vital checklist items actionned by AEP	75

54	Program cost and profit per aircraft analysis	78
55	Hourly operating cost versus north Canada market	79

List of Tables

1	Static margin variability at different CG positions	19
2	Weights of all components	25
3	Comparing ANSYS results to the analytical solution	35
4	Baseline material and dimensions	39
5	Reaction forces for a one gear landing	41
6	Expected life of hinges	43
7	Hinge moment (HM) and hinge moment coefficients for primary flight control surface	44
8	Actuator sizing and PCU envelope design parameters	44
9	Comparison of hinge moment coefficients (Roskam method and SU2)	45
10	Undamped natural frequency and damping ratio of the Arctic Fox	63
11	Recommendation for Arctic Fox	63
12	Heading, airspeed and approach path slope deviation	73

ACRONYMS

A	Amps
AC	Advisory Circular
AC	Aerodynamic Center
AC	Alternating Current
ACARS	Aircraft Communications Addressing and Reporting System
AEO	All Engine Operative
AEP	Autonomous Emergency Procedures
ALD	Actual Landing Distance
API	Application Programming Interface
ASD	Accelerate-Stop Distance
ATR	Avions de Transport Régional
AWM	Airworthiness Manual
BFL	Balanced Field Length
BL	Buttock line
CAR	Canadian Aviation Regulations
COP	Coefficient of Performance
CDR	Conceptual Design Review
CFD	Computational Fluid Dynamics
CG	Center of Gravity
C2	Command and Control
DC	Direct Current
DPO	Dual Pilot Operation
EDP	Engine Driven Pump
EMA	Electro-Mechanical Actuator
ECS	Environmental Control System
FEA	Finite Element Analysis
FS	Fuselage Station
FHA	Functional Hazard Analysis
FLD	Factored Landing Distance
GDP	Gross Domestic Product
GDS	Global Distribution System
GNSS	Global Navigation Satellite System
HF	High Frequency Radio
HM	Hinge Moment
IAM	Identity Access Management
ICTC	Information and communications technology council
IFR	Instrument Flight Rules
LiDAR	Light Detection and Ranging
LUCA	Large Unmanned Cargo Aircraft
ILS	Instrument Landing System
MAC	Mean Aerodynamic Chord

MFD	Multi-Function Display
MGI	Mckinsey Global Institute
MLW	Maximum Landing Weight
MS	Margin of Safety
MTOW	Maximum Takeoff Weight
NASA	National Aeronautics and Space Administration
NNC	Nutrition North Canada
OEI	One Engine Inoperative
OEM	Original Equipment Manufacturer
PCU	Power Control Unit
PID	Proportional, Integral, Derivative
PDR	Preliminary Design Review
PTU	Power Transfer Unit
RFP	Request for Proposal
RMO	Remotely Managed Operation
RMS	Root mean squared
RPM	Rotations per minute
SAE	Society of Automotive Engineers
SATCOM	Satellite Communications
STOL	Short Take-off and Landing
SU2	Stanford University Unstructured
TCAS	Traffic Collision Avoidance System
TOD	Take-off Distance
UAS	Unmanned Aircraft Systems
UOIT	University of Ontario Institute of Technology
V	Volts
V1	“Commit to fly” Speed
V2	Take-off Safety Speed
VR	Rotation Speed
VF	Variable Frequency
VHF	Very High Frequency Radio
VOR	VHF Omnidirectional Range
VTOL	Vertical Take-off and Landing
WL	Water line
WAN	Wide Area Network

Project Contributions

Anthony Aubry

My administrative role this year was one of the 3 project manager position, which led me to help organize the group, resolve conflicts and help team members in need. My technical role over the first semester was engine/performance, where I selected the engines and propeller with Jeewan, while keeping the constraint diagram up to date. I also calculated the takeoff, landing, climb and cruise performance, as well as help Mehrshad to design the flaps. I also helped Alex and Angie with mission analysis for aircraft sizing. In the second semester, I determined the required time, fuel and payload for each remaining mission in order to determine the number of aircraft needed. I also reviewed the CG limits in flight and on ground to support stability and landing gear design. Furthermore, I designed and modeled the nacelle in CATIA v5 in order to perform a CFD validation/verification of its aerodynamic effect on the wing. I also assisted Jon for the H-stab design, Hamza for the takeoff flight testing, and Jeewan in the automation rollout.

Ahmed Badr

In the first semester, the administrative role was market analysis, conducting research on the flights across the north along with the situation in the north. The technical role was stability and control directional stability making sure that the aircraft is statically stable. The second semester the technical role was flight testing – landing to verify if the aircraft can land safely on different runways.

Jie Bao

For my administrative role, I helped manage the database sheet during the first semester and I was in the poster team alongside Angie, Rebecca, and Devin. The task involved the design and printing of the poster. My technical role consisted of assessing the static stability to support the wing emplacement on the fuselage, with its respective distance to the empennage and the initial sizing of the horizontal stabilizer. In the second semester I completed the longitudinal stability analysis by assessing the dynamic stability and the related handling qualities for cruise condition.

Brian Barcelo

My administrative role was configuration control, which consisted of designing a database to record all decisions and calculated values related to design. This allowed for transparency and traceability throughout the design process. I also developed an input/output matrix during the first semester to help the project managers determine which deliverables were depending on which technical teams. This semester, I helped the report team by proofreading Parts A, B, C and the conclusion. I primarily worked on preliminary sizing and modeling of the skin, ribs and spars of the wing on 3Dexperience last semester. My technical role this semester was to design and validate the engine mount structure.

Hamza Bensouda

During the fall semester, I was tasked in determining the avionics required for the aircraft. It included a list of flight instruments, their weight, cost, electrical loads and the design of the cockpit layout. For the winter semester, I took care of the flight testing for takeoff with the help of X-Plane. I was able to validate the calculated take-off performance values for speeds and distances that were initially obtained during the fall semester.

Kerolos Boulos

During the fall semester, my task was to create a 3D model of the Arctic Fox. The first iterations were modeled using openVSP to run some aerodynamics analysis and have a visual representation of the aircraft. The final version was assembled on 3Dexperience with the Obinna. In the winter semester, I took care of the environmental control system and the thermal management of the avionics bay.

Joshua Cayetano-Emond

My administrative role for both semester was that of assembling and formatting the reports submitted. I also acted as co-team leader with Ben during the initial sizing phase of the first semester. My technical role during the first semester was aerodynamics, where I helped assess the longitudinal stability with Jie and go over preliminary sizing of the empennage. During the second semester, I was on the wind tunnel team, where I acted as team lead and helped with the construction of the rig and elaboration of the procedure. Finally, I acted as support for automation strategies after the wind tunnel data had been analyzed.

Philip Corriveau-Pelletier

For my administrative role I helped with the invitations and catering for the mid-year design review. I was also the time keeper for presentations and provided feedback to most of my colleagues on their presentations and time management. My technical role was focused on the design and integration of the fuel system with validation of fuel level sensors for the second semester. I also built the first part of one of our Roskam estimate sizing tool and started with autonomy infrastructure research before moving on to fuel system design.

Devin Crossman

In the fall semester, I built a tool for building the constraint diagram and did research on regulations and avionics related to autonomy. I also created a preliminary model of the aircraft in X-Plane and created a promotional video for our midterm design review. In the winter semester I refined the X-Plane model with assistance and input from the team. I created an X-Plane plugin to assist with flight testing and to demonstrate the ability to control the aircraft autonomously during the take off, climb, and cruise phases of flight. I also provided support to team members creating their own plugins for X-Plane. I performed the stall characteristics flight test. I created another promotional video for the final presentation and also worked to design and print the poster for the poster presentation.

Angelina Cui

On the administrative side, I was in the poster team to design and print the poster. For the technical roles, in the first semester, I worked on designing the cockpit layout. I also helped with avionics selection and mission analysis. In the second semester, I worked with Xinlu to design an icing avoidance system and demonstrate it by creating a plugin for X-Plane. I also revisited the design of the panel and the cockpit layout from the first semester and iterated on the design.

Xinlu Dai

On the technical side, in the first semester, I estimated weights of all components and determined CG positions for each of them. Then, I created an Excel sheet, containing all the equations and calculating the CG. In the second semester, I worked with Angelina to develop a route revision system for icing avoidance. I designed the strategy for the system and helped Angelina code the plugin. Also, I revisited CG by updating the weight excel sheet regularly, and drew the new CG excursion diagrams. On the administrative side, I helped with the catering and poster presentation cleaning up.

Nicolas Gaucher

In the first semester, I was part of the loads and structural layout team. Emphasis was put on building excel tools to determine the overall highest loads the aircraft is experiencing as well as size some structural components. In the second semester, I sized structural elements of the cargo section of the aircraft using the loads obtained in the first semester as well as a new load found by Obinna. The elements sized were: stringers, frames, bulkheads, transversal and longitudinal beams, struts and skin panels. I also drew the entire layout using AutoCAD.

Emerald-Jayne Henao

My administrative roles included formatting the presentation slides for the Mid-Year Design Review presentation. In the second semester, I helped the Report team to proofread the final report. My technical roles in the first semester involved the development of the mission and business case, as well as a market analysis in which I developed one of the three aircraft sizing tools. I was also a part of the Fuselage and Cockpit Design team, and helped to design the fuselage. In the second semester, my technical role was to develop the Identity Access Management system in order to implement communications security for the Arctic Fox. I also aided in defining new terminologies for discussions about autonomy and autonomous flight.

Jordan Hubscher

My technical role in the first semester involved the research and decision making behind the flight control system network and the protocol standards the Arctic Fox would adhere to. My technical role in the second semester was that of software development and cryptography research. I was involved in the research and development of the key management system for the Arctic Fox.

Nicholas Iacuessa

My administrative roles included leading the invitations write up and distribution management for the public relations team for the final design review. As well, I was part of the team to set up the NCADE office into a greeting and refreshments area. My technical roles included conceptual design of the landing gear assembly and investigation into a more electric aircraft in the first semester. In the second semester, I worked on the design of the human factors experiment and safety protocol. Furthermore validation and verification was done through test pilot flight data and the development of an autonomous emergency checklist script by means of a plugin designed for X-Plane.

Arapi Kandiah

During the first semester, my technical role included determining the wing configurations such as the wing shape, position, and wingtip of the aircraft considering the conditions that our aircraft should fly in. This semester, I was able to do the preliminary design of the wing box including the skin, ribs, and stringers. With the help of the results from Brian from the first semester, I validated the design by doing multiple calculations, iterations and the ANSYS software.

Itamar Keren

My administrative role during the first semester was initially Project Manager. The task later became too much for me to manage given my other commitments. My technical role focused on mission analysis where I helped with the data acquisition and processing for food requirements, critical routes and subsidy options along with Alex. In the second half of the year, I was part of the wind tunnel testing team where I helped draft and construct the test rig as well as develop and adjust the test procedures. Lastly, I assisted the report team by proofreading.

Jonathan Leo

The administrative responsibility that I volunteered for was to support the customer and public relations team by writing the first draft of the invitation letter and reviewing the later revisions with other members. On the technical side, the majority of my work was put into the horizontal stabilizer and elevators in the first semester. My work continued in validating the hinge attachments with FEA, as well as calculating the hinge moment for the rudder. Other work was done on the whole empennage design to work with the changes done on the aircraft to improve the take off distance and to respect static stability in pitch. I also helped other members model their components and integrate their parts into the empennage assembly.

Cristian Leon

During the first semester, Xinlu and I worked together on the Weight and Balance (CG calculation) of the aircraft. Afterwards, I worked on the cost analysis, in which I obtained the RDT&E and Production cost. For the second semester, I started my research in Operational cost and landing gear; however, the team needed someone to do the hydraulic system from scratch, so I volunteered. For the hydraulic system, I worked on the conceptual and regulatory research, the system design, the CAD and a FHA that allowed me to come up with a sequence of events and actions that the automatic system of the aircraft has to follow in case of emergency. I am still working on the Amesim validation.

Tiffany Lucia

During the first semester, my technical role was to size and CAD the vertical stabilizer and rudder of the aircraft. Specifically, I came up with preliminary sizing for the vertical stabilizer and rudder surface area as well as for the ribs and skin and used 3DEX to CAD. I was also on the Customer and Public Relations team the first semester and I was tasked with creating and distributing the invitations as well as assisting with the catering. The second semester, I was part of the Human Factors team where I worked alongside Nicholas Iacuessa to design, implement and conduct an experiment that would give insight on how implementing autonomous systems on an aircraft impacts the human-machine interface.

Andrew Malaty

In the first semester, I was part of the systems team and was tasked with working on the pneumatic system. I designed a heat transfer model for both the anti-icing system as well as the environmental control system. During the second semester I worked on refining the anti-icing heat transfer model to not have any variables that were guessed (all estimated or measured). I was part of the wind tunnel testing team and specifically in charge of the anti-icing portion of the test. I designed and built the control and measurement system for the heated leading edge.

Benjamin Maniraguha

I assumed a leadership role in my assigned group in the first 7 weeks of the project prior to the introduction of technical and administrative roles. My administrative role was configuration control, this included managing the configuration control google sheets tool, specifically for the systems group in the first semester. My technical role was designing the flight control system. I worked on picking the appropriate power system for our aircraft, sized the actuators and obtained all specifications for the actuator envelope for all three primary flight control surfaces. I used CFD to find the control surface hinge moments to validate the design decision of electrical actuation. Additional involvements included being a part of the cargo considerations task force.

Daniel Minkin

For my administrative role, I was one of three Project Managers for the team throughout the year. This included weekly meeting organisations, project organisation, overall Gantt Chart creation, leading the team and helping with miscellaneous tasks. On the technical side, in the first semester I worked to conceptually design the landing gear for the aircraft including the wheels, tires, position and control/actuation specifications as well as conduct initial research on hydraulic systems with Nicholas Iacuessa. In the second semester I furthered the landing gear development by designing the attachment points of the landing gear to the fuselage and then validating and verifying with a finite element analysis.

Mehrshad Moghadamazad

During the first semester, my technical role was to design the Arctic Fox wing and flaps. To do so, I developed several MATLAB tools to select a proper wing airfoil, determine wing parameters, lift distribution, wing lift-AOA graph, wing stall angle, and so on. In addition, I found an estimation for the flaps hinge moments. During the second semester, my technical role was to validate the MATLAB tool and method that I used to design the wing in the fall semester using CFD analysis (ANSYS Fluent and XFLR5). CFD analysis was conducted for both low and high aspect ratio wings. Moreover, the MATLAB results were compared with the wind tunnel testing results.

Obinna Ofielu

My administrative role in both the first and second term involved editing, formatting and assembling the project report. In the first semester, my roles on the technical side included market research, organization and creation of the project CAD drawings on 3Dexperience and OpenVSP. In the second semester, I worked to create the internal structure of the wing of the Arctic Fox. This included determining the loads, designing and validating the spars, wing-fuselage attachment and ailerons. I was also involved in generating design variables from OpenVSP and CAD drawings for the internal structure on 3Dexperience.

Rebecca Rajs

My administrative role in both the first and second semesters was as one of three Project Managers. In the first semester I was leading and providing support to the structures and loads team. More specifically I worked on the overall design of the fuselage, including overall sizing and design based on the specific nature of the aircraft's mission. In the second semester I continued to provide support to those working on structures. I designed and sized the aft section of the fuselage, including the rear ramp cargo door. I was also part of the group responsible for the design of the poster.

Alexandre Renaud

For the administrative role, I was part of the team to organize the design reviews, i.e. the catering, the guest list and the invitation. On the technical side, I was part of the market analysis and business case team where I did research and established the communities database. Furthermore, I worked on the mission analysis and optimizing initial aircraft sizing in order to obtain a payload-range diagram. During the winter semester, I was part of the wind tunnel testing team where I helped with the test proposal and procedure, the wing and rig assembly, testing and post processing the data. Finally, in the final stretch, I finalized the cost analysis with the program cost and the operating cost, in order to determine the profitability of the stakeholders.

Noah Sadaka

On the administrative side, I was on the report assembling and formatting team for the midterm and final reports. I also helped the project management team, was a group leader for the initial design phase of the first semester, and administered the 3DEXperience space. On the technical side, I determined the main technologies of the electrical system in the first semester, and designed, CADed, and validated the electrical system in the second semester. I also worked on a stakeholder analysis, and re-examined the feasibility of airdrops.

Akolade Salawu

During the first semester I was involved the creation of an excel tool for the initial sizing of the aircraft. I was also part of the loads and structural layout team, I also created an excel tool for the v-n diagram, initial calculation of the aircraft loads and the initial CAD of the fuselage structure. For the second semester I worked with the wing team on the design and validation of the center wing box. I was also involved in the creation of the CAD rendering of the internal structure of the wing and overall assembly of the various CAD rendering.

Jeewan Singh

For the first semester, I was in the performance & engine selection subteam with Anthony. In this role, I aided in the selection of the engines and preliminary propeller requirement which was completed by my teammate. I also worked on steady climbing, level turning and gliding flight performance. In the second semester, I worked on the strategy for increasing autonomy for the aircraft. In this role, I conducted a trade study to identify the most feasible flight management mode, identified the regulatory and infrastructural hurdles, and defined an operational path towards increasing autonomy. On the administrative side, I was part of the report proofreading team.

Report Contributions

Name	Contribution
Anthony Aubry	Sections 4.4.3, 5.2, 5.3, and 5.5.3
Ahmed Badr	Section 5.8.3
Jie Bao	Sections 4.4.2 and 5.7
Brian Barcelo	Section 5.4.7
Hamza Bensouda	Section 5.8.2
Kerolos Boulos	Sections 4.1 and 5.6.2
Joshua Cayetano-Emond	Exec. Summary & Sections 4.2 and 5.5.1 (paragraphs 1-3)
Philip Corriveau-Pelletier	Section 5.6.5
Devin Crossman	Sections 3.2, 4.3, 5.8.1, and 5.8.4
Angelina Cui	Sections 5.6.6 (helped by Devin) and 5.6.7 (with Xinlu)
Xinlu Dai	Sections 4.6 and 5.6.7 (with Angelina)
Nicolas Gaucher	Section 5.4.2
Emerald-Jayde Henao	Section 1.2
Jordan Hubscher	Section 5.9.4
Nicholas Iacuessa	Sections 4.5 and 5.9.3
Arapi Kandiah	Section 5.4.5.3
Itamar Keren	Sections 5.5.1 (paragraph 4), 6, and 6.1 (paragraph 1)
Jonathan Leo	Section 5.4.9
Cristian Leon	Section 5.6.4
Tiffany Lucia	Section 5.9.2
Andrew Malaty	Section 5.6.1
Benjamin Maniraguha	Section 5.4.10
Daniel Minkin	Sections 1.1 and 5.4.8
Mehrshad Moghadamazad	Sections 4.4.1 and 5.5.2
Obinna Ofieldu	Exec. Summary & Sections 2.1, 3.5, 5.1, 5.4.5, 5.4.5.1 and 5.4.5.2
Rebecca Rajs	Sections 5.4.3 and 5.4.4
Alexandre Renaud	Sections 2.2, 2.3, and 5.10
Noah Sadaka	Exec. Summary & Sections 3.3, 3.4, and 5.6.3
Akolade Salawu	Sections 5.4.1 and 5.4.6
Jeewan Singh	Sections 3.1, 5.9.1, and 6.1 (paragraph 2)

1 INTRODUCTION

1.1 Introduction to AERO 490

At the beginning of the fall semester (2018), the Aerospace Capstone team, consisting of 30 students from various engineering disciplines, received a Request for Proposals (RFP) to develop a conceptual design for a new aircraft. Throughout the fall semester, design decisions were made on the aircraft and systems based on the customer needs identified in the RFP. In the second semester, the team then performed validation and verification on the design of the aircraft up to that point to see whether the design was feasible. This report summarizes the design decisions, the validation and verification, and describes the aircraft's current design.

1.2 Problem Statement

A company (the Company) issued a request for proposals to develop the next generation of aircraft. The Company determined that the unmanned air vehicles (UAV) market is set to grow at a rapid pace. As such, they have decided to establish themselves as a market leader.

The successful introduction of UAVs in the aviation industry depends on three main efforts. First, technology needs to be developed to enable the safe and efficient operation of the vehicle during a mission. Second, infrastructure needs to be in place to allow the operation of the vehicle. Third, a regulatory environment and proper regulations must be implemented to allow both manned and unmanned air vehicles to share common airspace.

Given that these obstacles must be resolved prior to introducing UAVs, the Company has decided that the best approach to leading the fleet in Canada's UAV market is to design an optionally-piloted cargo aircraft for deployment in Canada's North. The aircraft will be introduced into existing infrastructure and regulatory environments so that the safety of the technology can be evaluated.

The Company's proposed mission is to deliver consumer and commercial goods such as food, clothing, fuel and potentially vehicles to Canada's northern remote communities.

Increasing the availability of these goods in the proposed areas could generate a reasonable expected return on investment (ROI) for the operator.

The Company believes that the aircraft will require a minimum range of 2000 NM. Furthermore, the aircraft is expected to land in many different environments in the North and thus, should have vertical take-off and landing (VTOL) capabilities, or something comparable since some remote communities may not have airports. It must also operate in icing conditions. Lastly, the aircraft must comply with the Canadian Aviation Regulations (CARs) and the Federal Aviation Regulations (FARs). If the regulations are not in place, new ones must be created in order to operate the aircraft.

2 BACKGROUND

2.1 Market Analysis

Weather conditions and insufficient infrastructure in Northern Canada cause infrequent deliveries and shortages of fresh produce as 75% of cargo transport to the region is done by air [1]. According to a 2016 - 2017 Nutrition North Canada (NNC) report, 54% of remote communities lack access to fresh produce as defined by Health Canada [2]. In a bid to mitigate this issue, the government of Canada established the NNC subsidy program. The NNC subsidy program is provided to suppliers and retailers that apply. The businesses must then pass the full subsidies received to the consumers. These subsidies are applied against the total cost of any product shipped by air to the eligible communities. This includes costs that accrue from “product purchasing, transportation, insurance and overhead” [3]. The program allows food suppliers and retailers to shift a portion of the cost to the federal government thereby lowering the cost to the final consumers. According to an NNC advisory board report in 2014, since the program was launched, demand for fresh produce increased [4]. This, in turn, increased flight hours of cargo operators to the North.

An analysis of the disparities in transport infrastructure between the different provinces proves that not all of the regions in Canada’s North are suitable for operation. For instance, while communities in Yukon and Nunavut were found to have existing and growing transport

infrastructure that provide year-round access by air and land, about 20 communities in the Northwest Territories have no year-round access by land and air. Ultimately, the Nunavik region is a prime location to establish a hub operation as it boasts a robust transport infrastructure as well as year-round access by water, land and air. More details of these results can be found in Appendix A.1.

To investigate the possibility of increasing access to more communities and opening new markets, means of reaching Northern Communities were evaluated. A Vertical Take-off and Landing (VTOL) configuration ensures that all communities with or without airports are reached. However, it is an expensive and unsustainable solution for the small market it targets. Alternatively, a Short Take-off and Landing (STOL) configuration ensures that all communities with airports in the North are reached while maintaining mission sustainability. This makes the Arctic Fox mission-specific for flying in the North while reaching more communities. The details of these assessments can be found in Appendix A.2 and A.3.

To open even more markets, airdrops and ski-landing gears configurations were evaluated. There are technical difficulties involved with implementing an airdrop solution such as a distribution infrastructure post-cargo-drop, cargo limits as fragile or heavy cargo may be difficult to drop [5], and design complexities. Ski-landing gears also present technical difficulties as they reduce the reliability of the aircraft due to an increased need for maintenance. Coupled with the expected cost of operating the Arctic Fox, a ski-landing gear configuration is unsustainable. More details on the performed trade study are in Appendix A.4.

Operating in all of Canada's North will not be sustainable; however, rolling out to a small-scale market will allow the Arctic Fox to gain more knowledge of the Northern market. More so, an STOL configuration allows the Arctic Fox to reach more communities in the North than the current aircraft flying the Northern skies.

2.2 Mission Analysis

Air transportation in the Canadian North is divided into two main business models: hub-to-hub and hub-to-point. The hub-to-hub aircraft model strategy is to bring a bigger payload

from a southern hub to a northern hub and is usually completed with large turbofan-powered aircraft such as Boeing 737s. The hub-to-point strategy is to redistribute smaller payload from a Northern hub to a point (remote community) and is usually accomplished with ATR-42 - a medium turboprop aircraft. Figure 1 represent both North Canada air transportation model, starting from Montreal to Iqaluit, and then Iqaluit to remote communities.

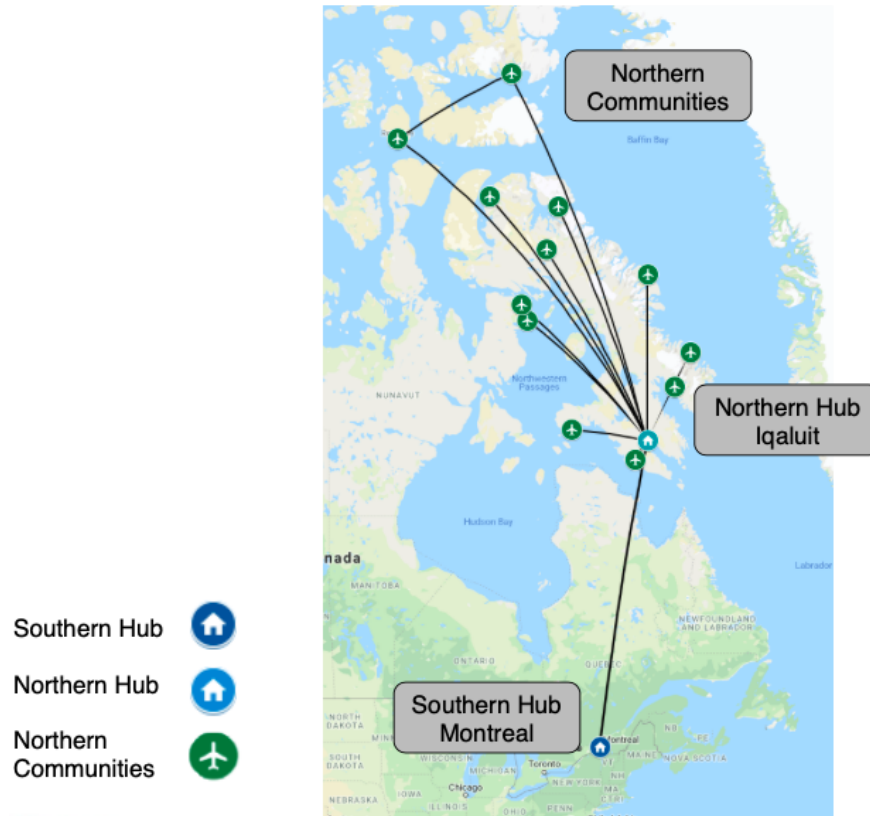


Figure 1: Current state of air transportation in Northern Canada

From a design point-of-view, one aircraft cannot compete in both markets and still outperform the competition. The hub-to-point market is an underserved market and delivering cargo to communities with shorter flights will increase the data gathering opportunities throughout different flight phases. Since First Air, the operator, is actively seeking to replace their ageing fleet of ATRs, the Arctic Fox was designed to outperform ATRs in a hub-to-point model.

Rankin Inlet, Iqaluit, Kuujjuaq, Cambridge Bay and Yellowknife are the five main Northern hubs serving the targeted market communities. Therefore, critical missions were established from these Northern hubs. They serve to define Arctic Fox's operating boundaries and limitations in term of its critical performance and lead the aircraft sizing exercise. Route limitations were established when the aircraft is operating at maximum payload capacity with a lower amount of fuel needed (maximum zero fuel weight or MZFW), when operating at maximum takeoff weight (MTOW) reaching a far community and trading payload for fuel, and when operating at maximum fuel weight and removing payload to reach the community. The complete details of the critical mission design process are found in Appendix B and further details can be found in Figure 5. .

From the list of the remote communities with air access, a weekly frequency of distribution and a total payload-per-trip were optimized. The optimization was based on the total weekly payload needed by the community and the total range to its closest hub. More details of this optimization study are found in Appendix B. It was established so that Arctic Fox can reach a maximum amount of communities to increase mission opportunities without affecting its operational limit of profitability, which is available in Figure 5.

2.3 Business Case

Weather patterns, seasonal fluctuations, competition, government regulations, economic sensitivity with subsidy program and the dilapidated state of infrastructure in the North are risks to consider to allow the main stakeholders, the original equipment manufacturer (OEM), the operator and the supplier or retailer to reach their profitability goals. A complete stakeholders' analysis is provided in Appendix C and in Section 3.3. The OEM's main objective is to be an industry leader in the development and production of unmanned vehicles. The OEM's short-term profitability is sacrificed to develop a new technology that will be extended in future applications, which will then lead to long-term profit. However, to justify the OEM's development and production costs, the aircraft must outperform the current aircraft operating in the North while remaining profitable and sellable. Then, after the first

phase, the profitability will be increased because of a reduction in operating cost due to a decrease in pilot recurrent salary and training associated with an autonomous aircraft. More details on this study can be found in Appendix C and in Figure 55 in Section 5.10.

The results from the operator profit analysis led to profitability for both dual-piloted and an autonomous aircraft configuration and are applicable for all the planned phases that will be discussed later. The profitability, when compared to ATRs, mainly results from an increase in mission opportunities due to the outperformance of both the Arctic Fox models in terms of takeoff and landing distances. Key outperformance points are mentioned; the complete analysis is found in Appendix C. More so, from the operating cost reduction advantages from autonomous flight. An improved profit gross margin of 38% with the autonomous configuration for Rankin Inlet phases as shown in Figure 2 and 23% is planned for the final phase as per Figure 3. Further details of this analysis are developed in Appendix C.

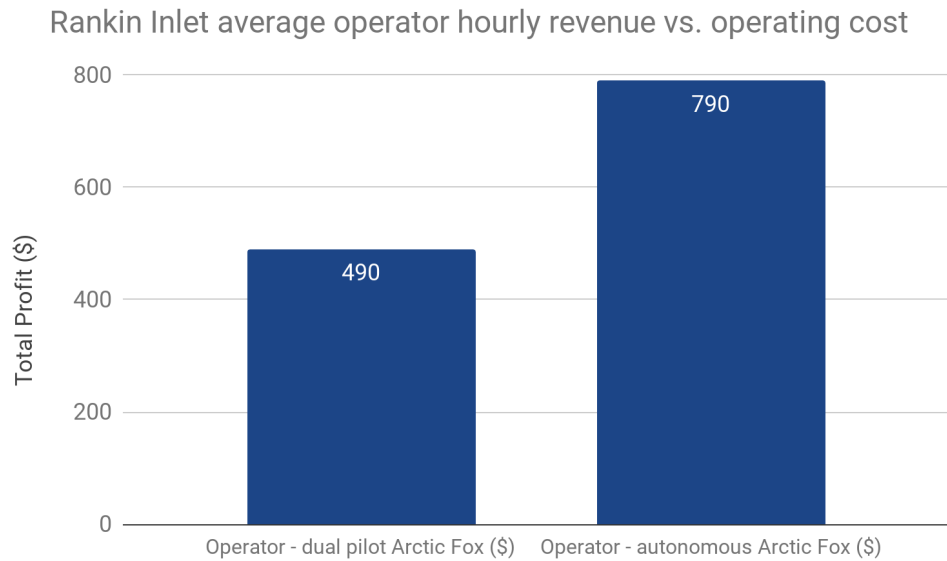


Figure 2: Rankin Inlet operator profit analysis

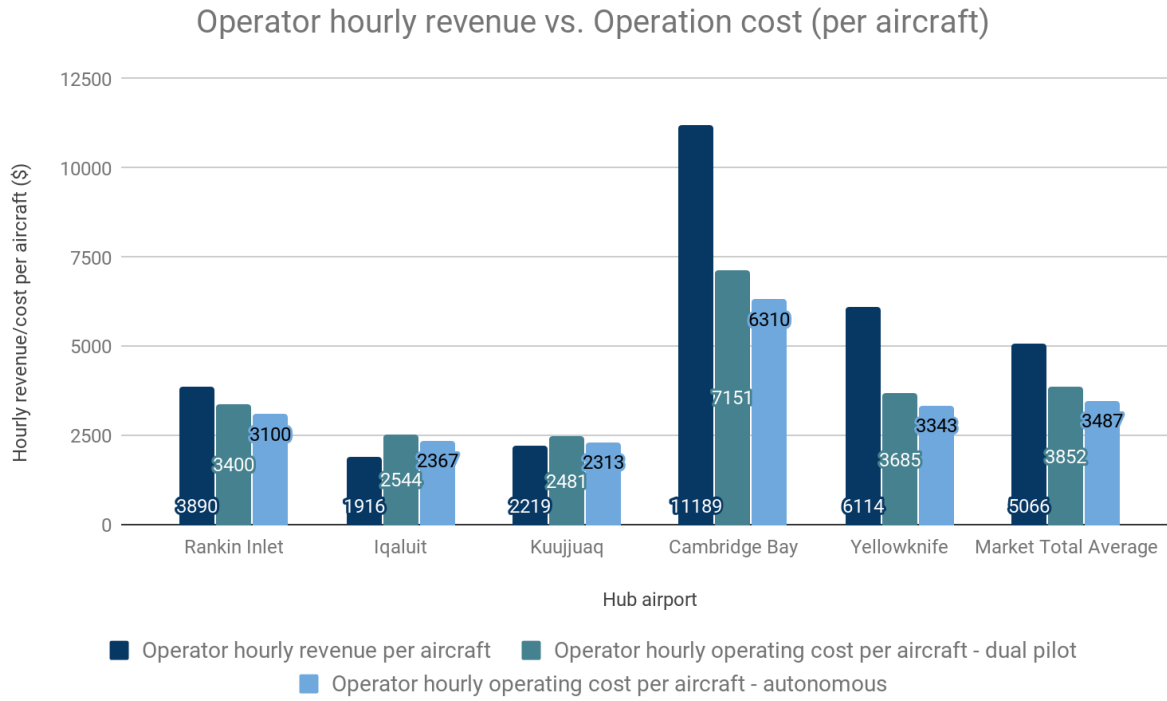


Figure 3: Overall market operator hourly revenue versus operating cost analysis

Designing a smaller aircraft allows the OEM to test and to prove the design safety and efficiency and to reduce the risk of higher development cost associated with a bigger aircraft model. More so, it should prove the market demand and stability. Once proven, the smaller scale technology and development can be expanded to a bigger scale model to increase market opportunities, and generally at lower program cost.

3 IMPACT OF TECHNOLOGY ON SOCIETY

3.1 Ethical

The RFP that the Arctic Fox aimed to address called for an optionally-piloted aircraft. Incorporating autonomous technology into aircraft brings up similar ethical questions like those for autonomous cars. For the case of the Arctic Fox, many such concerns are resolved due to the area of implementation being Northern Canada. In addition to not having any humans on-board, low population density and low aerial traffic aid in addressing classical ethical problems [6]. One such ethical problem is self-sacrifice, where the dilemma posed

consists of an autonomous car being confronted with making a decision of either driving off a cliff (resulting in the death of its occupants) or slamming into an oncoming school bus (possibly jeopardizing more lives). For the case of an autonomous aircraft flying in sparsely populated Northern Canada, this question is easier to answer. For example, given a malfunction during landing, the pre-programmed response algorithm would be set up to ensure that no human lives are put at risk since the self-sacrifice of the aircraft only involves loss of cargo. On the other hand, an ethical conundrum of a deer running onto the runway while the aircraft is landing or taking off is just as relevant for autonomous aircraft as it is for autonomous cars, and may manifest itself in other ways such as a flock of birds.

In the current preliminary design study, two options to incorporate autonomy into the aircraft were considered. The first - a remotely managed operation where pre-programmed decision-making algorithms are in-charge of flight functions. The second, an AI autonomous system that flies the aircraft but is also able to make independent decisions. Through the trade study shown in Appendix D, the second option was found to be an unsustainable path towards achieving aircraft autonomy because of the immaturity of AI technology and the lack of clarity in the human-machine interface for AI systems.

Future steps in the design process include other ethical concerns. A major concern in the programming of the decision-making algorithms is to ensure that no inherent personal biases seep in. An appropriate method to guard against this is to incorporate technical expertise from a diverse group of programmers. The programming shall also involve incorporating crash/emergency landing sequences. The guiding ethical principle for such cases should include but not be limited to, protection of human life, property, and maintaining the integrity of sovereign First Nations land. Finally, the implementation of aircraft equipped with sophisticated cameras and tracking equipment poses the concern of right to privacy infringements. Robust regulatory and legal safeguards would be required to ensure no misuse of this advanced technology occurs.

3.2 Legal

As a remotely operated autonomous aircraft, the Arctic Fox has unique legal considerations. Similarly to conventional transport aircraft, the Arctic Fox must adhere to the Canadian Aviation Regulations (CARs). Recently, Transport Canada updated the CARs and introduced a new section, (Part IX), specifically to address remotely piloted aircraft systems like the Arctic Fox. The regulations and guidance material currently available are mostly targeted at smaller UAVs operated within visual line-of-sight. Because the Arctic Fox is a larger aircraft operating beyond visual line-of-sight (BVLOS), a special flight operations certificate (SFOC) must be obtained by the aircraft operator [7, 903.01].

The Arctic Fox is a testbed for autonomous flight technology. The reliability data obtained while operating autonomously is useful to prove the safety of the autonomous system; however, regulations and guidance material addressing the concerns of autonomous aircraft still need to be developed. A specific area for regulatory development to focus on is the interface between the remote human pilot and the onboard autonomous system. This interface differentiates the roles and responsibilities of the human pilot and autonomous system, establishes the required level of situational awareness to fly BVLOS, and provides the means to control the aircraft remotely.

Some examples of regulations that apply to the Arctic Fox are: the remote pilot must be able to take immediate control of the aircraft [7, 901.32], the UAV must give right of way to other aircraft [7, 901.17] and the aircraft must be equipped with collision avoidance transponders [7, 702.46]. In addition to aviation regulations, the aircraft is also subject to other legal requirements such as protecting privacy, not trespassing and minimizing harmful environmental impact. The design requirements of the Arctic Fox were partially derived from the applicable regulations.

3.3 Social

Through stakeholder analysis, the impact of the Arctic Fox on Northern communities was examined. Inuit in Nunavik, the Northern portion of Quebec where there are a num-

ber of Inuit communities, are represented by the Makivik Corporation, who also manage, invest, and administer funds from the James Bay Northern Quebec Land Claim Agreement [8]. Makivik invests by owning profitable businesses, such as Air Inuit and First Air, both targeted operators for the Arctic Fox [9].

Through these investments in airlines, Makivik has been able to provide millions in funding for community programs, local cultural organizations, youth associations, and more [10]. As Makivik also represents the Nunavik Inuit at the governmental level, increased profits allow Makivik to increase their political presence and result in greater subsidy programs [11]. As one of the Arctic Fox's requirements is to provide the operator with a good return on investment, its usage by First Air and Air Inuit would increase Makivik's funds and allow for greater investments in the communities.

3.4 Environmental

Northern Canada is a delicate environment, with pollution having 10 to 100 times the impact than in other environments due to soot collecting on snow and increasing the absorbance of the ground [12]. Nevertheless, food and other cargo still need to be sent to Northern communities, and there are few options to do so.

During the warmer months, bulk items and non-perishables are sent by boat and stored in the communities for the year [13]. While some communities have seasonal road and rail access, the vast majority do not [14]. Delivering large quantities of perishable food in the summer is problematic, as it needs to be stored in a climate-controlled environment. Unfortunately, many communities are off of the electrical grid, and rely on diesel generators, resulting in food storage having a high environmental cost, especially given the risks of diesel spills [15]. Given the challenges of storing food for long durations, and the lack of reliable year-round road access, food deliveries by air are the only feasible option.

The Arctic Fox will help reduce the environmental footprint of transportation to the North. Compared to the aircraft currently being used, it can carry more payload for longer-

range missions, requiring fewer flights, thus reducing the environmental impact of air transportation in the North.

3.5 Economical

Understanding the economic impact of the Arctic Fox on Northern communities requires dispelling some public perceptions on Unmanned Aircraft Systems (UAS). Public concern about automation is focused on the potential for mass unemployment caused by a surplus of human labour. These debates are largely misguided. According to findings by the Information and communications technology council (ICTC), autonomous vehicles offer inclusivity and economic participation for underrepresented groups in Canada — such as indigenous people while effectively growing the total employment in the Canadian economy [16]. These benefits are projected to grow for every year after implementation. The Arctic Fox, as discussed in section 5.9, is designed to go through a dual pilot operation (DPO) to a remotely managed operation (RMO). The anticipated world-wide pilot shortage, with automation, means that any displaced pilots will easily find new employment [17]. Although pilot jobs will be lost going from the first level to the next, new jobs of a different nature will be created in the second. The change in nature of these jobs will demand rethinking education and training, providing income supports and safety nets for displaced people with the help of government bodies and policymakers.

Coupled with shifts in the nature of employment, the Arctic Fox is bound to lead to increases in performance benefits. These benefits include increased profits, reduction in operating costs, and increased cargo throughput for the operators. According to a test by Mckinsey Global Institute (MGI), the implementation of “automation technologies could bring a range of performance benefits for companies” [18, p. 17]. The test developed hypothetical case studies to understand the economic impact of automation beyond labour substitution. One of the results showed that, calculated as a percentage of operating cost, automation could drive aircraft maintenance down by 25%. Since the Arctic Fox will be reaching more communities in the North, there will be an increase in cargo throughput for

the operator. The relative cost of implementing an autonomous aircraft like the Arctic Fox is “modest compared to the real value it can create” [18, p. 11].

The Arctic Fox represents the potential to contribute to the economic growth of the North. This is pertinent in a time when the region is experiencing a decline in growth rate and working-age population [19]. The expected decline in growth rate will lead to an economic growth gap. The Arctic Fox could compensate for these demographic trends. From the results of tests performed by MGI, automation in the aerospace industry is estimated to inject 0.8 - 1.4% of GDP by purchasing power parity (PPP) annually, assuming that all of the displaced labour rejoins the workforce [18, p. 15]. This ensures that living standards are maintained or improved as labour force wanes.

4 CONCEPTUAL DESIGN

4.1 Overview

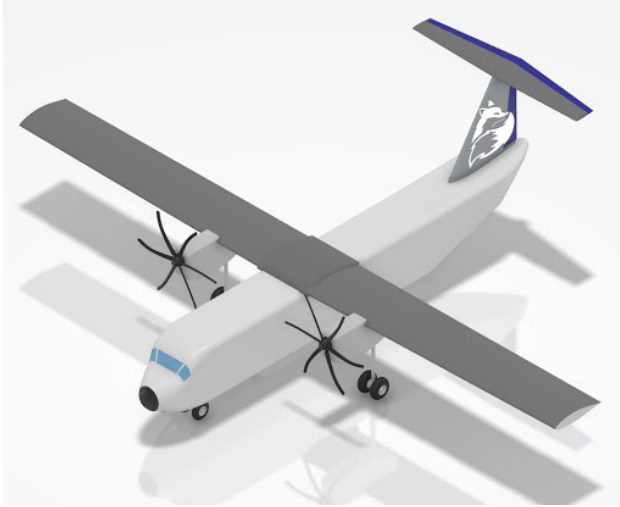


Figure 4: The Arctic Fox in the first semester

The Arctic Fox is designed to transport 10 800 lbs of perishable food, with a gross weight of 37 637lbs. The aircraft, shown in Figure 4, has a rectangular fuselage with cross-sectional dimensions of 9.5 ft high and 8 ft wide. The total length of the aircraft is 70 ft, where 13 ft is dedicated for the cockpit and 34.5 ft is for the cargo bay. The tail section has a rack angle of 12 degrees with the horizontal. The rigid wings are designed to have a root chord of 9.2 ft and a tip chord of 8.3 ft with a total span of 87.7 ft. The T-tail configuration is composed of the vertical stabilizer and the horizontal stabilizer. The vertical tail is designed with a NACA 0012 airfoil with a root chord of 12.15 ft and tip chord of 4.07 ft. The vertical stabilizer has a span of 12.53 ft and a front sweep. The horizontal tail is also designed with a NACA 0012 airfoil with a root chord of 5.23 ft and tip chord of 3.20 ft. The span of the of each horizontal stabilizer is 15 ft.

4.2 Aircraft Sizing

The initial aircraft weight was calculated through an iterative process that was conducted following a method outlined by Roskam [20, p. 5-85]. By benchmarking against similar aircraft in its category and evaluating the mission profile to estimate fuel to weight ratios

as well as necessary payload and range to accomplish the mission, an initial gross take-off weight was obtained. Once this weight was found, the above estimated ratios were revised by inserting in actual design values of the Arctic Fox until the final gross take-off weight of 37,600 lb was obtained. A payload-range diagram was then constructed and a maximum payload of 10,800 lb was found and a maximum range of 1170 nautical miles, as seen in Figure 5.

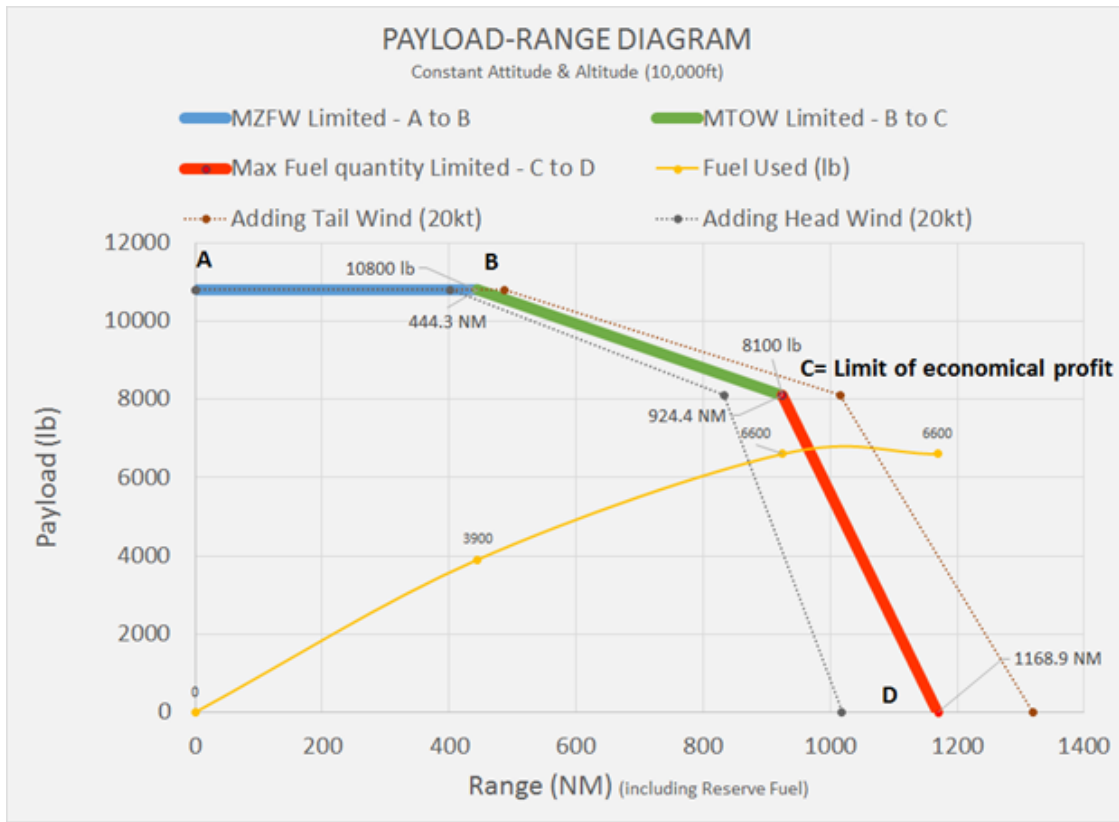


Figure 5: Payload-Range diagram of the aircraft

Evaluation of the different constraints posed by the aircraft missions led to determining how those would affect the design and physical characteristics of the aircraft. Following a method outlined by Roskam [20, p. 89-192], a constraint diagram was constructed, as shown in Figure 6. This tool allowed the equal comparison of some mission performance constraints, with the design space respecting all constraints shown in white in the top-left corner.

The preferred design point would be the lowest one, as it results in the smallest engines. However, a higher wing loading is also desired to minimize the wing area. The chosen design point is therefore driven by the takeoff run and landing distance, which is not surprising given the short runways in Northern Canada. Using the known gross weight of the aircraft and multiplying by the ratios given by the constraint diagram, a wing area of 768 ft² and a thrust of 11,500 lbf were necessary. Details on the development of the constraint diagram tool can be found in Appendix E.

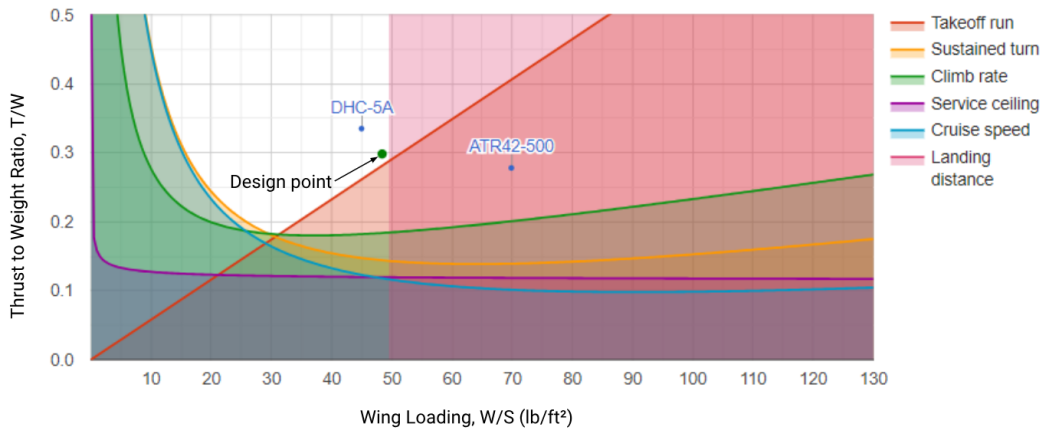


Figure 6: Constraint diagram of the aircraft

4.3 Autonomy Technology Review

The technology that allows an aircraft to automatically fly a particular lateral and vertical flight path and perform automatic landings is already well established. The Arctic Fox is a testbed for unmanned air vehicle (UAV) technologies. Enabling it to conduct missions autonomously under the management of a remote human pilot, the Arctic Fox utilizes a system of systems including elements such as triple redundant flight computers, lidar, instrument landing system (ILS) radios, command and control (C2) radios, global navigation satellite system (GNSS), inertial navigation system (INS), collision avoidance system (CAS), attitude and heading reference system (AHRS), radar altimeters, weather avoidance system, automatic anti-icing, etc. Although not yet fully designed, the ground control station is similarly outfitted with several critical components of advanced technology to provide the human pilot with the necessary situational awareness.

In order to safely incorporate autonomous UAVs into shared airspace with manned aircraft and over populated areas, it is necessary to determine the reliability of the autonomous system. The Arctic Fox project will record reliability data such as the mean time between failures (MTBF) of the equipment, whether the data gathered is accurate, and whether the decisions made and the actions taken by the autonomous system were appropriate. For example, data will be collected on the Arctic Fox's ability to autonomously

- maintain separation minima
- detect and avoid intruder aircraft
- detect and avoid bad weather conditions
- recognize and update 3D topography of mission areas
- resolve emergency issues such as engine fires, malfunctioning equipment, and loss of the command and control link
- provide adequate situational awareness to the remote pilot station

The data obtained will be used to demonstrate the airworthiness of the autonomous system and assess the feasibility of incorporating unmanned aircraft into common airspace. By having access to the data, our customer will gain an advantage when designing the next-generation of autonomous aircraft. The data will also be valuable in helping regulators to create new regulatory guidance material and standards for autonomous UAVs.

4.4 Overall Performance

4.4.1 Aerodynamics (Wing Design)

The Arctic Fox is a low-speed cargo aircraft with short take-off and landing distance, so its wing airfoil should be capable of producing high amounts of lift during flight. In order to find a proper wing airfoil, ideal (C_{li}) and maximum (C_{lmax}) lift coefficient required for the airfoil were calculated using equation 4.1 and 4.2, respectively.

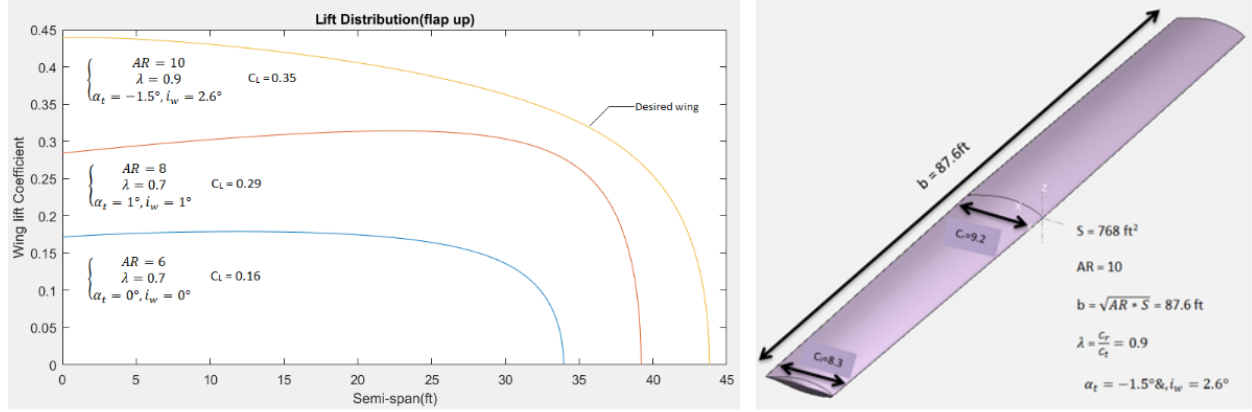
$$C_{li} = \frac{2W_{avg}}{\rho V_c S 0.95(0.9)} = 0.4 \quad (4.1)$$

Where, W_{avg} is the average weight of the aircraft during the cruise(lbf), ρ is the air density at cruise altitude(slug/ft³), V_c is the cruise speed(ft/s), and S is the wing planform area(ft²). In this formula, W_{avg} is divided by 0.95 and 0.9 for two main reasons. First, other aircraft components such as tail and fuselage contribute to lift production positively or negatively. Second, the wing lift coefficient of the 3D wing is different from 2D airfoil [21, Ch. 5].

$$C_{lmax} = \frac{2W_{TO}}{\rho_0 V_s S 0.95(0.9)} - \Delta HLD = 1.5 \quad (4.2)$$

Where, W_{TO} is the take-off weight(lbf), ρ is the Air density at sea level(slug/ft³), V_s is the stall speed(ft/s), S is the wing planform area(ft²), and ΔHLD is the lift coefficient added by flaps (Fowler flap).

Among different airfoils with $C_{li} = 0.4$ and $C_{lmax} = 1.5$, NACA 653-418, which has the highest lift to drag ratio with enough thickness, was chosen [21, Ch. 5]. The details of airfoil selection are found in Appendix F.



Wing lift coefficient required = 0.35

Figure 7: Lift distribution and wing parameters

To determine the wing parameters such as aspect and taper ratio a MATLAB tool using lifting line theory was developed. Then, wing parameters were determined based on two criteria.

1. To have enough lift for cruise. In preliminary wing design, the wing is designed for cruise conditions. Then, flaps are designed based on lift required during take-off and landing.
2. To have a lift distribution which its concentration is closer to the root. This creates some advantages for the wing design such as stress reduction at the wing root due to bending moment.

In order to select and design flap parameters, a MATLAB tool was developed to calculate the wing lift coefficient after flap deflection, as shown in Figure 7. Based on the lift coefficient required for take-off and landing and using the MATLAB tool, Fowler flap was selected and sized as shown in Figure 8.

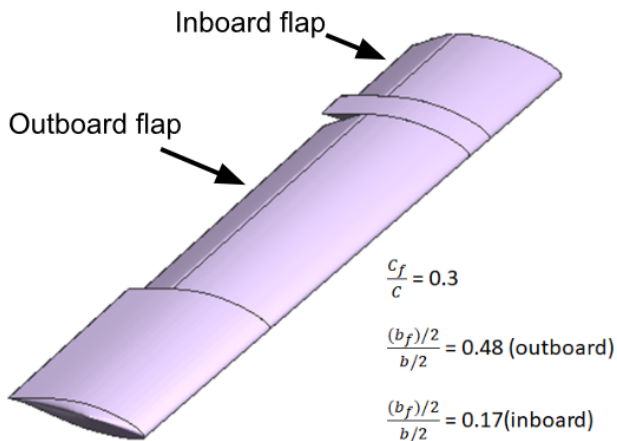


Figure 8: The Arctic Fox wing and flaps

4.4.2 Static Margin

The airplane pitches up or down with respect to the location of the CG. A statically stable aircraft will always return to equilibrium following a longitudinal disturbance. However, the aircraft loses its stable quality as the CG moves past the neutral point. The latter term is the aft CG limit for stable flight. This behaviour is explained by the change of the negative pitching moment stability sign to positive, $\delta C_m/\delta a$. The static margin is the distance between the neutral point of the aircraft and its CG. The neutral point was found to be at 62% MAC or at 5.25 ft aft the AC of the wing, as shown in Figure 9.

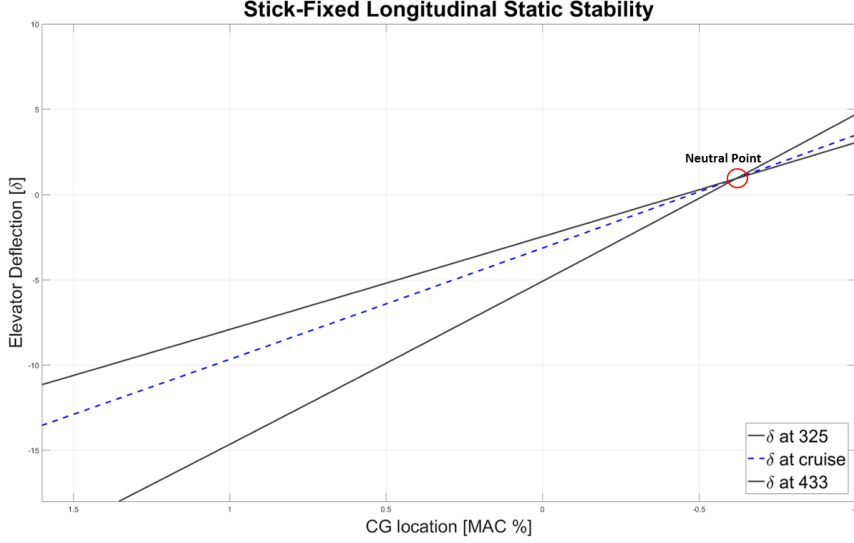


Figure 9: Static stability

The neutral point is fixed with the Arctic Fox configuration. So, if the CG is at the neutral point, the corresponding elevator deflection required to balance the pitching moment at the neutral point will be the same for three different cruise speed (325 ft/s, 395 ft/s, and 433 ft/s). The resulting static margin of the most forward and aft CG position is shown in Table 1.

	Most forward CG Position	Most aft CG position
CG Position	1% MAC	36% MAC
Static margin	61% MAC	26% MAC

Table 1: Static margin variability at different CG positions

Alternatively, the neutral point may also be calculated using the airplane geometry [22, p.408]. However, the calculation necessitate wind tunnel testing to obtain the required accurate aerodynamic variables. In overall, the static stability is critically dependent of the weight distribution of the Arctic Fox. Therefore, during the conceptual phases, the initial aircraft configuration decisions must satisfy the static margin.

4.4.3 Aircraft Performance

The cruising altitude was selected to be at a maximum of 10,000 feet in dual pilot operations since the Arctic Fox is an unpressurized aircraft which cannot operate above this altitude without additional oxygen supplies onboard as described in CAR 605.31 [23]. At this altitude, flying at low speeds and for short missions, the most fuel-efficient power plant type is the turboprop [24]. In order to reduce the total cost of the engines and the maintenance time and cost, while still having a redundant design, a two engine installation was selected. Benchmarking against other turboprop aircraft of similar gross weight (30,000 lb to 50,000 lb) on the basis of the number of engines validated the decision.

4.4.3.1 Takeoff Performance

From the constraint diagram, each engine and propeller combination must produce at least 5,650 lbf of thrust during takeoff. In order to meet this thrust requirement and reduce certification cost of the propeller and engine assembly, the PW127N engine, producing 2,750 shp [25], was selected with the Hamilton Standard 568F propeller, containing six blades forming a diameter of 13 ft [26]. The combination produces 6,240 lbf of thrust per installation at sea level and standard atmospheric conditions, calculated using the following equation from Roskam [20, part VII, Ch. 5].

$$\bar{T} = 5.75P_{TO} \left(\frac{\sigma ND_p^2}{P_{TO}} \right)^{1/3} \quad (4.3)$$

where \bar{T} is the mean takeoff thrust in pound-force ; P_{TO} is the all engines combined takeoff power in shaft horsepower (5,500 shp) ; σ is the air density ratio (1) ; N is the number of engines (2) ; D_p is the propeller diameter in feet (13 ft)

The selection of the PW127N engine was also affected by the fact that the targeted operators in Northern Canada currently use ATR-42 and DHC-8 Q300, which are powered by PW100 family engines (PW120 and PW123). Hence, the engine selected will be a less expensive investment for the operators, since it will not require major changes of equipment, training and methodology.

From the calculated thrust, the lift and drag parameters with flaps at 25° and the CAR 724.44 [27] regulations on gravel runway operations, the distance for one engine inoperative (OEI) takeoff and all engine operative (AEO) accelerate-stop distance (ASD) on dry gravel runways were calculated. The mean acceleration between the takeoff speeds (V_{EF} , V_1 , V_R , V_{LOF} and V_2), defined in FAR 25.107 [28], was used to calculate those distances as per [29] and the details of this calculation can be found in Appendix G. The calculation of both distances over a range of decision speed (V_1) yields the balanced field length (BFL), which is the runway length that must be available in order to be certified for takeoff at a given weight. The BFL at maximum takeoff weight (MTOW) of 37,637 lb at sea level and standard atmosphere was found to be 2,442 feet using the regulated 15% added distance for gravel runway from CAR 724.44 [27].

Only two airports in the northern market chosen have runways shorter than this BFL, meaning that the Arctic Fox can takeoff at MTOW from 54 of the 56 airports. For the other two airports (Grise Fjord and Kimmirut), the takeoff weight determined from the market and the mission analysis of these communities is less than 30,000 lb. At a takeoff weight of 30,000 lb at sea level and standard atmosphere, the BFL is 1,486 feet, which is shorter than both runways.

4.4.3.2 Landing Performance

From the lift and drag parameters with flaps at 40° and the CAR 724.44 [27] regulations on gravel runway operations, the actual landing distance (ALD) and the factored landing distance (FLD) were calculated. The mean acceleration between the landing speeds (V_{ref} , V_{TD} and V_{FB}), defined in FAR 25.125 [28], were used to calculate those distances as per [29] presented in details in Appendix G.

In order to certify for operation on gravel runways, the FLD must be shorter than the available landing distance of the runway, meaning that the aircraft must be able to come to a full stop within 80% of the gravel runway available, while still using the added 15% distance correction factor from CAR 724.44 [27]. At the maximum landing weight (MLW)

of 37,000 lb at sea level and standard atmosphere, the FLD is 2,323 feet without the use of reverse thrust. Hence, the aircraft can be certified to land at MLW at 54 of the 56 airports chosen, while the other two airports would require the use of reverse thrust or would only be certifiable under a lower landing weight.

4.4.3.3 Cruise Performance

The steady level-flight cruise velocity was calculated using the drag polars from OpenVSP [30], the approximated cruise power setting of 4,264 shp at sea level [31] modified for the 10,000 feet altitude and the following equation derived from Roskam [20, part VII, Ch. 5].

$$V = \left(\frac{2P_{alt}\eta_p}{C_D S \rho} \right)^{1/3} \quad (4.4)$$

where V is the aircraft velocity in feet per second ; P_{alt} is the power available at 10,000 feet in shaft horsepower (3,560 shp) ; η_p is the propeller efficiency (0.7) ; C_D is the cruise drag coefficient of the aircraft (0.037) ; S is the wing area in square feet (768 ft^2) ; ρ is the air density at 10 000 feet in slugs per cubic feet (0.00176 slugs/ ft^3)

This resulted in a cruise velocity of 225 knots and a maximum velocity of 245 knots at an altitude of 10,000 feet. The details of the calculations are presented in Appendix G. The propeller efficiency calculated from Gudmundsson [32] was low compared to other turboprop aircraft of similar gross weight and was reviewed once the preliminary design phase began.

4.5 Systems

4.5.1 Electrical System

The design of the electrical system was driven by the number of aircraft components needing electrical power. A trade study was conducted for the electrical system schemes, comparing variable frequency for 115 and 230 VAC generation, 28 and 270 VDC generation and 400 Hz AC generation. The results of the trade study are shown in Figure H.0.1 in Appendix H, which concluded that 230 VAC generation would be optimal. This is advantageous because of the reduced current needed for the system. Reducing the current minimizes the resistance through the wires, thus allowing smaller diameter wires, compared to the 115

or 28V schemes. As well, generating at variable frequency removes the need for a constant speed drive, thus reducing the weight and complexity of the system [33].

4.5.2 Primary Flight Control System

The primary flight control system of the Arctic Fox will be electrically actuated. This design decision was the result of a trade study performed comparing electrical, mechanical and hydraulic power solutions. Some advantages of electrical actuation are high power transmission efficiency and a reduced power distribution weight. Disadvantages include heavy components at the actuator level, the impact on the electrical system (power demand and weight) and lastly, single point failures i.e actuator jamming. In the conceptual design phase, the rudder and elevators were split to mitigate against single point failures, in the event of a jammed split surface, control is maintained by the other surface. Each split surface is actuated by 2 EMAs. In the event of a single point failure of one of the actuators used for roll control, control would be maintained by a dual actuator system over a summing lever. The lever's position corresponds with the sum of the positions of the actuators attached to it, as detailed in Appendix I.

4.5.3 Fuel System

The fuel system conceptual design aimed to satisfy the maximum mission range requirement of 6,600 lb of fuel. The volume of the fuel tank required is 135ft³. A wet symmetrical wing design was chosen based on a trade study comparing it to a fuel bladder wing design. Fuel stored within the wing acts as a counter stress on the wings which helps to reduce changes in the wing dihedral angle on takeoff. As well, it helps to reduce wing flutter by providing rigidity to the wings [34]. Fuel bladders were discouraged due to the space requirements in the cargo bay and longitudinal center of gravity consideration of added weight near the tail or nose.

4.5.4 Landing Gear Layout

The landing gear configuration was selected by considering a series of options with their advantages and disadvantages: taildragger, tricycle, quadricycle, monowheel, and

tandem/bicycle [32, p. 550]. The results of the trade study are shown in Appendix J. The tricycle configuration was selected for its ground stability, its increased ability to land in crosswinds, and ease of loading and unloading cargo because the aircraft lies horizontally on the runway. The landing gear was positioned using the method provided by Gudmundsson [32, pp. 567-569]. The landing gear placement was driven by the location of the CG of the aircraft and was placed to avoid incidents such as side tip-overs and tip back. As well, the landing gear is placed so the nose landing gear, as a rule of thumb, may carry 10-20% of the gross weight when the aircraft is not in the air. This is because a high nose gear load results in difficulties rotating the aircraft on takeoff, while too little weight results in difficulty steering the aircraft due to reduced friction with the ground. [35, pp. 232-233] [32, p. 568].

The landing gear layout is presented in Figure 10.

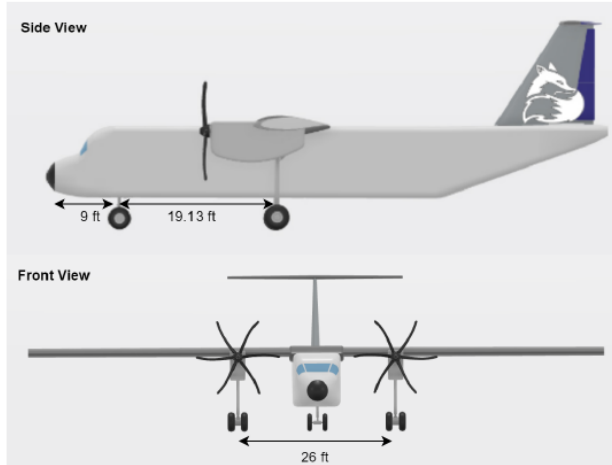


Figure 10: Landing gear layout

4.6 Weight and Balance

The objective of weight estimation is twofold: to ensure the aircraft's weight is within the allowable limit and to provide the stability team with the CG position to ensure that it is within the allowable range.

Group	Component Name	Weight (lb)	Location of CG of each part		
			x, Fuselage station line, ft	y, Buttock line, ft	z, Waterline, ft
Structure group	Wing (two)	6688.8	34.7	0.0	18.6
	Horizontal Tail	262.8	75.4	0.0	32.0
	Vertical Tail	404.1	72.8	0.0	37.2
	Fuselage	4999.1	40.8	0.0	14.4
	Main Landing Gear	873.6	36.5	0.0	9.0
	Nose Landing Gear	436.8	15.0	0.0	9.0
Propulsion Group	Engine Section	2120.0	28.0	0.0	16.6
	Fuel System	156.2	34.7	0.0	18.6
	Nacelles	1200.0	30.0	0.0	17.0
Equipment Group	Propellers	900.0	25.0	0.0	18.0
	Flight Controls (wing)	240.0	36.5	0.0	19.5
	Flight Controls (H-stab)	220.0	75.0	0.0	31.5
	Flight Controls (V-stab)	80.0	74.6	0.0	24.0
	APU Installer	250.0	71.0	0.0	29.0
	Electrical	803.1	26.7	0.0	12.0
	Avionics	900.0	19.0	0.0	13.6
	Anti-icing (wing)	15.2	31.4	0.0	19.5
	Anti-icing (V-tail)	2.0	68.9	0.0	24.0
Useful Load group	Anti-icing (H-tail)	3.3	71.6	0.0	31.5
	Insulation	39.6	34.1	0.0	14.4
	Cargo	8100.0	40.0	0.0	15.0
Crew	Crew	390.0	14.0	0.0	15.8
	Fuel	4500.0	34.7	0.0	19.0
	Total Sum	33584.7			

Table 2: Weights of all components

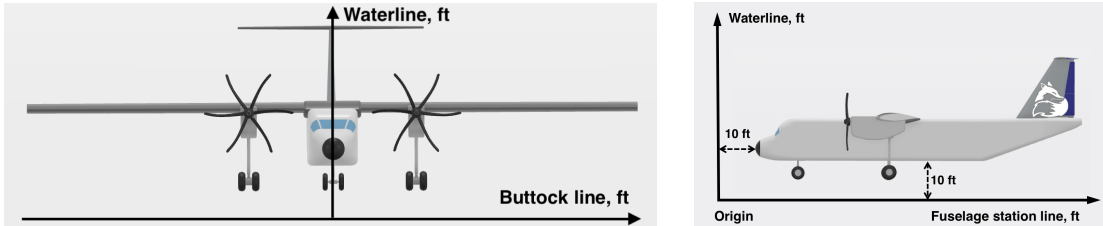


Figure 11: Coordinate system

The coordinate system to locate components is shown in Figure 11. Weights of aircraft components are listed in Figure 2 were estimated by three methods. Weight estimation equations from [35, ch. 15] were used for structure and propulsion components; data of similar aircraft were used for equipment components, and mission profile helped define useful loads. Due to limited time, weights of some components were roughly benchmarked, such as the avionics and the electrical system.

The gross weights from Table 2 for three critical missions are 5-10% less than that from initial aircraft sizing. The most aft CG was at 63.5% of mean aerodynamic chord (MAC) from the leading edge, obtained by removing any removable component whose CG is in

front of the aircraft CG, referred to [21, pp. 590-606]. Similarly, the most forward CG was obtained at 36.8% of MAC from the leading edge. This range fell within the longitudinal CG envelope calculated by the stability team.

5 PRELIMINARY DESIGN AND V&V

5.1 Overview and Dimensions

Dassault Systemes' 3Dexperience and CATIA v5 were used to communicate the designs of the Arctic Fox. Figure 12 shows the Arctic Fox in orthographic and isometric views. The surfaces of the Arctic Fox were modelled chiefly with generative surfaces. Files with more details of the design of the exterior of the Arctic Fox can be found in Appendix K.

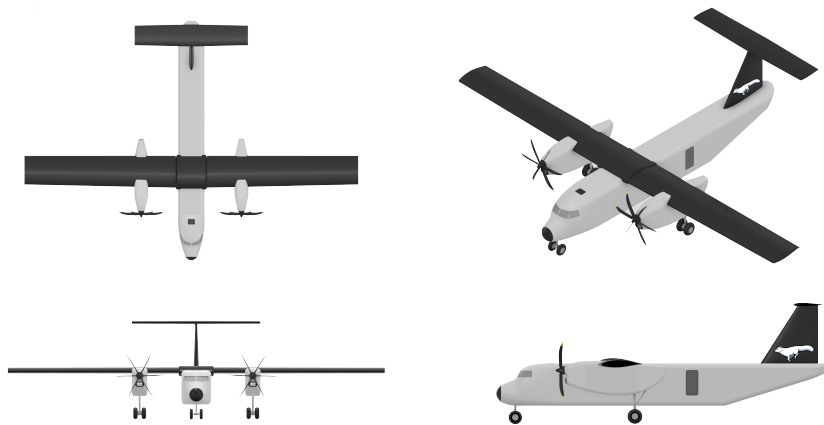


Figure 12: Orthographic and isometric views of the Arctic Fox

System designs were illustrated using adaptive swept surfaces to represent feed, wire, and hydraulic lines. Figure 13 shows the subsystems of the Arctic Fox.

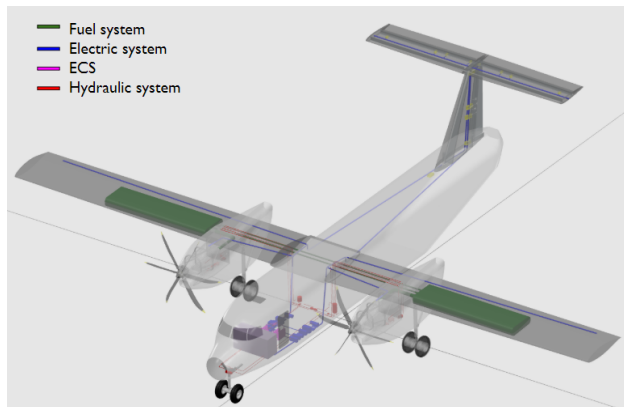


Figure 13: System architecture of the Arctic Fox

5.2 Weights and CG

With major re-designs of several components during the preliminary design phase, more accurate and detailed weight estimations were obtained. The MTOW of the Arctic Fox was increased to 38,405 lb, which is shown along with all the components weights in Appendix L.

The updated positions and weights of components resulted in a most aft CG of 69.25% MAC from the wing leading edge when flying with maximum payload and minimum fuel, while the most forward CG is at 41.06% MAC when flying with one full pallet of cargo in the most forward position and minimum fuel. In order to avoid instability during cargo loading and unloading, the main landing gears were positioned behind the most aft CG on ground, which was calculated to be 86.79% MAC. The details of the CG limits determination can be found in Appendix L. The range of flight CG limits falls within the longitudinal CG envelope calculated by the stability team and the landing gear limits calculated by the landing gear team.

5.3 Aircraft Performance

With major re-designs to the empennage, main landing gears and engine nacelles during the preliminary design phase, the MTOW and MLW of the Arctic Fox were increased. At the current MTOW of 38,405 lb, the BFL of the aircraft at sea level and standard atmosphere on a gravel runway increased to 2,536 feet. This change did not affect the capability of the aircraft to takeoff at MTOW from the same 54 of 56 targeted airports mentioned previously.

At the current MLW of 38,000 lb, the FLD of the aircraft at sea level and standard atmosphere on a gravel runway increased to 2,357 feet. This change did not affect the capability of the aircraft to land at MLW at the same 54 of 56 airports targeted.

The propeller efficiency calculated and used to find the cruise velocity during the conceptual design phase was found using a propeller viscous profile efficiency of 0.75 [32, Ch. 14]. This value is typical for a fixed pitch propeller, but too low for a constant speed propeller like the Hamilton Standard 568F. Hence, the viscous profile efficiency was changed to 0.85,

which is a typical value for a constant speed propeller. This resulted in an overall propeller efficiency of 0.8, falling in the expected range for mid-sized turboprop flying at low speeds [32, ch.14]. The iterative calculations of the propeller efficiency are detailed in Appendix M. This change of propeller efficiency in cruise increased the normal cruise velocity of the Arctic Fox to 236 knots and its maximum velocity to 256 knots.

5.4 Loads and Structures

5.4.1 V-N Diagram

The operating flight envelope of an airplane is presented in a v-n diagram. The v-n diagram is contingent on four factors: aircraft gross weight, the configuration of the aircraft, (clean, external stores, flaps and landing gear position), the symmetry of flight loading (since a rolling pull-out at high speed can reduce the structural limits to approximately two-thirds of the symmetrical load limits), and the applicable altitude. A change in any one of these four factors can cause a change in operating limits.

The maneuvering and gust v-n diagram presents the limits to which the airframe must be designed for adequate strength to withstand all maneuvers and turbulent air to which the plane would be subjected. For the arctic fox, the v-n diagram was constructed for symmetric flight at 10,000 ft (service ceiling), and clean configuration as shown in Figure 14, detailed calculations can be found in Appendix R;

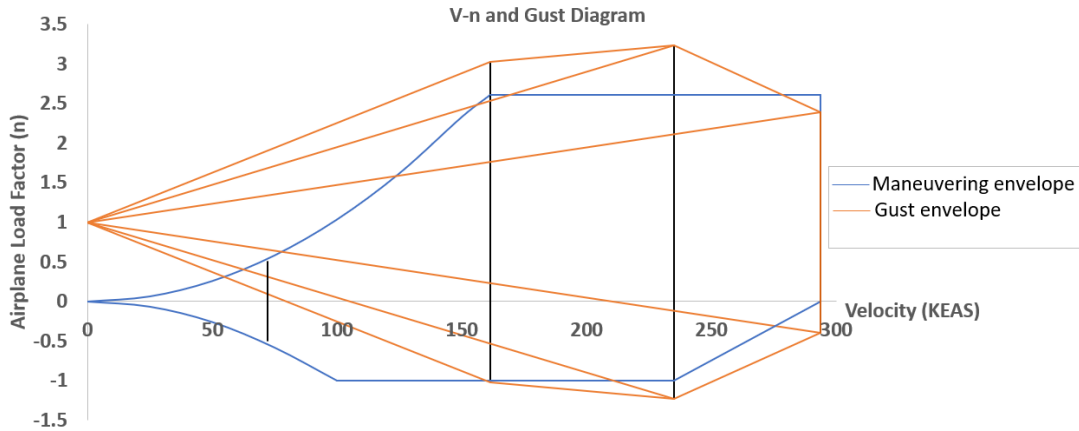


Figure 14: V-n diagram

The maneuvering envelope (the area enclosed by the blue curves), has a maximum positive load factor of 2.6 and a maximum negative load factor of -1. The condition for the maximum positive load factor is a 2.6g pull-up maneuver at dive speed and a low angle of attack and the condition for the maximum negative load factor is -1g maneuver at cruise speed.

The gust envelope (area enclosed by the orange curves), has a maximum positive load factor of 3.23 and a maximum negative load factor of -1.23. The condition for the maximum positive load factor is positive and negative gust at 50 ft/s at cruise speed. The gust envelope is more critical than the maneuver envelope because it has a higher maximum positive and negative load factors. The critical v-n diagram is at maximum weight, maximum altitude and for landing configuration.

The v-n diagram does not take asymmetric maneuvers such as sideslip into account. The load analysis for this maneuver must be done separately and then compared with the result from the v-n diagram.

5.4.2 Fuselage Structural Layout

The structural layout of the fuselage has been designed to resist the highest loads an aircraft can be subjected to in all three axes of motion; pitch, roll and yaw. These loads are due to the following maneuvers: pulling out of a dive (pitch axis), recovering from a roll at the maximum roll angle (roll axis) and deflecting the rudder in the event of an engine failure to maintain maneuverability (yaw axis). The layout designed, represented excluding the skin in Figure 15, consists of a semi-monocoque structure consisting of stringers, longitudinal and transversal beams, struts, skin panels, bulkheads and frames.

Assuming the fuselage behaves like two cantilever beams attached to the wing, four tapered longitudinal beams have been sized, two aft and two forward, to resist the pitch axis bending loads calculated in Appendix N. These longitudinal beams consist of an I cross-section made of 7075 T-6 aluminum that go through I beam bulkheads connected to the wing box front and rear spar to transfer the loads between the wing and the fuselage.

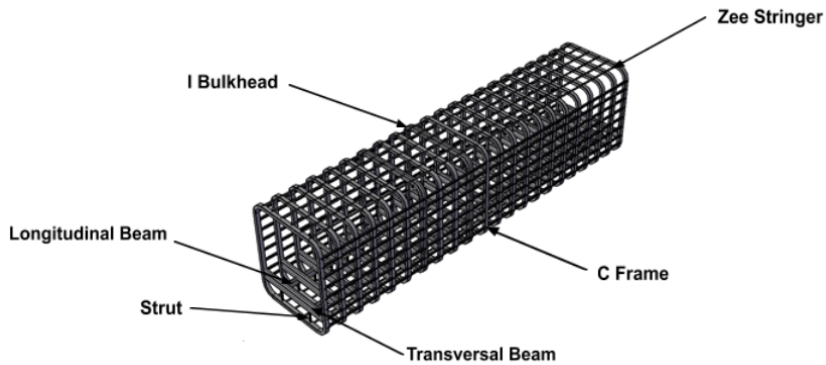


Figure 15: Fuselage structure of the Artic Fox

Furthermore, transversal I beams along with compression I beam struts were sized to resist the distributed weight of the cargo payload. Assuming the transversal beams to be fixed at both ends, and the cargo payload to be evenly distributed, the highest bending moment in each transversal beam was calculated in Appendix N and used to size them. Two I compression struts per transversal beam were sized to resist the compression loads arising from the distributed cargo weight calculated in Appendix N. Both these components were sized using 7075 T-6 aluminum.

Longitudinal Zee stringers were sized to resist the combined bending moment in the Pitch and Yaw axes. Lastly, bending loads arising from the rudder deflection in the event of an engine failure were calculated in Appendix N. Having 28 stringers, eight on both sides and six on the top and bottom, the direct stress arising from the bending moments have been found for each stringer as a function of its area, which has been selected in order to have a positive margin of safety (MS) for the highest loaded stringer. Using Aluminum 7075 T-6 and an area of 0.163in^2 , the margin of safety for the highest loaded stringer is 12%, which is positive. C frames were also designed, using the same aluminum, to maintain the shape of the fuselage as well provide attachment points for the stringers.

Skin panels were sized to resist principally torsional and bending loads. Torsional loads, arising from the aircraft returning to its original position after a roll maneuver, have been calculated in Appendix N. Skin panels on all four corners of the fuselage have been sized

using methods found in [36, ch. C9]. Using Aluminum 2024 T-3, a radius of curvature of 13.14in and a thickness of 0.035in, the margin of safety was calculated to be 17%. Applying a more simplistic method outlined in Appendix N to size the rest of the skin, shear stresses around the fuselage, arising from the highest torsional loads, have been calculated. Using a thickness of 0.035in, the margin of safety is of 10.07.

5.4.3 Aft Fuselage Structure

The aft fuselage structure was designed to resist critical bending moments and shears. Given the distribution of weights along the length of the fuselage, the method outlined in Bruhn was used to find the bending moments and shears at various fuselage stations [36, Ch. A5]. The critical load case for both bending and shear was a 1G flight case combined with a maximum elevator deflection. The critical axial load occurs during the 4.83G flight case.

Due to the tapered shape of the aft fuselage, the cross-section changes at each frame bay. Each cross-section was designed and analyzed using a structural idealization of the skin and stringers. The final cross-sections of the aft fuselage are the result of optimization of stringer areas, number of stringers, and skin thicknesses. All of the cross-sections consist of Z-shaped stringers of variable area with a constant depth of 1.375in. The stringers on top of the fuselage have an area of 0.255in^2 each, and the stringers on the sides each have an area of 0.453in^2 . The skin has variable thicknesses throughout each frame bay based on the changing loads. The minimum skin thickness is 0.04in, and the maximum thickness is 0.067in. The stringers are made of aluminum 7075-T6, and the skin is made of aluminum 2024-T3. These materials were chosen based on their material properties as well as historical data [37, Ch. 11].

The derivation of the flight loads, as well as details of the aft fuselage cross-sections and their stress analyses, including margins of safety, can be found in Appendix O.

5.4.4 Cargo Door Structure

Based on historical data as well as the Occupational Safety and Health Administration guidelines, when a ramp is down, the angle it makes with the ground must be less than 25° for safe use of a forklift [38]. The cargo door itself spans from the second frame to the tenth frame of the aft fuselage. The final design of the cargo door is approximately 158in long, resulting in an angle of roughly 20° .

When the door is lowered, the section of the floor between the start of the aft fuselage and the second frame lowers as well. This section of floor is attached to the door by a continuous hinge which was sized using the loading requirements as well as supplier specifications [39]. This configuration was chosen in order to reduce the overall length of the cargo door while respecting the ramp angle requirements, thus reducing the overall weight.

The cargo door is attached to the fuselage at the second frame of the aft fuselage. It is attached by two lugs, each sized to carry 100% of the critical load. The lugs are made of 7075-T6 aluminum.

Further details and analysis of the structure can be found in Appendix O.

5.4.5 Wing Structure

The internal structure of the wing supports the lift load, the weights of the fuselage, landing gears, engines, propellers, fuel systems, and control surfaces. Figure 16 shows the internal structure of the wing with its constituent parts. For brevity, details of the aileron design are presented in Appendix P.5.

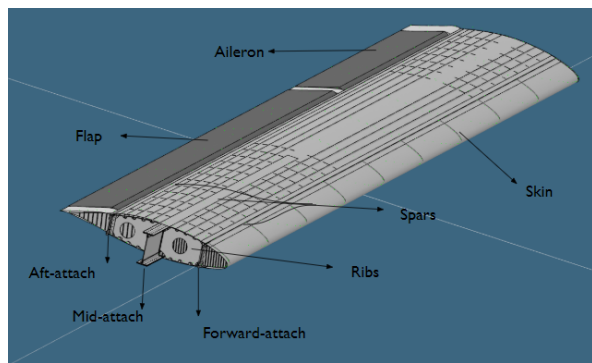


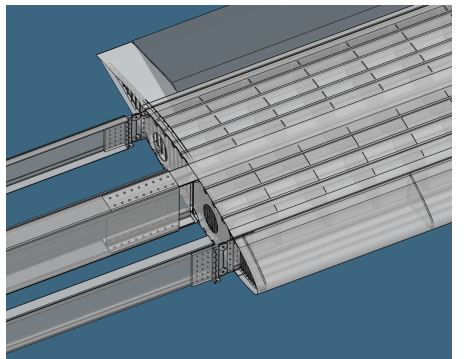
Figure 16: The internal structure of the wing of the Arctic Fox

5.4.5.1 Spars

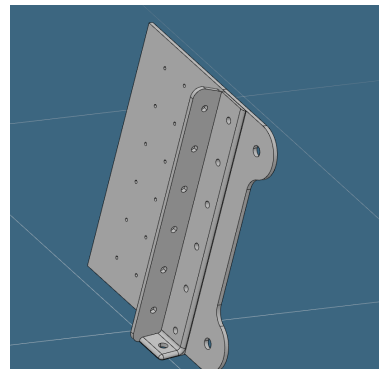
The wing features two tapered spars that run from wing root to tip and a 16ft auxiliary mid-spar. The spars are at 15, 40 and 70% of the wing chord. The I-beam spars are made of 2024-T81. The decision matrices for the material and cross-section selections are in Appendices P.1.1 & P.1.2. Load analysis was performed at different load cases, which were determined from airworthiness specifications as per CAR 525.301 [40]. The ultimate loads, load envelopes, summaries, and design considerations are presented in Appendix P.1. The minimum moment of inertia (I_z & I_x) for each spar was obtained with regards to the tensile strength of 2024-T81, the max bending moments and the distances from the neutral axis to the top surface. The web thickness of the spars was evaluated to ensure structural integrity due to shear forces and shear buckling. The details of these assessments can be found in Appendix P.1.0.4. When sizing holes for spar optimization, methods outlined in [41, ch. 13] were applied. From those methods, 6-diameter elliptical holes with 13.3-inch spacing were determined for spars. This configuration produces a weight reduction of 5%. More details of this evaluation are in the sizing tool in Appendix P.1.0.5.

5.4.5.2 Wing-Fuselage Attachment

The wing-fuselage attachment features a main attachment located at the mid-spar and two other attachment points located at the front and rear spar. The critical loads discussed in Section 5.4.5.1 drive the design of the attachments seen in Figure 17.



(a) Wing-fuselage attachment with spar carrythrough



(b) Forward-attach

Figure 17: Wing-fuselage attachment of the Arctic Fox

The aft and forward lugs were tested in axial and transverse loading conditions. The axial loading conditions include shear-bearing, tension, lug and bushing yield, and shear-off failures. The test guidelines are in Appendix P.2. The MS for the tests and details of fasteners are also presented in Appendix P.4.

To validate the theoretical analysis of the wing-fuselage attachment, finite element analysis (FEA) was performed on the forward-attach because it carries the highest load of the three spars. The applied loading conditions are shown in Appendix P.3.1. The ANSYS results differ from results obtained from the analytical solution as seen in Table 3. The diagrams of these loading conditions are in Appendix P.2.1. The differences in the results are due to the number of elements [42], stress concentrations arising from fastener-holes, and the absence of the bolt in the model since the analytical solution considers both the lug and pin to be acting together as their structural integrity are dependent [37, ch. 7]. Stress and deformation results of the FEA are in Appendix P.3.2.

	Analytical results	ANSYS results	% Difference
Shear-bearing failure (psi)	33,701	49,288	31.62
Tension failure (psi)	85,834.1	83,062	3.34
Margin of Safety	0.83	0.87	4.94

Table 3: Comparing ANSYS results to the analytical solution

5.4.5.3 Ribs, Skin and Stringers

The ribs are designed to the shear-buckling of the wing skin, and the ultimate loads discussed in Section 5.4.5.1 and detailed in Appendix P. There are 31 ribs located 18 inches from each other along the wingspan to keep the aerodynamic shape of the wing. They transmit the wing loads from the skin of the wing to the three spars. Considering the compressive-buckling of flat rectangular plates in [36, ch. C5], the thickness of the ribs of the Arctic Fox is 0.03 inches. The initial spacing of the ribs were 24 inches based on the preliminary spacing of transport aircraft given in [20, p. 220]. Due to the low margin of safety obtained from a rib spacing of 24 inches, the rib spacing was changed and finalized to 18 inches. Compar-

ing the material properties and strengths of different aluminum alloys, aluminum 7075-T6 was the material used for the ribs of the wing due to its high compression strength. The rib was assumed to be an unstiffened web-shear beam according to the description given in [41, p. 534] to add cutouts for weight optimization. From the cutout analysis method, two cutouts were laid out with a 9.5-inch diameter and a 15-inch spacing as illustrated in Figure 18.

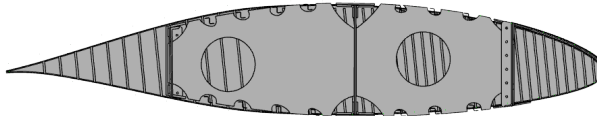


Figure 18: Rib configuration of the Arctic Fox

The skin is designed to cover the wing structure, as well as withstand torsional and bending loads. Aluminum 2024-T3 was the material used for the skin and stringers due to its high fatigue performance. The skin thickness of the Arctic Fox is 0.06 inches. This was determined by evaluating the buckling of flat sheets under combined loads [36, ch. C5], the structural idealization method from Megson detailed in Appendix Q, and the gravel landing conditions in Northern Canada. The maximum bending stress determined from the structural idealization method was 10828 psi, and a margin of safety of 5.74 was obtained, which concluded that the wing skin chosen was correct.

Sixteen Z-shaped stringers are attached to the skin and designed to prevent buckling under shear and torsional loads and to keep the skin from bending. The skin and stringers are illustrated in Figure 19. The thickness of the stringers is 0.05 inches. This was determined using the diagonal tension web NACA TN 2661 method from [41, p. 485-498]. The stringers were equally spaced by 6.5 inches between the front and mid spar, and 6.2 inches between the mid and rear spar, detailed in Appendix Q. The stringer thickness and spacing of the Arctic Fox were validated using the structural idealization method in Appendix Q and gave a maximum stress of 30,223 psi and a margin of safety of 0.36, which showed that the wing box will be able to withstand all ultimate loads.

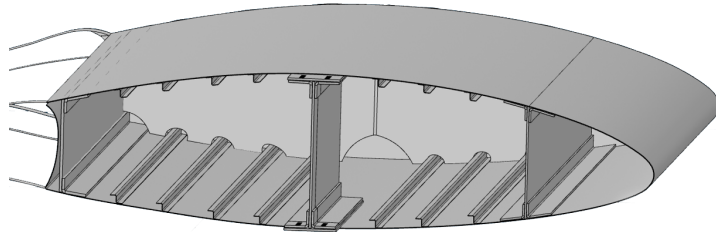


Figure 19: Skin and stringer configuration of the Arctic Fox

5.4.6 Centre Wing Box

5.4.6.1 Spars, Stringers, and Skin

The Arctic Fox is a high wing aircraft with lug attachments joining the wings to the fuselage and the centre wing box is the attachment point for the wing to the fuselage. The centre wing-box comprises of three spars; I-beam front spar, C-beam rear spar and a hollow rectangular beam mid spar. The front and rear spars are made of 7075-T6 alloy. The load analysis was performed for different load cases with regards to regulations, which are detailed in Appendix R.

The spars are made of spar caps and webs. The minimum moments of inertia for each spar required to withstand the ultimate loads were calculated and the spars were designed to have greater moments of inertia.

The stringer and skin panels of the centre wing box are the same as that of the wing, as they are designed to withstand the torsion and bending loads. The skin has a thickness of 0.06 inches and is made from Aluminum 2024-T3. The skin thickness was designed for buckling using the idealized method and with the maximum loads applied, the margin of safety was determined to be 1.245.

The stringers were designed for buckling under shear and torsional loads, using the diagonal tension web method from [41, p. 485-498]. There are 16 Z-stringers equally spaced between the front and rear spars. The stringers were sized to have a thickness of 0.05 inches and are made from 2024-T3. This was validated using the idealized structure and the max-

imum applied load, which resulted in a margin of safety of 0.21. Detailed calculations for the design and validation can be found in Appendix R.

5.4.6.2 Centre Wingbox Attachment

The wing is attached to the centre wing-box with lug attachments at the front and rear spars, and the mid spar of the wing is inserted into the mid hollow beam of the centre wing-box and fastened to it. The female mate of the lugs shown in Figure 20 is designed to withstand axial and transverse loading conditions.

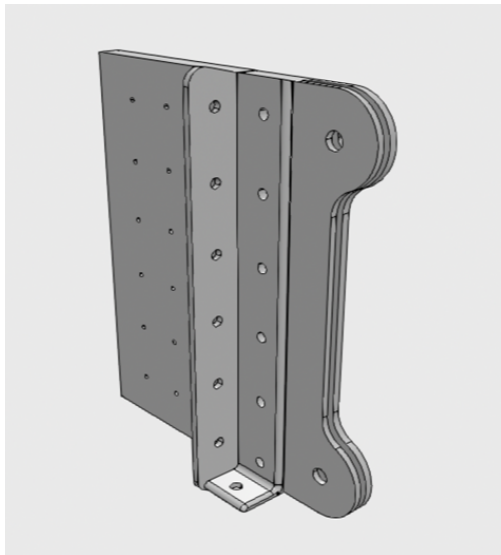


Figure 20: Female lug attachment

This load analysis and design details can be found in Appendix R. The same design theory and procedure used for the design of the male lugs were used for the female lug. The theory was validated for the male lug using FEA done for the front spar detailed in Appendix P.

5.4.7 Engine Mount Design

The engine mount consists of a truss structure that transfers powerplant loads to the leading edge wing spar. The design must withstand limit and ultimate load factors related to load conditions defined in the regulations, which are detailed in Table S.0.1 in Appendix S.

Gust load factors were taken from the v-n diagram shown in Figure 14, while gyroscopic and aerodynamic load factors were considered in the load case matrix through various roll, pitch and yaw maneuvers. The forces and moments were then resolved at the CG of the engine for all load cases. The load case matrix, the tabulated forces and moments, and all relevant equations are found in the Appendix S.

The initial powerplant mount design and attachment points were based on turboprop installation layouts found in Niu and Torenbeek [37, p. 447], [43, p. 40]. Surveys of the truss structures on the Beechcraft King Air at the TC hangar and on the Dornier 328 at ENA shown in Figures S.0.1 and S.0.2 in the Appendix S validated the overall design. The baseline material and dimensions were found through benchmarking [44], [45] and are summarized in Table 4.

Specification	Value
Diameter	2 in
Thickness	0.120 in
Material	AISI 4130 Alloy Steel
Specification	MIL-T-6736

Table 4: Baseline material and dimensions

The initial engine mount structure was modelled using CATIA v5. For verification, ANSYS was used to perform finite element analysis (FEA) to determine the critical load case. Through iterations, two additional truss members joining the top of the centre ring and the leading spar attachment truss members were added to eliminate the stress concentration occurring at the bottom of the centre ring where truss members are fastened, as shown in Figure 21. The truss member and ring dimensions were revised using an updated CAD model of the PW127N engine, and the diameter and thickness were increased to 2.50 inches and 0.25 inches respectively due to equivalent stress values exceeding the yield strength of the material. Through FEA verification of the final design, the worst load case was determined to be crash load case 29, yielding a maximum equivalent stress of 8.73×10^6 psf, which is

below the material's ultimate tensile strength of 1.17×10^7 psf and offers a 34.0% margin of safety. An exhaustive list of all equivalent stress and margin of safety values for all load cases is found in Appendix S.

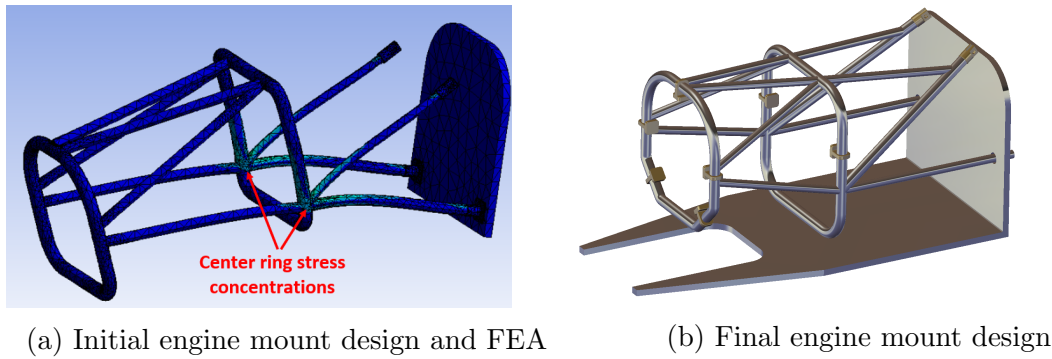


Figure 21: Engine mount design iterations

5.4.8 Landing Gear

Due to the landing gear configuration, the main landing gear was to be stored inside the engine nacelles. The necessary calculations can be found in Appendix J. The landing gears need to be longer to reach the ground from the engine nacelles and also be stored in them, which complicates the design. The engine nacelle is restricted in size, as it adversely affects the lift to drag ratio of the wings if increased. A software called “Linkage” was used to do a kinematic study of different landing gear actuation options as shown in Figure 22. Option 1 proved to be the best option due to the amount of space taken up by the landing gear when stored as well as actuator stroke length minimization and force requirement.

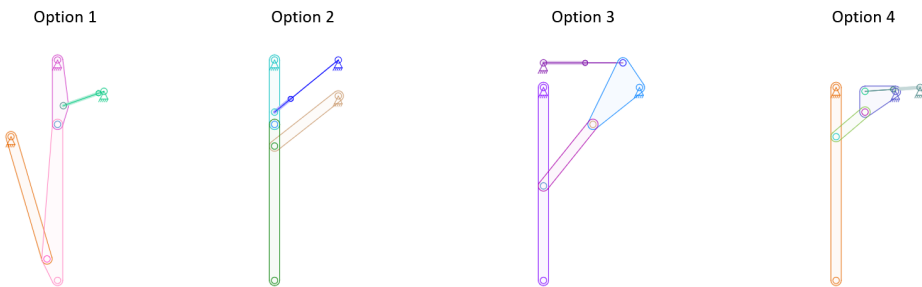


Figure 22: Main landing gear options

The aircraft will be flown in a meteorologically challenging environment in Canada's North. Because of these challenges, the landing gear structure must be able to withstand a landing on one main gear with a vertical speed up to the allowable legal amount of 12 ft/s as per CAR 525.723 (b) [40]. An Excel tool was created based on the [36, p. A2.23-A2.30] reaction forces calculation methods in order to determine the required attachment points dimensions for the chosen critical case as depicted in Figure 23.

The landing gear dimensions and the max landing weight were used in the tool as inputs to calculate the reaction force that will be translated to the attachment points. It then uses a double shear calculation to determine the necessary dimensions of the lug attachment using a 10% safety factor [46]. The calculated dimensions of the landing gear attachments can be found in Figure J.0.1 in Appendix J.

In order to verify the dimensions of the attachment points, ANSYS was used to perform a finite element analysis, which can be found in Appendix J. The attachment points are made out of 7075-T6 aluminum because of its high ultimate and shearing strengths [47]. Table 5 shows the difference between the tool's results and the ANSYS results and is used to validate the excel calculations.



Figure 23: Critical case landing

	Inner main lug	Outer main lug	Drag strut lug
ANSYS result	2772 lbf	34954 lbf	59544 lbf
Excel tool	5610 lbf	32787 lbf	58615 lbf
Difference	-3138 lbf	2167 lbf	929 lbf
% Difference	-53%	6.61%	1.85%

Table 5: Reaction forces for a one gear landing

As ANSYS is able to take into consideration the deflection of the landing gear struts while the Excel tool does not, the results on each attachment point differ from expected, especially for the “Inner Main Lug” which has a difference of 53%. However, the ANSYS results confirm that the critical attachment point is the one that attaches to the drag strut. The safety factor that the ANSYS results show is slightly lower than that of the tool, at 6%. This means that a slight redesign in the attachments is required in order to make them stronger.

After the successful verification of the excel tool, it was used for the nose landing gear attachment design, with the main differences being that the impact force is lower and the orientation is straight and level due to the main landing gears already being touched down. The dimensions of the attachment can be found in Figure J.0.2 in Appendix J.

5.4.9 Empennage

The empennage design, which consists of the horizontal and vertical stabilizers, were sized along with the elevator and rudder. The final specifications of the sizing are shown in Figures T.1.1 and T.2.1 in Appendix T. Due to initial problems with longitudinal static stability and take off distances, the horizontal tail was redesigned, resulting in the final empennage design shown in Figure 24.

The trade study that resulted in the T-tail configuration was still valid due to the advantages to provide stability and control introduced at the conceptual design phase. More details on the selection of the tail configuration are located in Figure T.3.3 in Appendix T. An influence to directional control were the effects of asymmetric thrust and crosswinds at takeoff which has an impact on the deflection requirement for the rud-

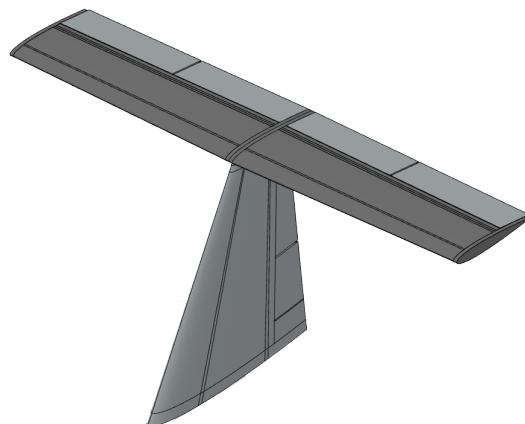


Figure 24: Empennage

der. Hence, the hinge moments were calculated using an excel tool based on the deflection angle and side slip angle needed to this particular takeoff scenario [20, p. 472]. The hinge attachments were designed to handle a hinge moment of 9333lbf*in acting on the rudder. To support the rudder, 4 hinges were needed and positioned adjacent to the actuators to avoid additional torsional moments acting on the hinges. The kinematics of the dogbone linkage was verified using CATIA v5 as shown in Figure 25.

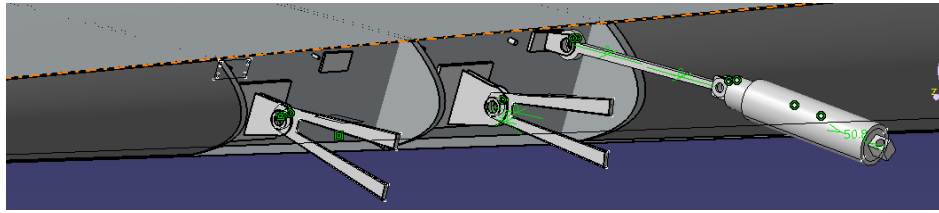


Figure 25: Hinge and dogbone kinematics for the rudder

Between aluminum 7075-T6 and aluminum 2024 T3, aluminum 2024-T3 has better fatigue resistance, hence that material was selected for the hinges [37, ch. 4]. Results were satisfactory because the margin of safety is 2.67 in the shear bearing failure case with an applied load of 2666lbf. The load acting on the hinge was calculated based on hinge moment and horn radius, assuming the worst case scenario of all hinge loads acting on a single hinge. The purpose was for redundancy in case several hinges fail. The hinge was analyzed for fatigue through FEA using ANSYS as shown in Figure T.4.1 in Appendix T. With the fixed boundary conditions applied at the fix supports of the hinge, the fatigue life was determined. After calculating the fatigue life using an excel tool based on [41, ch. 9] , the values were compared as shown in Table 6.

Fatigue analysis for Hinge	FEA using ANSYS	N2 (Michael Niu's Method)	% Difference
Life in cycles, N	1×10^6	3.52×10^6	15.7%

Table 6: Expected life of hinges

After comparing the two values from Table 6, the difference in the fatigue life for the hinge is 15.7%. This is mostly due to values taken off the logarithmic graph used for extrapolation and to calculate the fatigue life [41, ch. 9].

5.4.10 Flight Control Actuators

Imperative to the sizing and validation of the actuators, the control surface hinge moments were calculated in the conceptual design phase using Roskam's method and are shown in Table 7.

Control Surface	Hinge Moment (lbft)	Hinge Moment Coefficients
Ailerons	249.58	0.52
Rudder	777.68	0.2146
Elevators	2234.75	0.2564

Table 7: Hinge moment (HM) and hinge moment coefficients for primary flight control surface

In the detailed design phase, the hinge moment values were used to size the flight control actuators and determine the electrical loads required to power the flight controls. A method outlined by Liscouet-Hanke et al. in [48], was used to size the actuators. The actuator mounting influences the space envelope of the actuator, so to minimize the space taken by them, a flange mount type was used for all three primary control surfaces. Following the process outlined in [48] and using some inputs based on the space available for actuator mounting, the electrical power output values were found to be as in Table 8:

	Ailerons	Rudder	Elevator
Power required for one actuator [W]	138.5	1101.9	2260.2

Table 8: Actuator sizing and PCU envelope design parameters

To evaluate the impact of EMAs on the electrical system the values obtained for the power demand needed to be validated and verified. [48] provide estimates for electrical loads required to power flight control systems, The power demand for the three main control surfaces was over 100 KW for a plane with 6 times the payload of the plane. By comparing

the payload of both aircraft, it was possible to scale down the power demand of the aircraft used in the study to that of the Arctic Fox. The results confirmed that EMAs would not result in an overdesign of the electrical system. The total electrical loads were smaller for the [49] estimates.

In addition, a verification of the hinge moment values was performed using computational fluid dynamics (CFD). With these hinge moment values, it was possible to find the corresponding power values and compare them to the design values. This comparison allowed increase the confidence level in the actuation power values since a 2D inviscid model results in larger pressure coefficient values and consequently, larger hinge moment and power demand values. The model provided the results shown in Table 9.

Control Surface	HM Coefficient (Roskam)	HM Coefficient (SU2 CFD Software)	Difference
Elevators	0.25	0.3	16.70%
Rudder	0.22	0.31	36.70%
Ailerons	0.52	0.75	36.90%

Table 9: Comparison of hinge moment coefficients (Roskam method and SU2)

While there is a variance between the hinge moment coefficients using both methods, the calculated power values are still very close to the initial estimates by [48]. This verification allowed to demonstrate that the implementation of EMAs will not result in an overdesign of the electrical system due to excessive power demand.

5.5 Aerodynamics

5.5.1 Wind-Tunnel Testing

Wind tunnel testing was performed to validate results obtained from Prandtl's lifting-line theory and the related MATLAB tool which was developed and used in the first semester. This tool is discussed in further detail in Section 4.4.1 Due to the difficulty of manufacturing a scaled version of the airfoil, a NACA0018 airfoil was provided. While this was not the same airfoil as the horizontal stabilizer or the wing, the MATLAB tool created allowed for easy

changing of the airfoil selected in its code. As such, the data obtained in the wind tunnel would allow for validation of the code.

The experimental wing has a chord of 17.5 inches and a span of 36 inches, for an aspect ratio of approximately 2. It was fitted with a heated silicon pad on the inner surface of the leading edge to test for icing characteristics in order to validate the anti-icing system model. A rig was manufactured out of steel tubing and a steel plate to hold the wing section on the provided pylon at the wind tunnel facilities. The section was then tested with a static load before being installed at the wind tunnel. Finally, using the rig, it was mounted onto a load cell at the wind tunnel facilities at the University of Ontario Institute of Technology (UOIT), as seen in Figure 26. Further details on the physical setup can be found in the procedure in Appendix U.

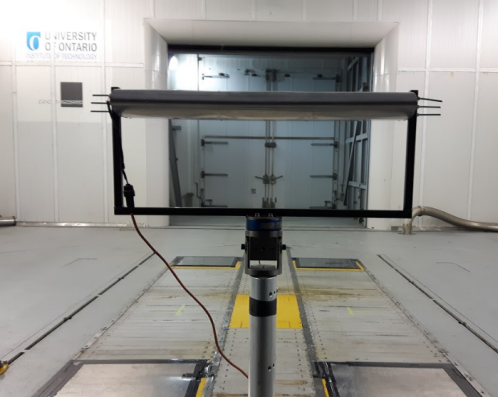


Figure 26: The wing section mounted once at the wind tunnel

The wing was subjected to freestream velocities and Reynolds numbers of 5×10^5 , 7×10^5 and 1×10^6 . A thirty-second average measurement of the lift and drag forces, as measured by the load cell, was taken for each Reynolds number. These measurements were done for angles of attack of 0.5, 10.2 and 19.8 degrees. Lift and drag coefficients were then calculated using the geometry and freestream properties of the air and with equations 5.1 and 5.2. These results were then compared with results from the MATLAB simulations as shown in Figure 27.

$$C_L = \frac{2L}{\rho u^2 S} \quad (5.1)$$

$$C_D = \frac{2D}{\rho u^2 S} \quad (5.2)$$

Where, C_L is the lift coefficient, C_D is the drag coefficient, ρ is the air density (slug/ft^3), u is the freestream velocity (ft/s), and S is the wing planform area(ft^2).

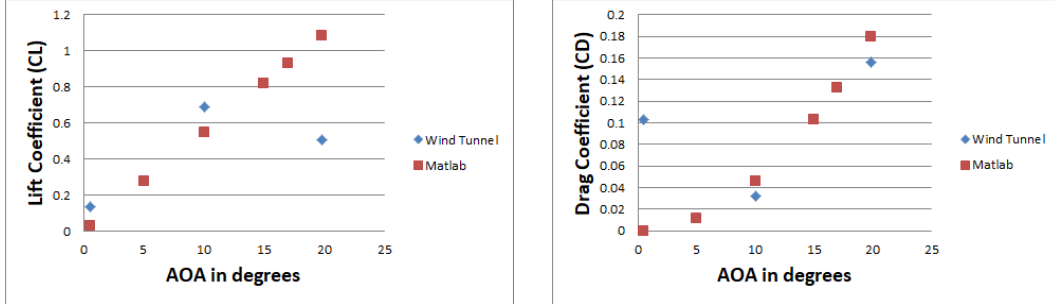


Figure 27: Lift and drag coefficients obtained from MATLAB and the wind tunnel

The second set of tests focused on icing. The detailed test procedure for which can be found in the Test Procedure document in Appendix U. The objective was to test for the amount of heating power required to prevent ice formation on the leading edge of the wing. A rheostat was used to control the current delivered to the resistive heating element on the leading edge. Three tests were performed using the wind tunnel at -20°C to produce winds of 44.7 kt and a sprinkler rig, as shown in Figure 28, with a water flow rate of 28 g/m²s in order to create a cloud water content of 1.25 g/m³. The first, tested for the amount of energy required to melt initial ice formations on the wing. This was required to determine if a lower power-output could be used to prevent critical ice formation on the leading edge. The second, tested the amount of energy required to prevent the formation of ice on the leading edge. This was achieved by setting the power output of the controller to the calculated energy requirement. The third test evaluated the energy required to melt a large layer of ice. This was achieved by allowing the wing to completely ice-over before turning on the anti-icing system. The video of this test can be found in Appendix U.



Figure 28: Sprinkler rig provided by UOIT to simulate icing

5.5.2 Wing CFD Validation

To further validate the MATLAB tool developed in the first semester, CFD analysis using ANSYS Fluent was conducted. Since it was not possible to perform CFD analysis for the actual wing size, the MATLAB results for two smaller wings with different aspect ratios (AR=2 and 6) were compared with the ANSYS results. In other words, the method and tool used in the first semester were validated instead of validating the designed wing. The wing with the aspect ratio of 2 is the wing tested in the wind tunnel with a NACA 0018 airfoil, and the wing with the aspect ratio of 6 is the horizontal stabilizer of the Arctic Fox with a NACA 0012 airfoil.

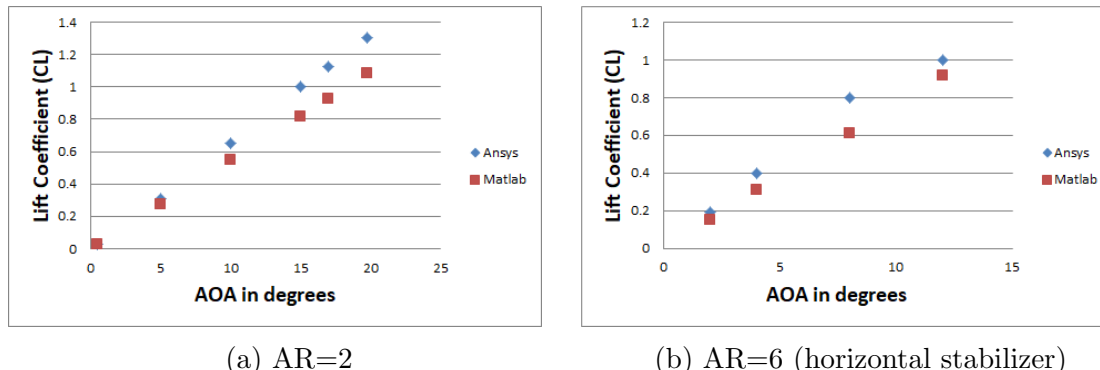


Figure 29: Lift coefficients obtained from MATLAB and ANSYS

Figure 29 indicates that the MATLAB results of both low and high aspect ratio wings are more conservative than the ANSYS results, which is desired and acceptable for preliminary design.

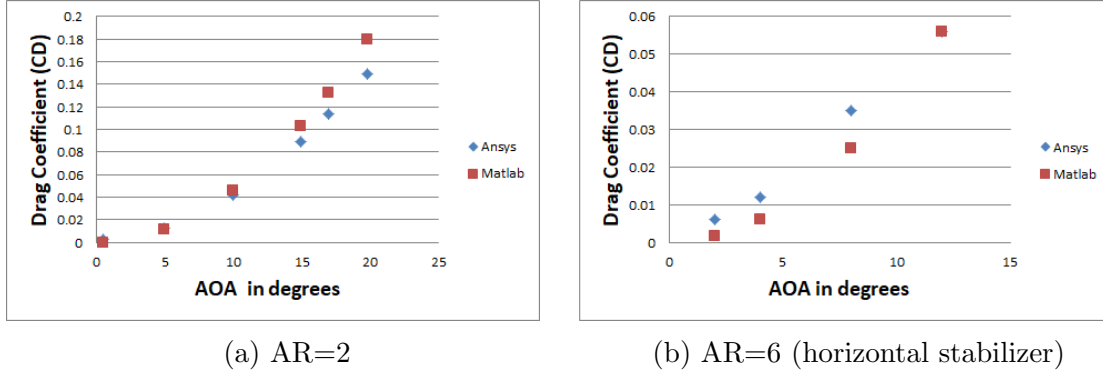


Figure 30: Induced drag coefficient obtained from MATLAB and ANSYS

It was expected that the induced drag coefficient measured by MATLAB for both low and high aspect ratios would be less than in ANSYS because the lift coefficients obtained from MATLAB were less (induced drag coefficient is proportional to C_L^2). However, above 15 degrees for the wing with AR=2, the MATLAB drag coefficient is higher than the ANSYS because the MATLAB tool (lifting-line theory) is not accurate for low aspect ratios [50, p. 324-374]. Comparison of drag coefficients obtained from MATLAB and ANSYS could be found in Appendix F.

Considering the fact that the aspect ratio of the Arctic Fox wing is ten, the MATLAB tool is an appropriate tool for preliminary wing design.

5.5.3 Nacelle and Wing

The nacelles of the Arctic Fox each house a PW127N engine and a main landing gear. Since a wet wing design was selected, the engines were positioned in front of the wing front spar as to respect the FAR 25.903 [28] requirement for the engine rotor burst zone.

The nacelle length was selected to accommodate the main landing gear attachment points positioning, the engine dimensions obtained from [25], and to create an aerodynamic profile from the landing gear attachments to the exhaust pipe exit. The maximum width of each

nacelle is located where the landing gear linkage and the wheels are stored, while the width decreases at the front and back of the nacelle to create an aerodynamic profile matching the width of the engine mount and the exhaust pipe respectively. The maximum height of the nacelle is located at the fuselage station line position of the retracted wheels, while the height at the front and back of the nacelle is reduced to aerodynamically join with the position of the air inlet duct and the exhaust pipe respectively. The nacelle used for aerodynamic validation is illustrated in Figure 31.

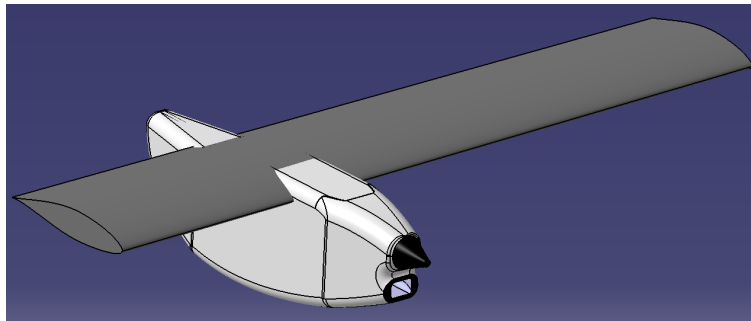


Figure 31: CFD nacelle

From computational fluid dynamics (CFD) simulations, the lift coefficient of the wing with the nacelle in cruise conditions was obtained for different wing incidences in order to determine the required wing incidence for level flight in cruise. The full procedure and the results of the simulations are detailed in Appendix V. The result is a wing at 1° incidence, compared to 2.5° during the conceptual design phase. The reduction is due to the conservatism of the MATLAB tool compared to the CFD simulations and to the increase in cruising velocity which caused the required cruise lift coefficient to decrease. The simulations also illustrated a stagnation point of approximately 1 ft in diameter below the exhaust, which can be seen in blue in Figure 32.

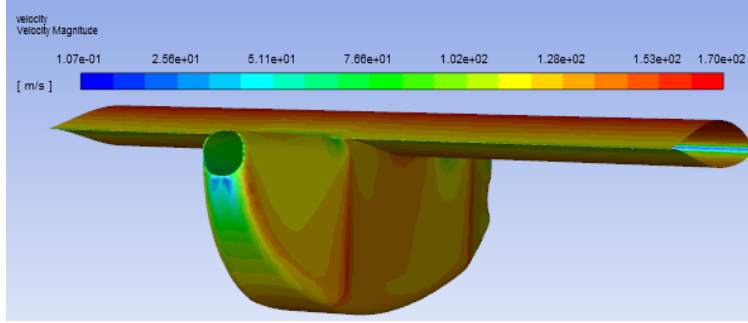


Figure 32: Exhaust stagnation point

The size of the stagnation point results in an increase in the drag created by the nacelle, which was reduced by moving the exhaust pipe exit down by 6 inches from its original position. The final nacelle shape is shown in Figure 33 with the locations of major components.

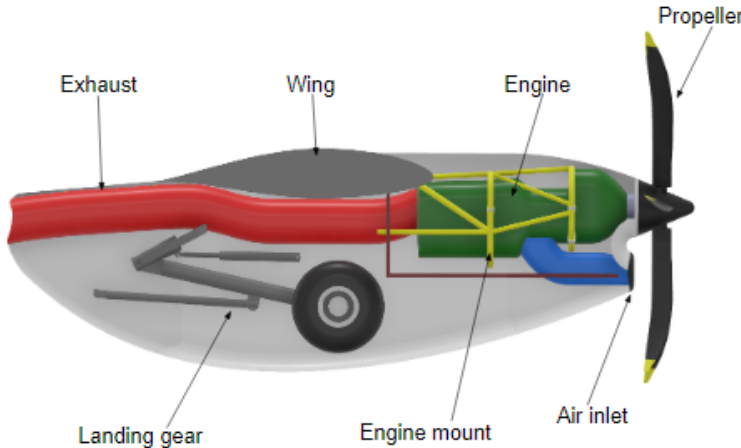


Figure 33: Final nacelle side view

5.6 Systems

5.6.1 Anti-Icing System

The anti-icing system of the Arctic Fox uses bleed air extracted from the engines to heat up the leading edge and prevent ice from forming on it. This method of anti-icing uses more power than the inflatable rubber boots de-icing method [51, pp. 239-258]. Anti-icing is more reliable since the rubber boots method may push the ice without breaking it if the surrounding ice is too thin [52].

The power required can be calculated with a convection and conduction heat transfer model. There are two main contributors of heat loss: steady-state heating, and power

required for heating the supercooled droplets of water hitting the leading edge. For steady state heating, the equation governing the phenomenon is $Q = hA\Delta T$, where the heat flow (Q), the heated area (A) and the temperature difference (ΔT) are known. The convective heat transfer coefficient (h) can be estimated with the Churchill-Bernstein equation which outputs the Nusselt number (Nu) with an input of the Reynolds and Prandtl numbers for cylinders with their axis perpendicular to the freestream [53]. The convective heat transfer coefficient can then be found using the definition of the nusselt number $Nu = hL/k$ [54].

Although there will be some error due to the assumption that the leading edge of the airfoil is a cylinder and that the thickness of the airfoil is the characteristic length. The power required for heating the supercooled droplets can be found by $Q = mc\Delta T$, where the mass flow rate is the estimated total water catch rate on the leading edge [55]. Using this model, the estimated power required to keep ice from forming on the leading edge at cruising speed is 708 kW, and 41.3 Kg/min of bleed air of the available 60 Kg/min will be required [25].

To validate this model, it was applied to the NACA 0018 airfoil climatic wind tunnel specimen which was used at the wind tunnel for aerodynamics testing. A silicon rubber resistive heated pad was installed on its leading edge. As explained in the wind tunnel testing procedures, the current delivered to the resistive heating element was varied and an ammeter and voltmeter were used to measure the power delivered to the system. The results of the experiment showed that 455.6 W were required to keep the airfoil at the threshold of ice accretion for the specimen airfoil, while 447.1 W were calculated after inputting the specific test parameters in the heat transfer model. This represents a difference of 1.87% which may be attributed to the use of the Churchill-Bernstein equation. Conservatively, a 3.5% increase on the calculated power required for the Arctic Fox yields 733 kW. This means that of the 60 Kg/min of available bleed air, only 43 Kg/min would be required. Detailed calculations and power requirements for the anti-icing system are provided in Appendix W.

5.6.2 Environmental Control System

The Arctic Fox is dedicated to the safe transportation of perishable food. The coefficient of performance (COP) of the air cycle machine and the vapour compression machine have been determined. As such, it requires a reliable refrigeration system which uses a vapour compression machine. This method of refrigeration provides a high thermodynamic efficiency compared to the air cycle machine [56]. The required cooling and heating loads can be calculated using a convection and conduction resistive model [57]. The operating conditions of the Arctic Fox were determined during summer and winter based on the locations of the mission analysis, which are detailed in Appendix X. The regulations and requirements concerning vapour compression machines for aircraft use can also be found in Appendix X. The convective heat transfer coefficient is calculated with the assumption that the aircraft fuselage is a flat plate and the air flow speed is at Mach 0.3 [58]. The calculated critical heat loads have been multiplied by a factor of 1.3 to take into account any overlooked heat transfer sources.

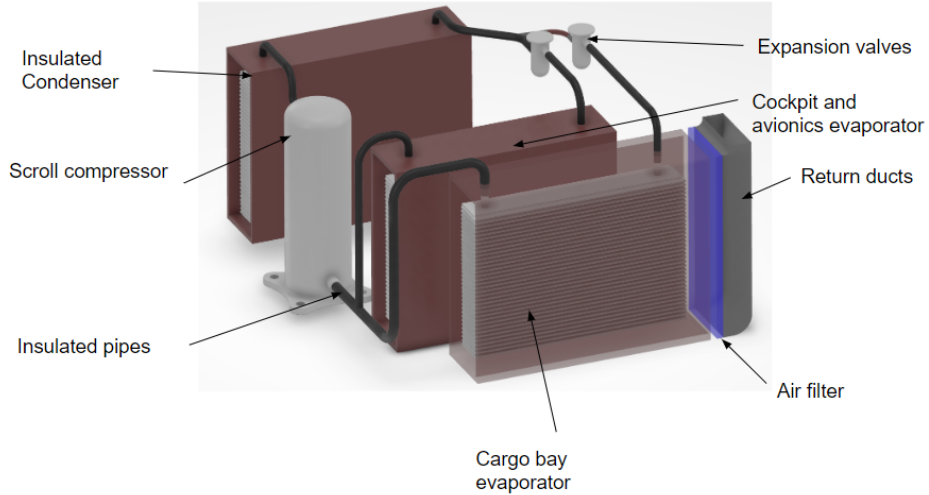


Figure 34: Main components of the environmental control system

The refrigeration system, using refrigerant R134a, has a COP of 3.33 and requires 2.94 kW to maintain the aircraft at a steady temperature. The critical cooling load of the aircraft may go up to 15 kW during hot days on the ground. For the comfort and health of the pilot,

the vapour compression machine is equipped with two evaporators as shown in Figure 34. One evaporator is dedicated to cool the cargo bay and the other to cool the avionics and the cockpit. The reason for this design is to provide the cockpit with air free of any contaminants that may originate from the cargo bay.

The Arctic Fox operates at subzero temperatures averaging at -22.5°C which results in it needing heating rather than cooling. A bleed air heat exchanger is an option but that would penalize the engine's efficiency. Consequently, the Arctic Fox is heated with the use of resistive electric elements of 3 kW, further reasoning is available in Appendix X. Moreover, the thermal cooling of the avionics is taking advantage of the cold operating conditions[59]. Assuming that the avionics bay is air sealed from the rest of the fuselage and that the rate of heat generated is greater than the rate of heat transfer with the surrounding environment, it is circulated through a closed loop where it is cooled at a skin heat exchanger under the cargo bay floor. If there is any temperature rise, a percentage of this recirculated air is exhausted from the plane and replaced by cool conditioned air. Under the unlikely event that there is smoke in the avionics bay, all air valves related to the avionics thermal management are closed except for the exhaust valve. The remaining air in the avionics bay is exhausted from the plane. A detailed scheme of the thermal management of the avionics is provided in Appendix X.

The refrigeration system was modelled in Siemens Amesim to validate the systems and size the required equipment such as the compressor and heat exchangers. This model is provided in Appendix X. The model is using steady state loads and results are still to come.

5.6.3 Electrical System

The Arctic Fox electrical system is powered by two 30kVA variable frequency 230VAC generators, with two 24V 44Ah NiCd batteries for emergency DC power, engine starting, and transient load damping, and a 9kVA ram air turbine generator (RAT) for emergency AC power. Electrical loads are powered through a split-bus system, as shown in Figure 35.

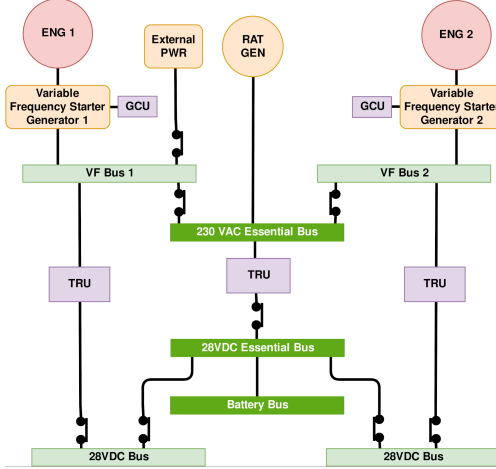


Figure 35: Electrical system architecture

Requirements and functions were derived from the CARs, and are provided in Appendix H. A functional hazard assessment was performed, and the failure to provide power to essential loads was defined as being “catastrophic” due to the avionics and flight control surface actuators being essential to safe flight. Fault tree analyses (FTA) were done for the failure to provide DC and AC essential loads, which gave failure rates of $5.05\text{e-}10$ per flight hour and $5.23\text{e-}10$ per flight hour, respectively, and are provided in Figures H.0.3 and H.0.4 in Appendix H. Component failure rates were provided by [60, 61], and as the function failure rates are less than $1\text{e-}9$ per flight hour, the system has sufficient reliability as required by FAA AC 23.1309-1E [62].

The cargo bay, cockpit, and exterior lighting, as well as the windshield heating power use were estimated from [20, Part IV, Ch. 7]. The avionics power use was estimated from [20, Part IV, Ch. 7], with additional autonomous systems power being estimated from [63]. Detailed calculations for the electrical load analysis are provided in Appendix H.

The entire electrical system was modelled in Siemens Amesim to validate the system architecture and size electrical components. This model is provided in Appendix H. An architectural modelling framework was used to model the system using steady-state loads, and the system was simulated using root mean squared (RMS) values. The batteries were sized to provide power to the essential DC loads for 30 minutes during cruise to meet CAR

551.201 [64], the RAT for providing power to the essential AC loads during the worst-case flight phase, and the generators for providing power to the entire electrical system in a single-engine failure case. Figure 36a shows that two 44Ah batteries are sufficient, Figure 36b shows that the RAT generator must have a rating of 9kVA, and Figure 36c shows that each generator must be able to provide 30kVA.

The major changes from the conceptual design phase were the removal of the APU, as the FTAs showed that the electrical system met the required reliability without it, making it unnecessary. DC engine starters were used so that the engines could be started using the batteries, and the static inverters were removed due to their inefficiency at high amperages.

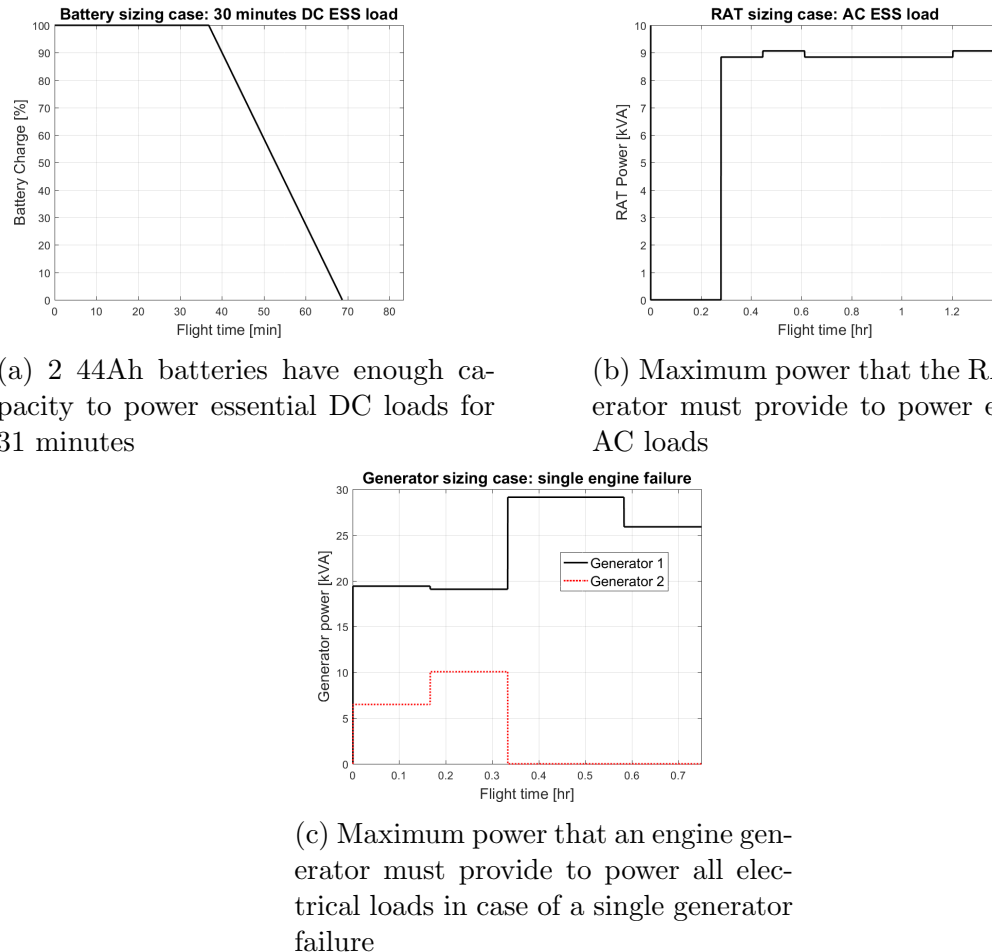


Figure 36: Electrical system sizing results from the Amesim model

5.6.4 Hydraulic System

The Arctic Fox has two independent hydraulic systems in order to maintain redundancy in case one system fails: system A and B. System A supplies hydraulic force to the Normal Brakes and the Nose Wheel steering systems; while system B actuates the Parking/Emergency Brakes and the Landing Gear systems. System A and B are powered by two separate Engine-Driven Pumps (EDPs), which allow the system to take its source of energy mechanically directly from both engines. System A is also equipped with an emergency mechanically-driven pump that will be powered by a 9kVA ram air turbine (RAT) in case of total engine failure; however, if only one engine fails, the system relies on a bi-directional Power Transfer Unit (PTU) that will transfer hydraulic power from one system to the other. Each system has a 5L reservoir that uses Skydrol as the hydraulic fluid that normally operates at 3000 psi. Since the hydraulic system will only be used during takeoff and landing, an electric clutch (EC) is mounted between the driven shafts that connect the engine with the EDP in order to engage or disengage the system. Thus, there is one clutch for each engine. Each system component was added in function to the mission requirements regarding the Hydraulic, Landing Gear and Braking systems regulations from the CARs, which can be found in Appendix Y. Figure 37 illustrates a complete schematic of the Hydraulic System and its normal operation.

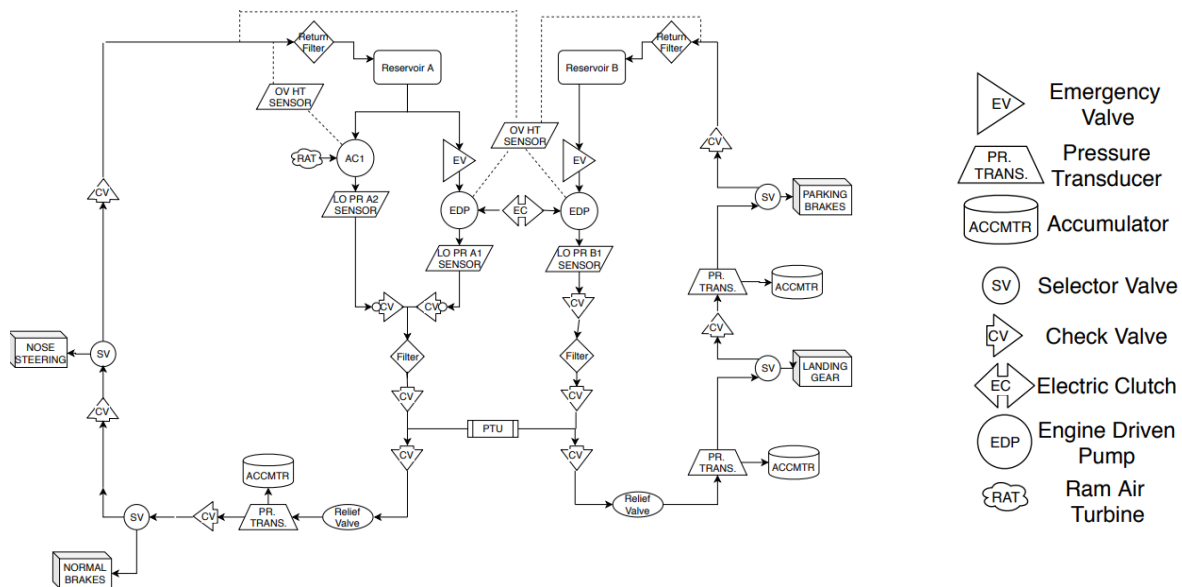


Figure 37: Hydraulic system configuration

A Functional Hazard Analysis (FHA) was completed, showing that in the event of any pressure loss, both systems are able to maintain normal operation. However, if there was a leak in either system, the affected system would end up losing its two actuators. If system A suffers a total failure caused by a leak, the Arctic Fox is able to totally brake within no more than two times the normal braking distance by using its thrust reversers, flaps and emergency brakes from System B. On the other hand, if System B suffers a total failure, the Arctic Fox is capable of lowering the landing gears by electrically removing the uplocks that keep the gear contracted to allow it to free-fall under gravity and aerodynamic forces. This analysis and more data related to the hydraulic system can be found in Appendix Y.

5.6.5 Fuel System

The Arctic Fox fuel system consists of 2 wet wing fuel tanks each 67.5 ft^3 capable of holding 6600lb of fuel. A wet wing design saves cargo room but requires more safety margins to protect the fuel tanks from debris hitting the wing, typical from gravel runway landings. To meet the safety margins the fuel tanks were placed 2 ft from the engine to meet with rotor burst certifications. The fuel tanks each contain a feed box, fuel boost pump, fuel transfer pump, fuel level sensors. Both fuel pumps have a dual pump system for redundancy and

are assisted by gravity due to the high wing placement. 10 fuel levels sensors are included in each tank to monitor the fuel level accurately during any of the four fundamental basic flight maneuvers. Combined, the fuel pumps consume approximately 4400 watts of power at max RPM and the 20 sensors consume 2.4 watts of power. This design was based on safety requirements [65]. Date sheets of these components can be found in Appendix Z

From a MATLAB simulation 3 cases were analysed. The simulation recorded the fuel level within the fuel feed tank and how much of an imbalance was created, between these 2 feed tanks, from several pump failures. With single engine boots pump failure fuel levels were balanced due to the fuel transfer pump keeping the tank level. With all pump failing the fuel levels were also balanced in both fuel feed tanks due to only the gravity feed being active. The worst case was dual pump failure within the same fuel tank because that engine would lose both its feed and transfer pump leading to the feed tank emptying itself with the gravity feed. While the worst case from an imbalance perspective is dual pump failure within the same feed tank any pump failing completely would lead to a forced landing to rectify the issue. The engines would still be partially operable under any combination of pump failure due to the gravity feed from the high wing configuration.

5.6.6 Avionics

The avionics system on the Arctic Fox is designed to satisfy the requirements of the autonomous strategy plan and to meet the equipment required for power-driven aircraft operating under instrument flight rules as specified in CAR 605.18. The Arctic Fox's instrument panel is shown in Figure 38, a complete list of the name and the functionality of all the instruments installed in the panel is provided in Table AA.0.1 in Appendix AA.

The glass cockpit design provides the necessary information and control for dual-pilot operation with an efficient interface utilizing several multi-function displays (MFDs). A backup system of gauges is also included to provide redundancy in the event of a loss of electrical power. Using more digital equipment will allow the real-time information received on-board to be transmitted to the ground control station.



Figure 38: Control panel

To support the system onboard and to meet the requirement for certification, antennas are installed in the Arctic Fox. Table AA.0.2 in Appendix AA provided a complete list of the name and the usage of all the antenna installed in the Arctic Fox, and the install location are shown in Figure 39.

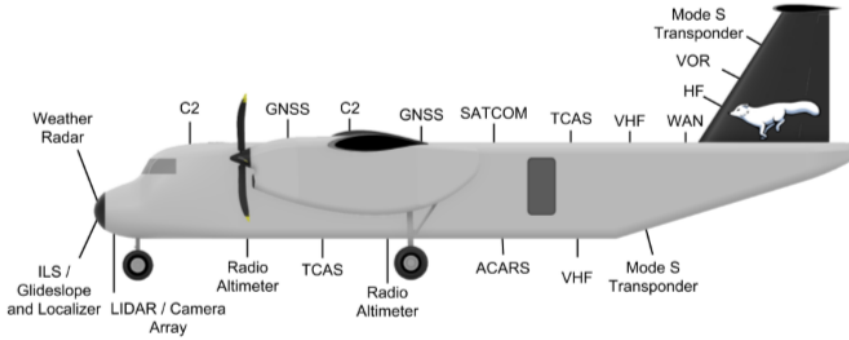


Figure 39: Installed antennas

Light detection and ranging (LiDAR) equipment and a camera array are installed on the Arctic Fox to support the end goal of the aircraft to be fully autonomous. LiDAR is a remote sensing technology which is able to detect winds, turbulence [66] and model the terrain by using laser [67]. LiDAR will be able to provide more accurate information with regard to the surroundings of the aircraft to assist with some operations such as landing, taking-off, and taxiing.

5.6.7 Autonomous Route Revision System for Icing Avoidance

The Arctic Fox is flying at 10,000ft during cruise, where there are low altitude clouds, containing relatively large water droplets [68]. In addition, snowstorms are common in Northern Canada, where the Arctic Fox will be operating. Therefore, the route revision system puts emphasis on icing avoidance. Figure 40 shows the design strategy of the route revision system.

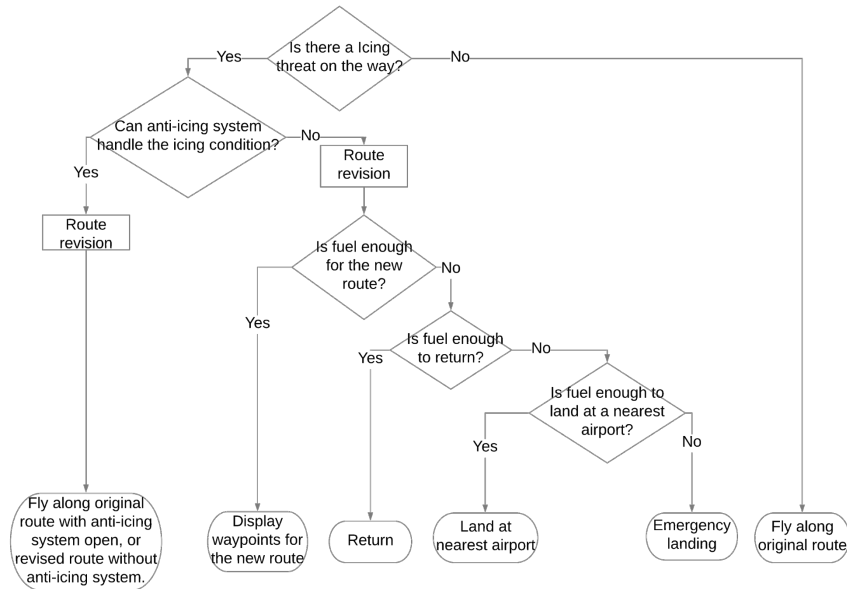


Figure 40: Icing avoidance system decision making flowchart

The system is simulated by creating a plugin in X-Plane. Figures AB.0.1, AB.0.2, and AB.0.3 in Appendix AB demonstrate scenes while the plugin is running under different situations. The scenario is set as the Arctic Fox is travelling along a straight line which is considered a fixed original flight route with a moving triangular icing area. Considering both service ceiling and cruise altitude are at 10,000 ft with pilots on board, the aircraft cannot ascend to avoid the icing area. Thus, the system will provide horizontal route revision instructions.

The system starts by predicting positions of the icing area and the aircraft depending on their movements. Then, by converting geographic coordinate system to cartesian coordinate

system and setting the departure airport as the origin, it obtains the time when the aircraft touches the icing area. The new waypoints will be the left or rightmost vertices of the icing area by that time. The system will choose one route with a minimum total distance among two choices and the authority to confirm the revised route is given to the pilot or the remote manager. Figure 41 visualizes the process of route revision.

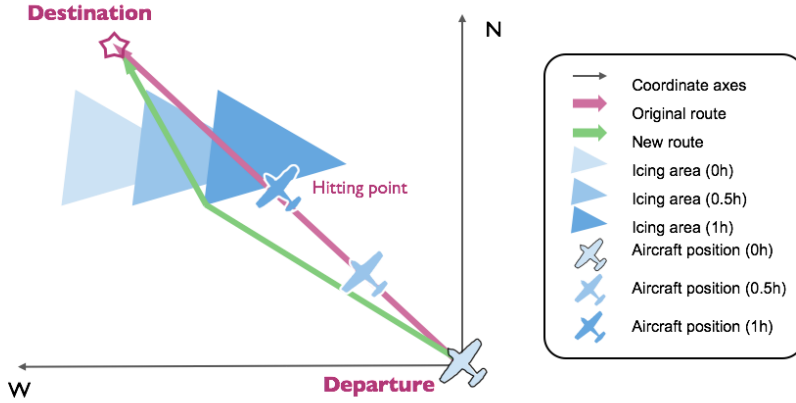


Figure 41: Route revision process for one way point

The current version of the system is able to operate either pre-flight route planning or in-flight route revision for icing avoidance. For example, when a second icing area appears abruptly, the system is able to continuously provide a solution. To become a more complete route planning system, it could be extended to avoid other harmful conditions such as turbulence, providing better protection for the Arctic Fox.

5.7 Stability - Cruise Condition

The handling qualities associated with the dynamic stability behaviour of the Arctic Fox were assessed to complement the stability study from the conceptual design phase. The longitudinal dynamic stability of the aircraft was estimated from [69, Chap. 4] and [70, Chap. 4]. This proposed approximate method relates the physical layout of the plane to its handling qualities. In other words, the Arctic Fox's physical layout is translated into a state-space motion matrix which is then solved using the approximate method and a MATLAB toolset. The latter method allows the obtention of the undamped natural frequency and the

damping ratio of the Arctic Fox. In turn, the handling qualities of the short and long period may be assessed. The results are as shown in Table 10.

	Most forward CG	Most aft CG
Undamped natural frequency, [rad/s]	5.79	4.15
Damping ratio	0.78	1.03

Table 10: Undamped natural frequency and damping ratio of the Arctic Fox

The two CG cases represents the top of climb and top of descent scenario of the flight. The detailed calculations are provided in Appendix AC.

The Arctic Fox displays stable behaviour over time. However, after consulting the O'hara Thumbprint plot and the U.S. Military Specification for flying qualities [22, Chap. 10], the undamped natural frequency of the forward CG case does not result in acceptable handling qualities, as shown in Appendix AC. The recommendation to the current design is to push, further aft, the wing and its related systems by 1.6 feet. As well as the electrical system by 4.3 feet. The design change will limit the most forward CG during the cruise segment from previously 1 MAC to 26 MAC (both positions are aft of the AC of the wing). The design change will prevent the horizontal stabilizer to counteract the moment generated from a large CG displacement. The resulting calculation is shown in Table 11.

	Undamped natural frequency, [rad/s]	Damping ratio short period	Damping ratio long period
New most forward CG	4.8743	0.8018	0.0303

Table 11: Recommendation for Arctic Fox

In turn, this will satisfy the handling qualities on the O'hara plot, shown in Figure 42.

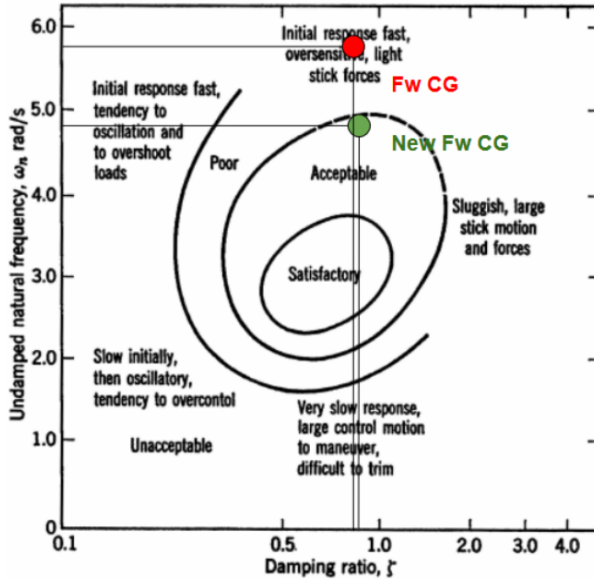


Figure 42: O’hara Plot

The recommended design will result in acceptable short period handling qualities. Furthermore, the conceptual design of the Arctic Fox will be classified as level 1 and level 2 for short and long period respectively on the Cooper-Harper scale for the category B flight phase (Cruise) [22, Chap. 10]. In other words, the recommended aircraft configuration will result in adequate flying qualities for the cruise segment and the desired performance is achievable with no more than minimal pilot compensation.

5.8 Performance Flight Testing

5.8.1 Simulation Model

The X-Plane flight simulator software was used to validate the performance of the Arctic Fox design. The model of the aircraft was built using the PlaneMaker tool included with X-Plane. A 3D model was created of the aircraft fuselage, engine nacelles, landing gear, wings, stabilizers, and control surfaces. X-Plane divides the aircraft geometry into smaller elements and employs blade element theory to calculate the forces applied to each element of the aircraft. Aerodynamic effects such as compressibility, downwash, and propwash are also simulated by X-Plane. Engine specifications for the PW-127, electrical loads, and data on the NACA 65-418 airfoil used on the Arctic Fox’s wings were also added to the model.

X-Plane allows access to the data calculated by the flight model. This data was recorded and used for the analysis of the flight tests. The simulator is also extensible through an application programming interface (API) which can be used to override or add additional functionality to the simulator. Plugins for X-Plane can be created natively with C++ or with third-party plugins such as FlyWithLua which provides a runtime and bindings to the X-Plane API for the Lua programming language. A plugin was created to simulate the ability to operate the aircraft autonomously by issuing commands to interact with the aircraft systems and use a PID (proportional, integral, derivative) controller to actuate the control surfaces. A sample screenshot and code excerpts from this flight testing plugin are available in Appendix AD. Other plugins were developed to display real-time graphs of the flight model variables of interest, to execute emergency engine fire procedures, and to analyze and potentially reroute the flight path in the event of adverse weather.

5.8.2 Takeoff Performance

Take-off is the most complex of all phases of flight to study for aircraft performance. The performance at take-off is needed to determine a flight envelope, which is a range of parameters where the aircraft can operate safely. Therefore, take-off was performed for the most critical conditions being a high ambient temperature and high altitude.

Take-off testing was all done at Telluride Regional Airport. This is called a high and hot test; the higher the altitude and temperature, the less dense air becomes and since engines are using air for combustion, the engines will deliver less shaft horsepower. Therefore, this is the worst case as it will result in the highest required distance or speed at take-off. The temperature set up in X-Plane for the testing was increased from the standard one at sea level. Telluride's altitude is 9078 ft which is higher than all the airports that the aircraft aims to deserve in Northern Canada. The flaps were set to 20 degrees before take-off to have a good trade-off between lift and possible drag.

The objective of the flight testing was to determine V_1 , V_2 , and V_R . V_1 corresponds to the maximum speed at which the pilot can make the decision to interrupt or continue his

take-off. V_2 is the minimum speed reached at a height of 35 ft above the runway surface. V_R is the speed at which the pilot pulls on the yoke to rotate the aircraft. All values were obtained after 10 trials on X-Plane to make sure of their consistency. The speed obtained for V_2 was 95 knots during a take-off AEO. V_R was theoretically calculated to be 82 knots and used as an initial assumption, but after testing, the actual V_R was 84 knots. Finally, the optimum V_1 speed was obtained with the BFL. V_1 is usually located within a range of 80-100% of V_R [71]. Therefore, ASD with AEO was determined at 4 different V_1 : 80%, 87%, 93% and 100% of V_R , same for the take-off distance (TOD) with OEI. As seen in Figure 43, once the 8 distances were obtained from X-Plane, 2 linear curves could be drawn for each of the 2 critical situations within the same graph. The intersection of the curve representing the ASD with the one defining the TOD represents the optimum speed V_1 which was 78 knots (92.8% of V_R) [71].

The BFL corresponding to that optimum speed V_1 was around 2450 ft which is shorter than the distance available on the runways at the airports in the North. Therefore, these values confirm that the design of the aircraft will be able to perform safely ASD with AEO or take-off with OEI at the airports in the North. The values calculated theoretically were 89.4% of V_R for the optimum speed V_1 and 2490 ft for the BFL which are quite similar. The numbers obtained with the testing on X-Plane were smaller since the drag and lift coefficients used to calculate the BFL theoretically were conservative.

5.8.3 Landing Performance

Landing flight tests allow the designer to confirm if the aircraft is able to land safely on short runways in different weather and runway conditions. The critical condition for a

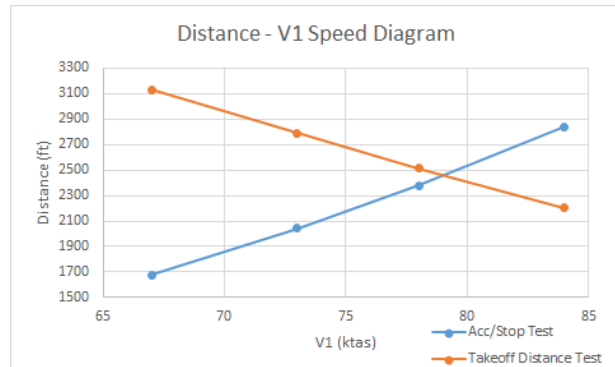


Figure 43: Optimum Speed V_1

landing test is to land the aircraft on a contaminated runway such as icy runway however the simulator does not support icy runway. The flight tests were conducted on dry and wet runways, with a maximum landing weight of 38,000 lbs. A flight test needs to meet a detailed list of criteria found in [72] to show compliance with the regulations. V_{REF} - the reference landing speed- should not be less than 1.3 of the stall speed [72]. The calculated value of V_{REF} is 88.4 KCAS. V_{REF} in this flight test is 90 KCAS, which is higher than the minimum allowable value of the reference speed. Therefore the reference speed obtained can be used to determine the landing distance.

The initial velocity, the final velocity and the time interval retrieved from X-plane were used to find the landing distance. The landing distance of the flight test on a dry asphalt runway is 1581 ft – the calculated value is 1840ft, the difference between the experimental and the calculated value is 14%. This difference is due to the drag polars in landing configuration that were roughly approximated during the conceptual design phase and the lift coefficients used in the calculations were conservative. The aircraft is able to land on 56 runways in the North with a maximum payload.

5.8.4 Stall Characteristics

The test procedure to determine the stall characteristics of the Arctic Fox was based on Advisory Circular (AC) 25-7D which provides guidance material on sufficient means to satisfy the regulatory requirements. It is necessary to conduct stall tests to determine the stall speed of the aircraft in various aircraft configurations and ensure there is adequate warning when a stall is imminent [72, 8.1].

Regulations require the stall to be demonstrated in straight flight and with a 30-degree bank angle [40, 525.201]. Before the stall test, the aircraft is trimmed for straight level flight at a speed between 1.13 and 1.3 times the anticipated reference stall speed VSR [40, 525.201]. The stall test is performed with the engine power off and again with the power set to 1.5 VSR for each configuration of the flaps, landing gear, CG, and weight. [40, 525.201]. Using the pitch control, the aircraft is decelerated at 1 kt/s until the aircraft stalls. When

testing the stall during a banking turn the test is also performed at a stall entry rate of 3 kt/s. The aircraft must be controllable up until the stall. The recovery after the stall should be prompt using normal operation of the controls [40, 525.203]. The amount of roll allowed during the recovery of straight flight stall is 20 degrees [40, 525.203]. For turning stalls, the amount of roll allowed is 60 degrees in the direction of the turn and 30 degrees in the opposite direction when the stall entry rate is 1 kt/s [40, 525.203]. At higher deceleration rates, the allowed amount of roll is 90 degrees in the direction of the turn and 60 degrees in the opposite direction [40, 525.203]. The complete test procedure and sample results are available in Appendix AF.

The Arctic Fox's stall characteristics were evaluated using the X-Plane simulator. Hazards that would exist in real-world testing include loss of control, overstress, collision, and controlled flight into terrain. To mitigate these hazards the test should be performed in airspace reserved for flight testing, at a minimum altitude of 7000 ft, with traffic collision and ground proximity warning systems equipped, and clear identification of the duties for the pilot flying and pilot monitoring.

The flight tests conducted determined that the stall characteristics were satisfactory for most configurations; however, the straight flight tests performed with the flaps fully deployed displayed an unacceptable amount of roll during the recovery. The reason for the excessive roll is likely due to aileron reversal at low speed. A potential solution to improve the roll authority during stall in a full flap configuration involves twisting the wing so the angle of attack (AOA) is higher at the root of the wing than at the tip. Other solutions involve re-energizing the boundary layer near the ailerons using slots or vortex generators which will delay the separation of air over the wing.

5.9 Autonomy

5.9.1 Autonomous Trade Studies and Program Roll-Out

In order to incorporate autonomy into the aircraft, an appropriate aircraft management format needed to be chosen. This was done by comparing different progression schemes. A

key component of this decision was the initial configuration as it directly related to the ability of the aircraft to be entered into service. The main challenge encountered in conducting this trade study was the comparison of time-variant schemes that involved subjective judgement. Eight progression models were considered, as shown in Figure 44:

	Timeline			
	Initial Rollout	Stage 2	Stage 3	Stage 4
1	Dual Pilot	Single Pilot	Remotely Managed	Autonomous
2	Dual Pilot	Remotely Managed	Autonomous	
3	Single Pilot	Remotely Managed	Autonomous	
4	Dual Pilot	Single Pilot	Remotely Managed	
5	Single Pilot	Autonomous		
6	Dual Pilot	Autonomous		
7	Dual Pilot	Remotely Managed		
8	Single Pilot	Remotely Managed		

Figure 44: Progression schemes

Six metrics were used to compare the above schemes. Namely, safety, crew resource management efficiency, feasibility, operability, cost, and potential for development. The requirements for the progression schemes, listed in Figure 45 were based upon these metrics. The result of this trade study showed the dual pilot-remotely managed progression scheme as the top option. The trade study can be found in Appendix D. Within this scheme, the operational model consists of two stages. Stage 1 corresponds to a dual pilot operation (DPO), under which the two pilots operate the aircraft with a more robust autopilot system as compared to current autopilots. This consists of introducing auto taxi and auto takeoff capabilities in addition to the already existing autoland capabilities.

Scheme shall conform to standards of safety
Scheme shall not interfere with current airport operational models
Scheme shall not cause undue stress, pressure or fatigue to operators
Scheme shall allow a gradual learning curve for operators and regulators
Scheme shall not attempt to incorporate immature technologies
Scheme shall have a well-defined man-machine interface
Scheme shall be able to operate with existing physical infrastructure
Scheme shall be able to operate with existing regulations
Scheme shall minimize operational costs
Scheme shall minimize development costs
Scheme shall minimize certification costs
Scheme shall permit collection of data relevant to transitioning from pilot on-board to off-board
Scheme shall minimize time interval between pilot on-board to off-board operation
Scheme shall provide an ambitious and attainable plan in response to the RFP

Figure 45: Requirements for trade study

Stage 2 corresponds to a remotely managed operation (RMO) under which the aircraft is flown by the autonomous system using pre-programmed decision-making algorithms. Two remote management options, namely one remote manager at the hub or one remote manager, one remote monitor at the point may be implemented to test and compare which option works better operationally.

The implementation of the chosen progression scheme into the area of operation is planned to be in phases. The initial roll-out shall occur at Rankin Inlet airport as a stage 1 operation where the pilots validate the capability of the autopilot system. Two aircraft flying two to three missions weekly would serve six communities close to Rankin Inlet. Figure 46 represents the six missions being flown out of Rankin Inlet.

Following this, under phase 2, two missions out of Rankin Inlet (to Arviat and Baker Lake) shall be operated as an RMO. The missions were chosen due to the frequency of their operation, allowing the collection of flight data for a higher number of flight cycles. The validation of the autonomous system includes (but is not limited to) assessing the

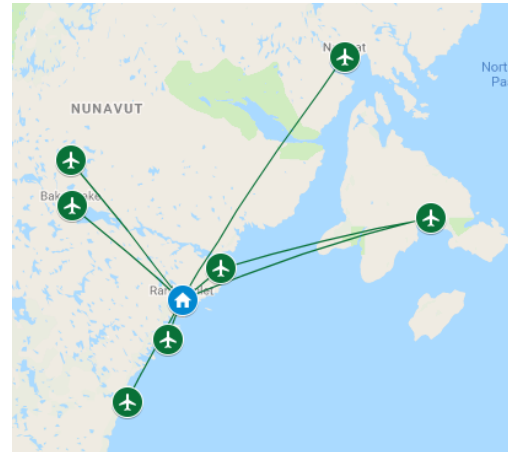


Figure 46: Missions from Rankin Inlet airport

system's capability in maintaining separation minima, analyzing the level of remote manager situational awareness and testing the reliability of lost link procedures.

Subsequently, the rollout for other markets is planned to be accomplished in a similar manner, where a stage 2 operation is implemented for Iqaluit (in phase 3), then Kuujjuaq and Cambridge Bay (in phase 4) and lastly, Yellowknife (in phase 5).

5.9.2 Human Factors

Given the autonomous nature of the aircraft, it was important to consider human factors and the effect that autonomous systems aboard an aircraft can have on the human-machine interface. An experiment was conducted to measure pilot performance and perceived workload of a pilot flying three approaches while experiencing emergency scenarios. An overview of the experiment can be seen in Figure 47.

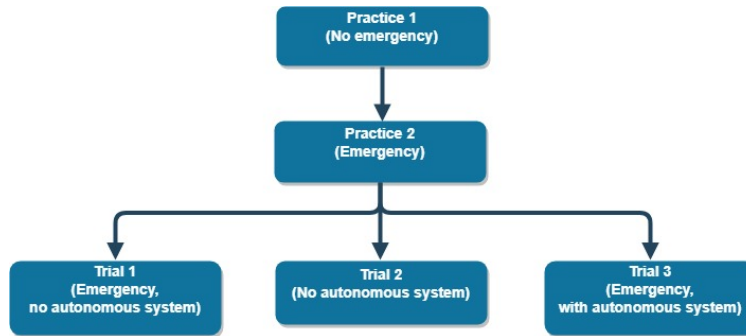


Figure 47: Experiment overview

The experiment protocol can be seen in Appendix AG. The pilot performance was measured through approach path deviation, heading deviation and airspeed deviation. The perceived workload was measured with the NASA Task Load Index which is based on temporal demand, mental demand, physical demand, performance, frustration, and effort, and can be seen in Appendix AG. For all pilot performance parameters, the collected data was plotted against its ideal slope and the deviation of the data slope from the ideal slope was compared. This was done for all three trials. Since the participants were asked to maintain 130 knots throughout the approach, the ideal slope was zero for the airspeed plot. An ex-

ample of the airspeed data collected for participant ID#49004 for trial 1 plotted against the ideal airspeed slope is seen in Figure 48.

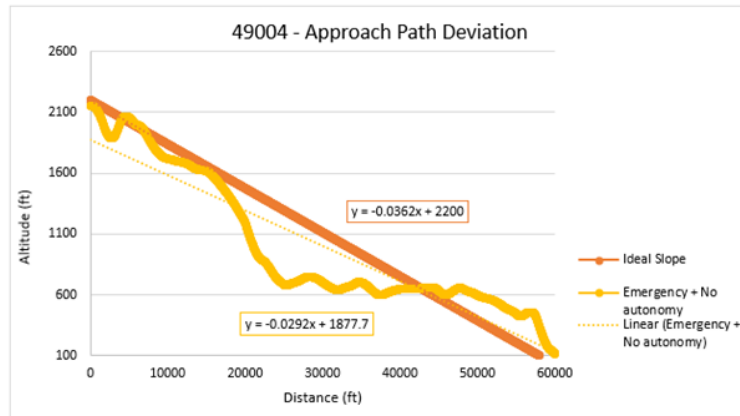


Figure 48: Approach path deviation from ideal slope for participant 49004 for trial 1

The heading ideal slope was also zero since heading is a measure of the degree that the nose of the aircraft is pointing. An example of the heading data collected for participant ID#49004 for trial 1 plotted against the ideal heading slope is seen in Figure 49.

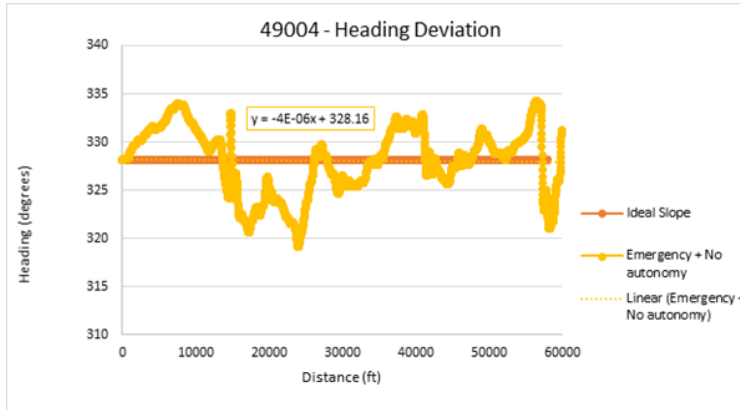


Figure 49: Heading deviation from ideal slope for participant 49004 for trial 1

The approach path ideal slope was determined through the 3-degree glide slope. An example of the approach path data collected for participant ID#49004 for trial 1 plotted against the ideal approach path slope is seen in Figure 50.

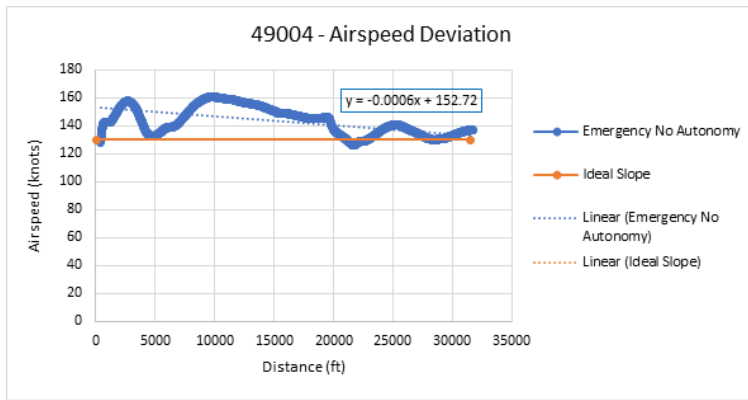


Figure 50: Airspeed deviation from ideal slope for participant 49004 for trial 1

The observation was that pilot performance improved in emergency situations when the autonomous system was implemented. As shown in Table 12, slope deviation was the least in trial 3 (emergency with autonomous system) for heading and approach path deviation and was smaller than the deviation in trial 1 (emergency with no autonomous system) for airspeed deviation.

	Average Heading Slope Deviation	Average Airspeed Slope Deviation	Average Approach Path Slope Deviation
Trial 1	9.47E-05	2.10E-03	3.34E-02
Trial 2	6.21E-05	4.00E-04	3.12E-02
Trial 3	4.17E-05	1.60E-03	2.79E-02

Table 12: Heading, airspeed and approach path slope deviation

As for perceived workload, on average, it was the least in trial 2 (no emergency) and the greatest in trial 1 (emergency with no autonomous system) as seen in Figure 51. Graphical analyses of all performance parameters and perceived workload for each participant trial can be seen in Appendix AG. The conclusion was that pilot performance improved in all three parameters and perceived workload decreased when the autonomous system was implemented.

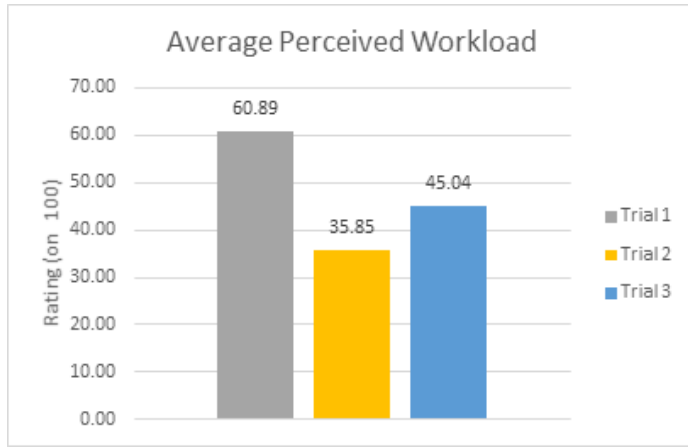


Figure 51: Average perceived workload

5.9.3 Autonomous Emergency Checklist

The results of the human factors experiments show that an autonomous emergency checklist increased pilot performance and decreased pilot workload during an emergency. The trial with an emergency and autonomy required the pilot to perform the vital checklist items, indicated by a box surrounding those items, to maintain safe flight. The vital items include idling the affected engine, feathering the propeller of the affected engine, and lowering the mixture/condition lever to stop. An experimenter would conduct the remainder of the checklist whilst saying each item aloud, and finally proclaiming the checklist for the given emergency was completed, once all items were actioned. An excerpt from the checklist is presented in Figure 52, and the full checklist can be found in Appendix AH.

ENGINE FIRE IN FLIGHT	
Power.....	as required
Prop (affected engine)	feathered
Feathered engine	complete Engine Securing Procedure
Condition lever	stop
Fuel selector	closed
Ignition	off
Fuel pump	off
Fire extinguisher (if fire persists)	actuated
Prop sync	off
Bus tie switch (inop. eng.).....	off
Electrical load	monitor
Crossfeed.....	if required

Figure 52: Excerpt from the checklist for engine fire in flight

The Autonomous Emergency Procedure (AEP) was developed using a scripting language called LUA and implemented using Flywithlua which is located in the X-Plane directory within the X-Plane system. In the event of an engine fire, the AEP is designed to perform the non-vital checklist items once the vital checklist items have been completed by the pilot. As shown in Figure 53, once all vital items are actioned, the conditions are satisfied and the AEP begins to action the other items so the pilot can continue to maintain safe flight. The script can recognize which engine is affected and take appropriate actions. The AEP source code, expanded images of the AEP in action and access to the video file of the AEP in action can be found in Appendix AH.

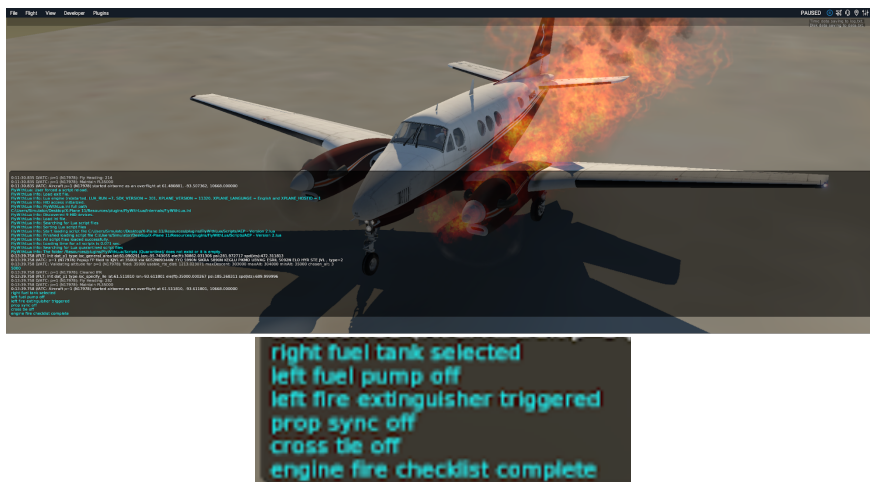


Figure 53: Vital checklist items completed, non-vital checklist items actionned by AEP

By proving its ability to increase pilot performance and reduce workload, the AEP can be developed further by performing the vital checklist items and autonomizing more emergencies, and aid in the development of a new infrastructure for autonomous aircraft.

5.9.4 Identity Access Management System

Currently, towered airports' air traffic control communicates to incoming aircraft via radio, unencrypted. Many commands are issued to the aircraft using a simple plain text identifier [73]. With this communication architecture, there is no protection regarding identity verification and authorization, nor is there any guarantee of data confidentiality or authenticity [73]. To ensure a secure channel of communication between incoming aircraft

and air traffic control, the proposed solution would be to implement an Identity Access Management (IAM) System that will track, store, and distribute the public key infrastructure of all registered aircraft and towered airports.

The IAM consists of three main subsystems. The first being the Global Distribution System (GDS). The GDS is the backbone of the IAM. The GDS features a highly available, high consistency, and a high level of security. The GDS is a distributed application that stores the public key infrastructure and access controls of the registered airports and aircraft. It is the GDS that verifies if an entity is allowed to access or manipulate a given resource. The last two subsystems of the IAM are the airport and aircraft clients. These applications communicate via radio and exchange public key and certificate information to validate the identity of the communicating entity. If valid, the entities will proceed to communicate over an encrypted channel. The full architecture and Software Requirements Specification document is available in Appendix AI.

Verification and validation of the IAM's feature were done using unit tests, which automated the boundaries of the encryption functionality of the airport and aircraft subsystems as well as the access control feature of the GDS. It was discovered late in the process that the XBee radios purchased to produce and validate the prototype of the system could not send a large enough payload to support the exchange of public key and certificate data between the airport and aircraft subsystems. Mitigation strategies would be to implement a sliding window protocol to deliver multiple smaller packets of data over radio in order to deliver the payload. This may increase latency significantly on top of the latent overhead of encrypting said payload. Another mitigation strategy would be to reduce data packet size altogether by having an end-to-end encrypted exchange of a secret key between the aircraft and the next airport on its flight path (i.e. when the aircraft is grounded) prior to take-off. This strategy will allow the aircraft and airport to communicate with a more efficient encryption algorithm quicker without having to rely on an internet connection to verify the identity of the entities while the aircraft is airborne.

5.10 Cost

After performing the market analysis, identifying the stakeholders and establishing critical missions, the business case is determined to ensure the stakeholders' profitability. The OEM, the operators and the retailer/supplier profit analysis is conducted under 3 different methods. The operator must achieve a positive revenue, throughout optimizing its cargo transportation, with the difference of its operating cost. Since retailer/supplier profit is affected by a multitude of factors, incomplete analysis of the total subsidy revenue is established and is available in Appendix AJ.

To assess the OEM profitability, a cost analysis method called "Modified Development and Procurement Cost of Aircraft (DAPCA) IV cost model" is used [35, ch.18]. Based on empirical data, this model is used to estimate the Program cost, which accounts for Research Development Testing and Evaluation (RDTE) and the Production cost. The Production cost includes the expenses generated by manufacturing materials and engineering products for the airframe, engines and avionics. The most cost determining input parameters are the aircraft empty weight, maximum aircraft speed and production quantity. A more complete analysis of the Program cost analysis is found in Appendix AJ.

From the Program cost analysis in Figure 54, the OEM break-even point arises after selling 140 aircraft, when considering a competitive selling price of 21 Million USD. An autonomy factor of 30% is added to the RDTE and the avionics cost to account for the autonomous development. A learning curve cost reduction, associated with an increase in aircraft produced is also included in the method. Since the DAPCA model is taken from 2012, a USD inflation factor of 3% per year is multiplied in the formulas until reaching 2019 [35, ch.18].

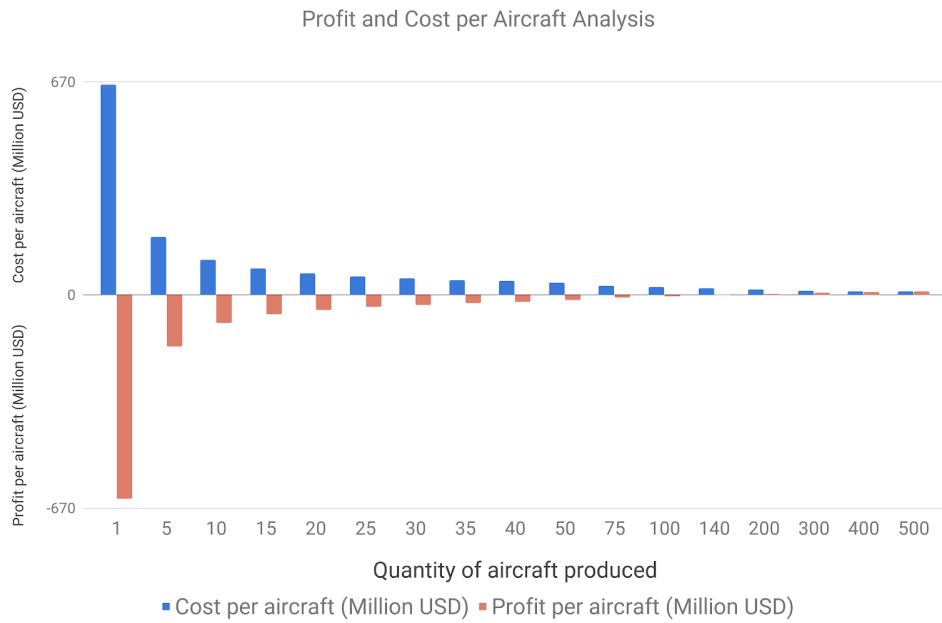


Figure 54: Program cost and profit per aircraft analysis

To complete the operating cost analysis, a Gudmundsson method [32, p. 46-49] was used for both dual-piloted and autonomous aircraft configuration, as well as for the market aircraft comparison with ATR 42-500 [74] and Dash 8 - Q300 [75]. The main parameters and inputs are the annual fuel cost, the engine overhaul cost, the maintenance cost, the annual loan payment, and the annual insurance cost. A maintenance factor of 0.5 is added to account for maintenance challenges from operating in Northern Canada. The price of the Arctic Fox is also included in the method. The results of the hourly operating cost analysis can be found in Figure 55 and further details can be found in Appendix AJ.

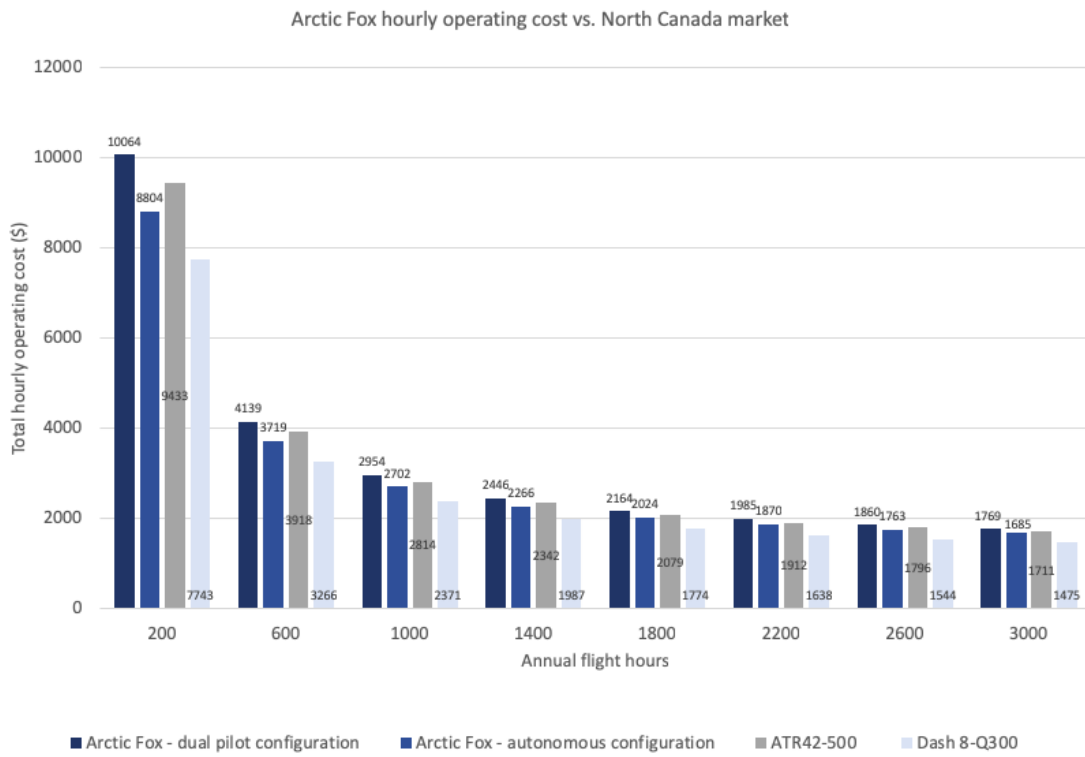


Figure 55: Hourly operating cost versus north Canada market

The operating cost associated with the dual-piloted aircraft is 140\$ per hour higher than the market competition in phase 1, evaluated at 1000 annual flight hours. For the phase 2 to 5, evaluated at 1400 annual flight hours, the operating cost of the autonomous aircraft are in average 96\$ per hour lower than the ATR 42-500 and competes with the Dash 8 - Q300. Although the operating cost is higher in phase 1, the operator remains profitable due to increased flight missions. The autonomous configuration and the decrease in operating costs ensure that profits are increased in phase 2 to 5.

6 CONCLUSION

The Arctic Fox is purpose-built for missions in the North of Canada. With a maximum ferry range of 1,545 NM, a factored landing distance of 2,357 ft on gravel at MLW and a balanced field length of 2,536 ft at MTOW on gravel, the Arctic Fox can fly into most airports situated in Canada's North with supplies. A total of 10,800lb of cargo, stored in the 1,500 ft³ cargo bay, can be transported over 603 NM.

The Arctic Fox includes essential systems such as an autonomous route revision system for icing avoidance and an anti-ice system using bleed-air from the engines to navigate Canada's Northern, icing prone, environment. Furthermore, the aircraft has EMAs for the flight control systems contributing to its more electric design.

Finally, the Arctic Fox will have the capability of multi-stage autonomy which will allow transitioning from dual-pilot and autopilot in the first stage, to fully autonomous in the final stage. This system is backed up with an identity access management system for secure communication between the autonomous aircraft and air traffic control and prevents cyber-attacks. Moreover, it comes equipped with an avionics system which satisfies the requirements of the autonomous strategy plan. This will reduce operating costs for the operators in the long term. It is predicted that the OEM will have a break-even point once the 140th aircraft is sold, with a competitive selling cost of 21M USD.

6.1 Future Work

In order to increase the dynamic stability of the Arctic Fox, the following is recommended to be changed in the design: move the wing and related systems aft by 1.6 ft and move the electrical system aft by 4.3 ft. Though the displacement of the electrical system should not result in any redesign, pulling the wings and related systems back would result in two major design considerations. Firstly, the landing gear position would need to move with the wing, yet would further have to be repositioned to meet CG changes. Secondly, moving the landing gear aft would increase the rotation speed during takeoff which would negatively impact the short takeoff capabilities of the Arctic Fox. The second change is most critical and would

have to be closely examined as it may result in the Arctic Fox no longer being a STOL aircraft.

Future work in defining the role of the remote manager and the autonomous system is required. A suggested outline for this role definition consists of the human readying the aircraft, assessing airworthiness before flight, and monitoring flight progress. Whereas the role of the autonomous pilot would include conducting ground and flight maneuvers, maintaining separation minima, and monitoring and resolving system failures. Consequently, the design of the human-machine interface is a crucial requirement in designing standard operating procedures. Additionally, further work to comprehensively identify avionic systems required on board and at airports is required before beginning the next step of the design process.

7 Appendices

This section includes all of the appendix material referred to in body of the report. The appendix contains an extensive collection of digital content such as CAD files, excel sheets or Amesim simulations. Except where noted otherwise, all of these files can be located on the common Aero 490 Google Drive. Whenever a file in the digital appendix is referred to, it will be described as a file path, preceded by a description of the file, as below.

An example of a digital appendix can be found in:

Digital Appendix: AERO 490 > Report > Final report > Digital Appendix >
Appendix Example > Example Appendix

All parameters referred to in this document and in the digital appendices can be confirmed with the general configuration control sheet seen in: AERO 490 > Excel File: Configuration Control

A Market Analysis

A.1 Details on Northern Communities

Digital Appendix: AERO 490 > Report > Final report > Digital Appendix >
Market Analysis > Business Case Data For Subsidy Program (2016 – 2017 data)

A.2 VTOL Communities

Digital Appendix: AERO 490 > Report > Final report > Digital Appendix >
Market Analysis > VTOL Communities

A.3 VTOL vs STOL tradestudy

Digital Appendix: AERO 490 > Report > Final report > Digital Appendix >
Market Analysis > VTOL vs STOL

A.4 Ski-landing vs Airdrop tradestudy

Digital Appendix: AERO 490 > Report > Final report > Digital Appendix >
Market Analysis >Ski vs Airdrop

B Mission Analysis

B.0.1 Critical Design Missions

To determine the critical missions that the Arctic Fox should perform, a complete market communities analysis is proceeded, considering the five main hubs. From the total fresh food products needed per day and per person, a total payload amount per community is established [2]. The range to the closest hub is researched on google map. With the range and the cruise speed known from aircraft performance calculations and simulations, a one way and a roundtrip flight duration is established considering refueling needed or not. With the total weekly payload known, an optimized payload transported per flight and a frequency of transportation to the community is defined, based on the maximal payload to not exceed to keep the aircraft in its designed weight envelope. Then, from the optimal frequency and the total mission flight time, a total weekly flight hours per community could be defined. Followed by a total weekly hub flight hours, a total number of aircraft to serve the hub is evaluated. The results of Rankin Inlet analysis is found in Table B.0.1. It was completed under the same methodology for the five main hubs. More details of the Rankin Inlet communities analysis can be found in the digital appendix. Digital Appendix: AERO 490 > Report > Final report > Digital Appendix > Mission Analysis & Business Case > \Mission Planning .xlsx" > Sheet: Missions Rankin

$$\text{Weekly Total payload per community} = \text{Total population} \times 4 \text{ lbs fresh food} \times 7 \text{ days}$$

$$\text{One way flight Duration} = \text{Distance (range) (nm)} / \text{cruise speed (knots)}$$

$$\text{Weekly total payload per community}/\text{optimal frequency assumed} \geq \text{Maximum payload of aircraft (10800 lb)}$$

$$\text{Total weekly flight hour per community} = \text{Optimal frequency} \times \text{Mission Flight time}$$

Community Name	Runway Length (ft)	Population	Cargo Needs (lb/week)	Subsidy rate (\$/lb)	Weekly Profit	One Way Flight Duration (h)	Distance (nm)	Alone	2nd Distance (nm)
Chesterfield Inlet	3600	437	12236	1.45	17757.46	0.22	49	N	206
Coral Harbour	5006	891	24948	1.86	46388.57	1.12	252	N	206
Repulse Bay	3400	1082	30296	1.91	57716.61	1.20	270	Y	-
Arviat	4000	2657	74396	0.91	67491.01	0.53	119	Y	-
Baker Lake	4195	2069	57932	1.50	86715.92	0.62	139	Y	-
Meadowbank Gold Mine	5359	600	16800	0.00	0.00	0.76	170	Y	-
Whale Cove	3937	435	12180	1.27	15469.33	0.19	42	Y	-
Total	8171	228788			291538.90				
Mission	Total Range (nm)	Cargo (lb/wk)	Frequency/wk	Cargo (lb/mission)	Mission Fuel	First Air weekly Profit	Refueling Needed	Mission Flight Time (h)	Weekly FH
Repulse Bay	540	30296	3	10099	4450	32400	Y	2.30	6.89
Arviat	238	74396	7	10628	2000	75600	N	1.01	7.09
Baker Lake	278	57932	6	9655	2500	64800	N	1.18	7.10
Meadowbank Gold Mine	340	16800	2	8400	2500	21600	N	1.45	2.89
Whale Cove	84	12180	2	6090	1250	21600	N	0.36	0.71
Chesterfield + Coral	507	37184	4	9296	3900	43200	N	2.16	8.63
					Rough estimates	259200		8.46	33.32

Table B.0.1: Rankin Inlet Communities lists and analysis

It is desired to complete a mission with a maximum payload possible at a maximum range possible. However, when sizing the aircraft, a maximum payload with a maximum is limited and constrained by the maximum fuel amount. If the payload or the range is increase over its limits, the aircraft weight must increase. The aircraft performance would then be affected by this rise in weight, and the constraint diagram will then give us a new optimal design.

Taking the critical missions into consideration, the optimized design was led by (1) Rankin Inlet to Arviat, (2) Iqaluit to Arctic Bay and (3) Iqaluit to Resolute Bay & Grise Fiord. Figure B.0.1 shows the critical design missions.



Figure B.0.1: Critical design missions

The rationale behind the thought process taken, was to consider the mission that will be performed at the maximum payload possible, under the limits of the aircraft optimization. This mission is Rankin Inlet to Arviat. The next mission considered was performed at a maximum take-off weight and for a maximal range, meaning that payload will start to be removed for fuel at this point. This mission is Iqaluit to Arctic Bay. Finally, the last mission considered is Iqaluit to Resolute Bay, which is the maximum range from a hub that can constraint the design. This trip will be the limit to the Arctic Fox operational limit of profitability, since a maximum range is performed and that payload is removed for fuel and to cover a longer distance.

C Business Case

C.1 Main stakeholder interconnection analysis

It is imperative to understand the interconnection between the stakeholders to understand how the profit is generated and how they can affect each other. From the request for proposal, the team goal is to design a conceptual design so that a Original Equipment Manufacturer (OEM) is able to sell it to aircraft operators such as First Air, Air Inuit, Canadian North, and even other market operator. However, to complete this exercise, only an analysis of the north canadian stakeholders is completed. The goal of the operator is to transport cargo, in the most efficiently manner possible. To do so, they charge a specific rate to the hiring company, based on the route and missions required to flight. The retailers and suppliers are hiring the operators so that the cargo is transported in the north of Canada, can reach the communities and northern residents. Since the transportation cost and fees are much higher in the north, a subsidized program exist to help the retailers being profitable. The final goal being to allow northern communities to eat fresh products, to be able to dress themself, to have freedom in their lifestyle. The revenues generated by the northern companies stays in the north and are explained in Section 3.3.

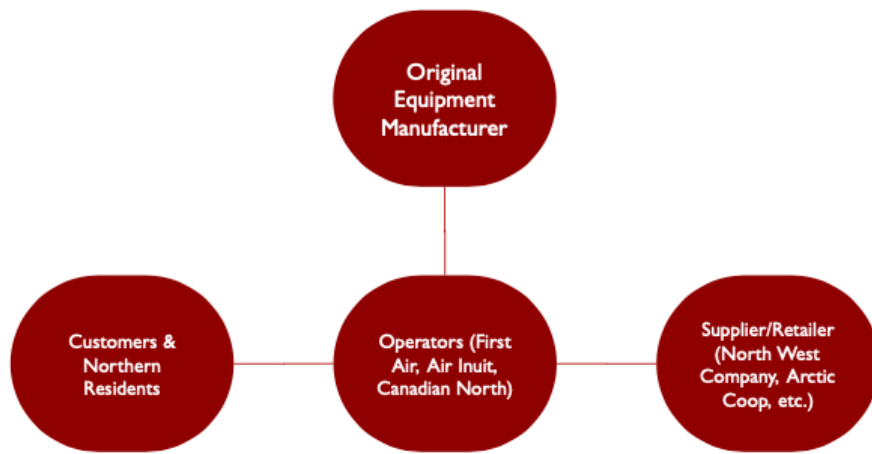


Figure C.1.1: Business case stakeholders of north canada food transportation

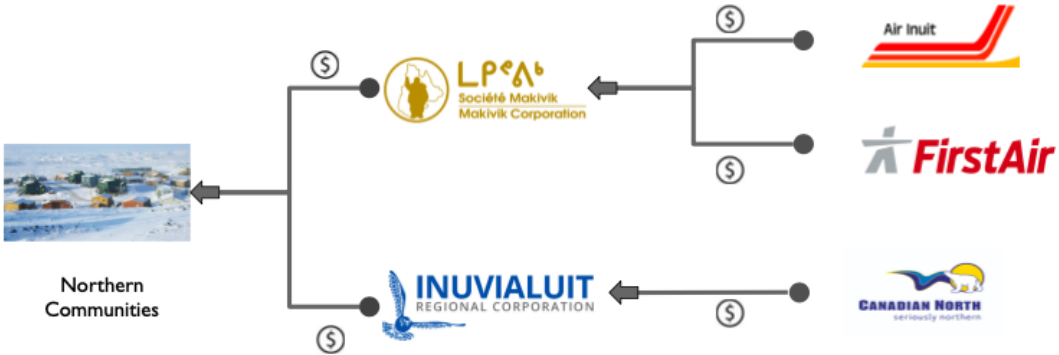


Figure C.1.2: Profit generated throughout business case stakeholders of north canada food transportation

C.2 Operating cost analysis

The operating cost analysis is completed to assess the operator profitability. It was performed by completing both Arctic Fox aircraft configuration, as well as comparing the north Canada market in order to ensure the competitiveness of the design. The ATR 42-500 and the Dash 8- Q300 aircraft are analyzed and compared to both Arctic Fox in terms of hourly operating cost. The analysis is performed by using the same method, i.e. the Gudmundsson operating cost analysis, that is extrapolated from business aircraft CFR Part 25 [76]. The ATR42-500 [74] and Dash 8- Q300 [75] specifications are used to complete the analysis (ex. Aircraft cost, maintenance factor, engine overhaul fund, annual inspection cost, etc.). The analysis procedures was completed for a range of annual flight hours.

This analysis detailed calculations found in Table C.2.1 and assumptions are found below:

Assumptions:

- Maintenance cost: 60\$/hr rate assumed
 - 4.1 ratio of man-hours to flight hours, (including higher north factor of 0.5)
- Storage cost (\$/year)
 - 68,000\$ (Higher in North Canada)

- Annual fuel cost (\$/year)

Fuel price higher in North Canada (average of 5.79\$/gal)

BHP cruise (PW127N)

SFC cruise (PW127N)

- Engine overhaul fund (2 x PW127N)

Overhaul cost = 900,000\$

HSI cost = 450,000\$

Interval = 8000 - 16,000 FH (since cold and dry environment)

- Crew cost and training

Dual-Piloted aircraft

Number of crew (2)

Assumed 150,000\$/year

Autonomous aircraft

Number of crew (1 for 5 aircraft)

Assumed 300,000\$/year

- Annual inspection cost

15,000\$ is assumed based on benchmarking

Maintenance Cost (\$ per year)		Def					
C_ap	49200	Maintenance Cost (\$ per year)					
F_mf	4.1	ratio of maintenance man-hours to flight hours					
R_ap	60	hourly rate for certified PowerPlant and Airframe (around 53-67 \$/hr)					
Q_flt	200	number of flight hours per year					
Maintenance to Flight hour ratio							
F_mf	4.1	North Factor	0.5				
F1	0	(Maintenance Performed by A&P Mechanic)					
F2	0.2	(Easy access to engine) or 0.02 if difficult					
F3	0.2	Because of retractable landing gear, otherwise fixed = 0					
F4	0.2	VFR radios are installed					
F5	0.2	IFR radios are installed					
F6	0.1	integral fuel tank installed					
F7	0.2	Complex Flap System, or 0 if simple					
F8	0.5	0 for 14 CFR Part 23 certification or 0.5 for 14CFR Part 25 certification					
Storage Cost (\$ per year)							
C_stor	67800	\$	Higher in the North !! - Electricity cost are high from heating				
R_stor	5650	storage rate (assume 1500\$ per month)					
Annual Fuel Cost (\$ per year)							
C_Fuel	186155.6319						
BHP_cruise	2132	typical horsepower during cruise					
SFC_Cruise	0.49	typical specific fuel consumption					
FF_Cruise	160.72	total fuel flow in gallons per hours		Jet Fuel	1.5274	1.489	1.5733
R_fuel	5.791302636	price of fuel in \$/gallons		price/liters	1.5299		
				liters to gallons	0.264172		
Annual Insurance cost (\$ per year)							
C_ins	210000						
C_ac	21000000	insured value of the aircraft, OPA increase !!					
Annual Inspection Cost (\$ per year)							
C_Insp	15000	Benchmarked					

Table C.2.1: Profit generated throughout business case stakeholders of north canada food transportation

Table C.2.1 is located in:

AERO 490 > Report > Final report > Digital Appendix >

Mission Analysis & Business Case > \Payload-Range Diagram .xlsx" >

Sheet: Initial Rollout_Operation Cost

Formulas: associated with Table C.2.1:

- Maintenance Cost = F_mf * R_ap * Q_flt
- Maintenance to flight hour ratio = 2 + F1+F2+F3+F4+F5+F6+F7+F8 + North Factor

- Storage Cost per year = $R_{stor} * 12$
- Annual Fuel Cost = $FF_{Cruise} * R_{fuel} * Q_{flgt}$
- $FF_{Cruise} = BHP_{Cruise} * SFC_{Cruise} / 6.5$
- Annual Insurance Cost = $C_{ac} * 1\%$
- Annual Inspection Cost = Benchmarked
- Engine Overhaul Cost = $N_{pp} * Rate * Q_{flgt}$
- Rate = Overhaul Cost/TBO + HSI Cost/ TBHSI
- Crew Cost = $R_{Crew} * N_{Crew}$
- $R_{Crew} = Salary / Q_{flgt}$
- Monthly Loan Payment = $(C_{ac} * 15) * i / (1 - (1/(1+i)^n))$
- Annual Loan Payment = Monthly Loan Payment *12
- Total Yearly Cost = Maintenance Cost + Storage Cost + Annual Fuel Cost + Annual Insurance Cost + Annual Inspection cost + Engine Overhaul fund + Crew Cost + Annual Loan Payment
- Hourly Operating Cost = Total Yearly Cost / Q_{flgt}

C.3 Performance outlook comparison of the Arctic Fox versus ATR 42 - 500 [77] and Dash 8 - Q300 [76]

The Table below shows the performance outlook of the Arctic Fox compared to the ATR 42-500 and the Dash 8-Q300.

	Arctic Fox	ATR 42-500	Dash 8-Q300
MTOW	38,405 lb	41,005 lb	43,000 lb
OEW	23,200 lb	25,794 lb	26,000 lb
Engine	PW127 M/N/NG	PW127 E/M	PW123 B/E
Maximum Payload	10,800 lb	11,684 lb	13,500 lb
Maximum Range	660 nm @ max payload	716 nm @ 48 pax	924 nm @50 pax
Maximum fuel load	6,600 lb	9921 lb	3,160 lb
Take-off distance	2,536 ft	3,822 ft	3,870 ft
Landing distance	2,357 ft	3,167 ft	3,415 ft

Table C.3.1: Performance outlook comparison of Arctic Fox versus North Canada market

- ATR 42-500 [77]:

Limited market for north Canada cargo transportation

Not able to takeoff and land at all northern airport

Increase in operational cost in icing environment

- Dash 8 - Q300 [76]:

Limited market for north Canada cargo transportation

Not able to takeoff and land at all northern airport

To improve the market reach of Arctic Fox, improved lifting devices and flight control systems to decrease the runway distance needed for takeoff and landing are designed. Airdrop configuration may also be added to reach more communities without air access.

C.4 Operator Profit Analysis

With the operating cost tool and with different aircraft competition specifications, the hourly operating cost versus north Canada market is established. Then, to establish the operator profitability, the operator total hourly revenue along with the total hourly operating cost have to be completed. First, to assess the operator hourly revenue, a total community cargo delivered in pound per week is done. Then, each missions flown by the operator is charged to the retailer or supplier or anyone hiring the operator to transport cargo, with a flat rate usually depends on the missions total range, complexity,

refuelling necessity and per how much payload the operator is capable to transport. Next, the total cargo delivered and revenue is determined per hub along with the total of aircraft needed to serve the particular hub. Finally, it is possible to compare the total hourly revenue per aircraft with the total hourly operating cost for both aircraft configuration. The operator profit analysis is available in Figures C.4.1 and table C.4.1 below, along with the formulas used to perform this exercise.

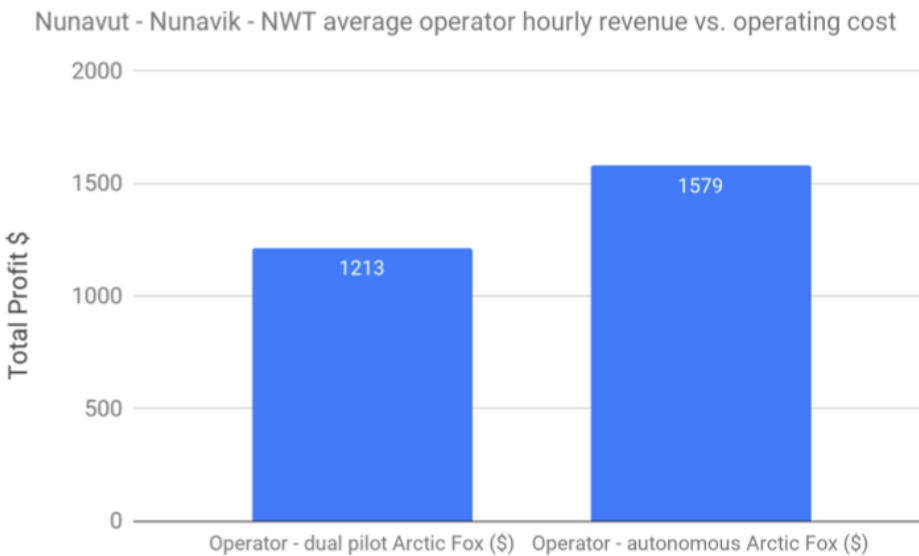


Figure C.4.1: Overall market operator profit analysis (Nunavut, Nunavik, NWT average operator hourly revenue vs. operating cost)

Figure C.4.1 is found in Digital Appendix: AERO 490 > Report > Final report > Digital Appendix >
Mission Analysis & Business Case > \Mission Planning .xlsx" >
Sheet: Summary

Airlines	Hub	Population Served	Cargo Delivered (lb/week)	Aircraft Needed	Operator hourly revenue per aircraft	Operator hourly operating cost per aircraft - dual pilot	Operator hourly operating cost per aircraft - autonomous	Hourly profit gross margin dual pilot vs. autonomous
First Air	Rankin Inlet	8171	228788	2	3890	3400	3100	38.05%
	Iqaluit	11104	310912	4	1916	2544	2367	28.23%
Air Inuit	Kuujjuaq	13200	369600	3	2219	2481	2313	64.20%
Canadian North	Cambridge Bay	5363	150164	1	11189	7151	6310	17.25%
Air Tindi	Yellowknife	3430	96040	1	6114	3685	3343	12.33%
Total	Market Total Average	41268	1155504	11	5066	3852	3487	23.16%

Table C.4.1: Operator profit analysis

Figure C.4.1 is found in Digital Appendix: AERO 490 > Report > Final report > Digital Appendix >
Mission Analysis & Business Case > \Mission Planning .xlsx" >
Sheet: Summary

Formulae used and flat rate assumptions:

Operator weekly revenue = SUM (Total mission weekly cargo needed * (mission flat rate or special flat rate))

Hub operator hourly revenue per aircraft = Total operator weekly revenue / (Total weekly flight hours * # Aircraft needed)

Total weekly flight hours = SUM (missions total range (round trip) * weekly frequency / Aircraft cruising speed)

Rankine Inlet flat rate of 1\$ per lb
Iqaluit flat rate of 2\$/lb & special rates for long flight
Kuujjuaq flat rate of 1.5 \$/lb
Cambridge flat rate of 1.2\$/lb
Yellowknife flat rate of 1.2\$/lb

Table C.4.2: Flat rate assumptions, according to Air indi [78]and Air North [79] rates.

The aircraft is assumed to be flying at maximum payload capacity at every flight, based on the range needed and the performance capacity taken from the payload-range diagram. The total aircraft needed per hub is assumed with a ratio of 1 aircraft per 55 total weekly flight hours, including loading, unloading and turnaround time (TAT).

C.5 Supplier/Retailer revenue analysis with subsidy

First, to assess the supplier hourly revenue associated with subsidy, a total community cargo delivered in pound per week is assessed. Then, the subsidy rate is multiply to the total payload received by the community, and finally added to give a total hub weekly profit. Then it is divided by the total flight hour flown and by the number aircraft flying the routes with this particular hub.

Community Name	Runway Length (ft)	Population	Cargo Needs (lb/week)	Subsidy rate (\$/lb)	Weekly Profit
Chesterfield Inlet	3600	437	12236	1.45	17757.46
Coral Harbour	5006	891	24948	1.86	46388.57
Repulse Bay	3400	1082	30296	1.91	57716.61
Arviat	4000	2657	74396	0.91	67491.01
Baker Lake	4195	2069	57932	1.50	86715.92
Meadowbank Gold Mine	5359	600	16800	0.00	0.00
Whale Cove	3937	435	12180	1.27	15469.33
Total		8171	228788		291538.90

Table C.5.1: Supplier/Retailer weekly revenue for Rankin Inlet hub

Table C.5.1 is found in Digital Appendix: AERO 490 > Report > Final report > Digital Appendix >
Mission Analysis & Business Case > \Mission Planning .xlsx" > Sheet: Rankin Inlet

Airlines	Hub	Population Served	Cargo Delivered (lb/week)	Aircraft Needed	Retailer hourly subsidy revenue
First Air	Rankin Inlet	8171	228788	2	4375
	Iqaluit	11104	310912	4	1448
Air Inuit	Kuujjuaq	13200	369600	3	2238
Canadian North	Cambridge Bay	5363	150164	1	13333
Air Tindi	Yellowknife	3430	96040	1	8530
Total	Market Total Average	41268	1155504	11	5985

Table C.5.2: Overall market total supplier/retailer hourly subsidy revenue

Table C.5.2 is found in Digital Appendix: AERO 490 > Report > Final report > Digital Appendix >

Mission Analysis & Business Case > \Mission Planning .xlsx" > Sheet: Summary

Formulas used:

Supplier weekly revenue = SUM (Total mission weekly cargo needed * (subsidy rate))

Hub supplier hourly revenue per aircraft = Total supplier weekly revenue / (Total weekly flight hours * # Aircraft needed)

Total weekly flight hours = SUM (missions total range (round trip) * weekly frequency / Aircraft cruising speed)

D Autonomy trade study

In order to compare the different options available to progressively incorporate greater autonomy into the Arctic Fox, the following trade study was conducted. The metrics used to compare were safety, crew resource management efficiency, feasibility, operability, cost, and potential for development. Based on these metrics, the following requirements were built.

Scheme shall conform to standards of safety
Scheme shall not interfere with current airport operational models
Scheme shall not cause undue stress, pressure or fatigue to operators
Scheme shall allow a gradual learning curve for operators and regulators
Scheme shall not attempt to incorporate immature technologies
Scheme shall have a well-defined man-machine interface
Scheme shall be able to operate with existing physical infrastructure
Scheme shall be able to operate with existing regulations
Scheme shall minimize operational costs
Scheme shall minimize development costs
Scheme shall minimize certification costs
Scheme shall permit collection of data relevant to transitioning from pilot on-board to off-board
Scheme shall minimize time interval between pilot on-board to off-board operation
Scheme shall provide an ambitious and attainable plan in response to the RFP

Table D.0.1: Requirements

Eight progression schemes were considered as follows:

	Timeline			
	Initial Rollout	Stage 2	Stage 3	Stage 4
1	Dual Pilot	Single Pilot	Remotely Managed	Autonomous
2	Dual Pilot	Remotely Managed	Autonomous	
3	Single Pilot	Remotely Managed	Autonomous	
4	Dual Pilot	Single Pilot	Remotely Managed	
5	Single Pilot	Autonomous		
6	Dual Pilot	Autonomous		
7	Dual Pilot	Remotely Managed		
8	Single Pilot	Remotely Managed		

Table D.0.2: Progression schemes

The comparison among the eight schemes resulted in two main choices. A scheme that begins with a single pilot operation that transitions to a remotely managed operation and finally a self-learning autonomous system. The second option: a dual pilot operation that transitions into a remotely managed operation.

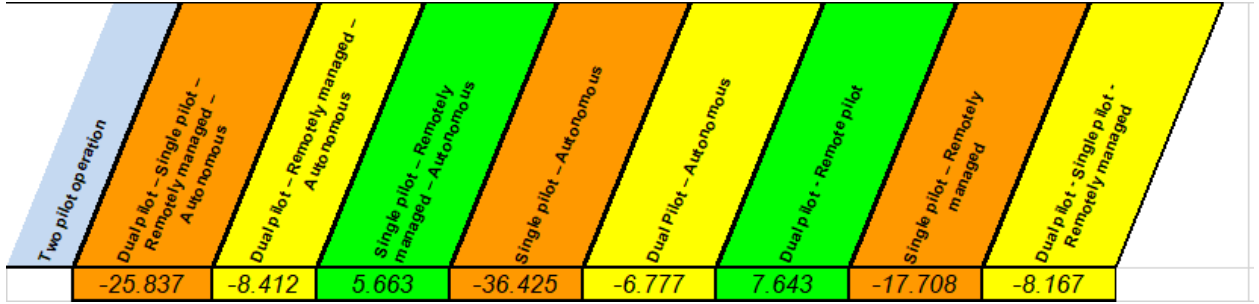


Figure D.0.1: Comparison of progression schemes

A further cost analysis was conducted for these two options to make a final decision by looking into the development and operational cost for each. Within the development cost, design & development and flight testing & certification were taken to be variable. Airframe design, configuration control and tooling design were assumed to be the same[80]. From the initial estimate from cost analysis team on dual pilot operation, a 50% increase in development cost for single pilot was assumed. Similarly, for remotely-managed and autonomous an increase of 100% and 200% respectively was assumed.

Operation	R&D (new cockpit), mil\$	T&E, mil\$	Total RDT&E, mil\$
Dual pilot	30	25	55
Single pilot	45	37.5	82.5
Remote managed	60	50	110
Autonomous	90	75	165

Table D.0.3: Cost analysis

For operational costs, only crew costs were taken to be variable, whereas other operational costs as seen in the figure below, were assumed constant. Information on average salary for crew were used to estimate the crew costs.

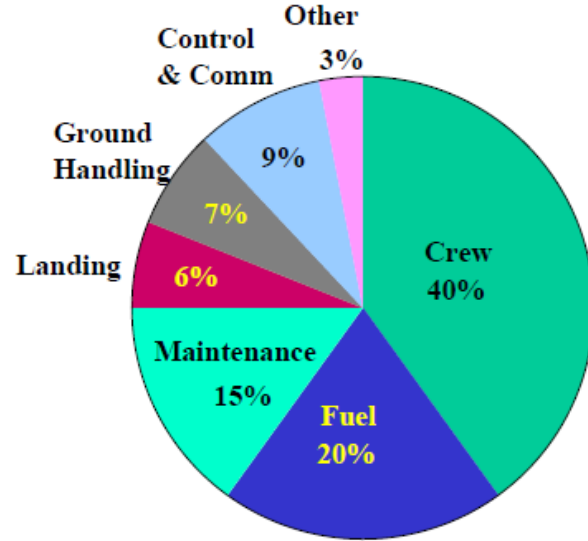


Figure D.0.2: Operational costs [80]

The development & operational costs and the comparison between the top two progression options are summarized in the following table and figure. As a consequence of these, the chosen progression option was Dual pilot operation - Remotely managed operation.

	Development, \$	Operational, \$
Dual-Pilot	55,000,000	180,000
Single-Pilot	82,500,000	140,000
Remote-Pilot	110,000,000	70,000+
Autonomous	165,000,000	60,000+

Table D.0.4: Development and operational costs

“+” refers to the additional ground station costs that are not included here

Functional Requirements	Two pilot operation	Single pilot - Remotely managed - Autonomous	Dual pilot - Remote pilot
BASELINE	Scheme shall conform to standards of safety	-	S
	Scheme shall not cause undue stress, pressure or fatigue to operators	-	S
	Scheme shall be able to operate with existing physical infrastructure	-	S
	Scheme shall be able to operate with existing regulations	-	S
	Scheme shall minimize operational costs	+	-
	Scheme shall minimize development costs	-	+
	Scheme shall minimize certification costs	S	S
	5.663		7.643

Figure D.0.3: Top two progression options

E Constraint Diagram

The design constraints tool is shown in E.0.1. The tool plots the relationships between thrust, weight, and wing area for various design parameters such as climb rate, cruise speed, and landing distance. The user can use sliders to vary the values of other variables in those relationships based on design requirements and observe the effect on the design space. The thrust, weight, and wing area relationships were obtained from aircraft design methods from Jan Roskam and Daniel Raymer. The tool is available online at <https://constraints.devincrossman.com>.

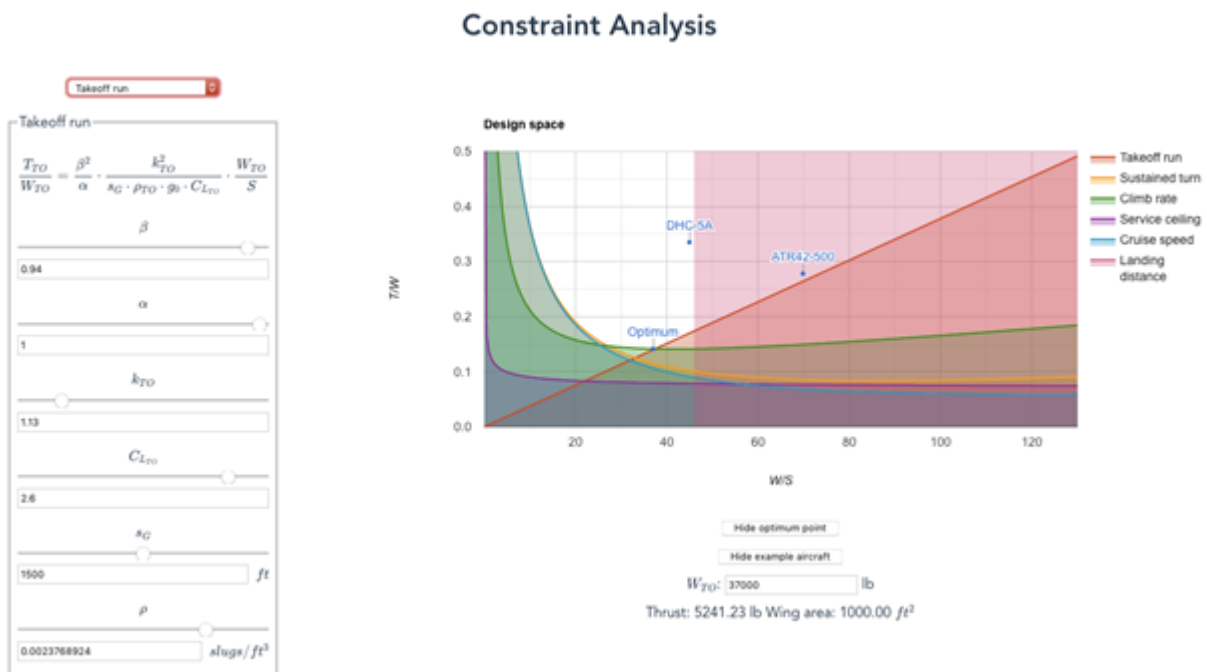
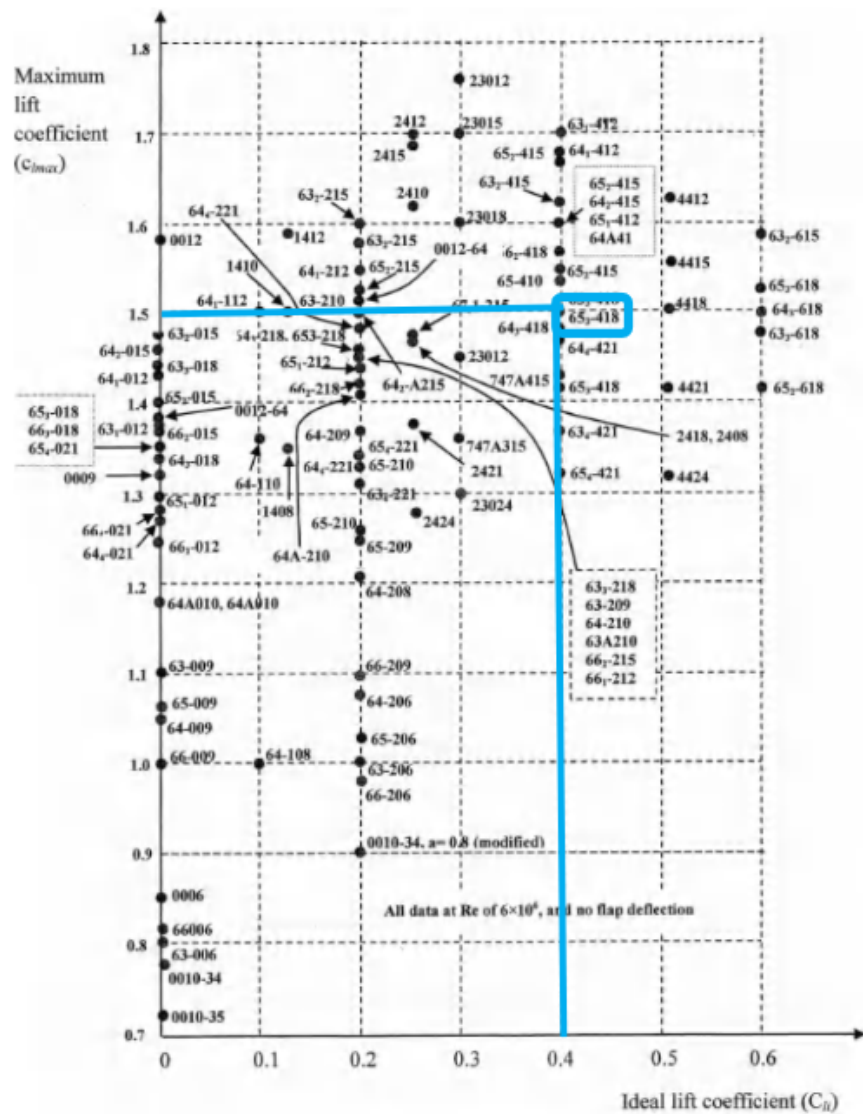


Figure E.0.1: Screenshot of the tool used to build the constraint diagram

The design constraints tool was developed using the Vue JavaScript framework. Vue is similar to other web app frameworks such as React and Angular but, rather than being monolithic, allows incremental adaptation. This makes it extremely lightweight and easy to use. A big advantage of using Vue is that it makes it easier to manage the state of application components. The code was written in TypeScript and is available online at <https://github.com/devincrossman/aircraft-constraints>.

F Aerodynamics



M. Sadraey, *Aircraft design*. Chichester: Wiley, 2013.

Figure F.0.1: Wing airfoil selection based on ideal and maximum lift coefficient required

Airfoil characteristics	NACA 63 ₃ -418	NACA 65 ₃ -418
$C_{l\max}$	1.5	1.5
C_{li}	0.4	0.4
$C_{d\min}$	0.005	0.0045
C_{mo}	-0.075	-0.0625
$(C_l/C_d)_{\max}$	128	140
$(t/c)_{\max}$	18%	18%
α_s	14 degrees	18 degrees
α_s (flap deflection)	12.5 degrees	11.8 degrees
α_0	-2.1 degrees	-2 degrees
α_0 (flap deflection)	-13.8 degrees	-14 degrees
Stall behavior	Abrupt	Moderate

Table F.0.1: Characteristics of two airfoils with $C_{li} = 0.4$ and $C_{l\max} = 1.5$

Both NACA 63(3)-418 and NACA 65(3)-418 have $C_{li} = 0.4$, $C_{l\max} = 1.5$, and enough thickness ($\max(t/c) = 18\%$). However, NACA 65(3)-418 has the highest lift to drag ratio (140), so it was selected as the wing airfoil of the Arctic Fox.

AR=2 & NACA 0018

AOA [deg]	C_D (MATLAB)	C_D (ANSYS)	% Difference*
0.5	0.0001	0.0030	96**
5	0.0115	0.0127	9
10	0.0459	0.0420	-9
15	0.1032	0.0890	-16
17	0.1325	0.1140	-16
19.8	0.1798	0.1489	-21

bottomrule

Table F.0.2: Comparison of drag coefficients obtained from MATLAB and ANSYS for NACA 0018

AR=6 & NACA 0012			
AOA [deg]	C_D (MATLAB)	C_D (ANSYS)	% Difference*
2	0.0016	0.006	73**
4	0.0062	0.012	48**
8	0.0249	0.035	29
12	0.056	0.056	0

Table F.0.3: Comparison of drag coefficients obtained from MATLAB and ANSYS for NACA 0012

$$(*) : \% Difference = \frac{C_{D,ANSYS} - C_{D,MATLAB}}{C_{D,ANSYS}} * 100$$

(**): High percent of difference is due to dividing by a small number

CFD analysis data and results

Digital Appendix: AERO 490 > Report > Final report > Digital Appendix >
Wing CFD Analysis

G Aircraft Performance Calculations

The calculation of the mean acceleration between segments of the takeoff and landing was done using the equation presented in figure G.0.1 [29], while using the root mean square velocity (V_{RMS}) of the segment for the dynamic pressure.

$$a = \frac{g}{w} [(T - \mu W) - (C_D - \mu C_L)qS - W\theta]$$

a = acceleration (ft/sec²), g = gravity (ft/sec²), T = thrust (lb), μ = braking/rolling coefficient, W = weight (lb), C_L , C_D = Lift and Drag coefficient at $\alpha = 0$, q = dynamic pressure = lb/ft², S = wing area (ft²), θ = runway slope (%), i.e. 2% = .02)

Figure G.0.1: Acceleration Equation

In order to determine the balanced field length (BFL), the speeds and distances must be computed for the OEI takeoff and the AEO ASD and V1 must be found at which both distances will be equal. This distance is known as the BFL. Each case is separated into multiple segments as shown figures G.0.2 and G.0.3 below [71].

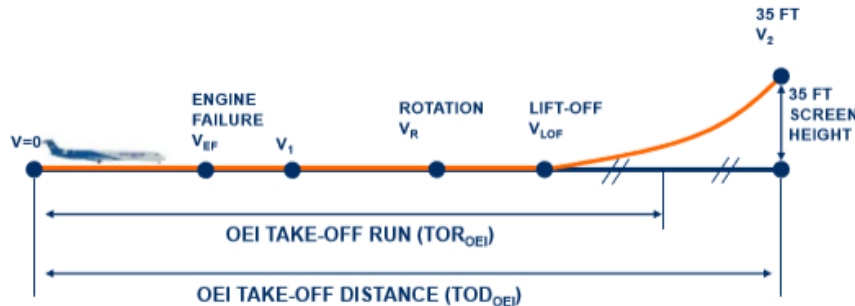


Figure G.0.2: OEI takeoff distance segments

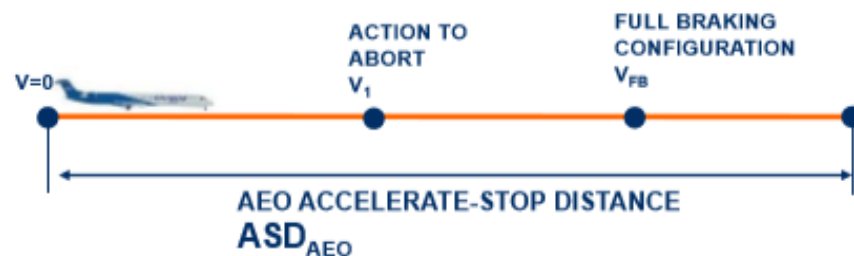


Figure G.0.3: AEO ASD segments

Using regulations from FAR 25.105 to 115 [28], the lift and drag of the Arctic Fox, and the acceleration equation, the following Excel spreadsheet is used to calculate each segment's

acceleration, speed, time and distance. This enables the determination of the total distance corresponding to a certain value of V_1 (ranging between 80% and 100% of V_R). The determination of the distance for the segments between V_R , V_{LOF} and V_2 was done using the OEI gradient at V_2 calculated from equation G.1 and figures G.0.4 and G.0.5 created from experimental takeoffs of different aircraft, while V_2 was determined using equation G.2. The equations and figures are from [71].

$$\gamma = \frac{T}{W} - \frac{C_D}{C_L} \quad (\text{G.1})$$

Where, γ is the gradient, T is the thrust in lbf, W is the weight in lb, C_D the drag coefficient and C_L the lift coefficient.

$$V_{2_{min}} = \sqrt{\frac{295.37W}{C_{L,V_2}S}} \quad (\text{G.2})$$

Where $V_{2_{min}}$ is V_2 for OEI in knots, W is the aircraft weight in lb, C_{L,V_2} is the lift coefficient at V_2 , S is the wing area in ft^2 .

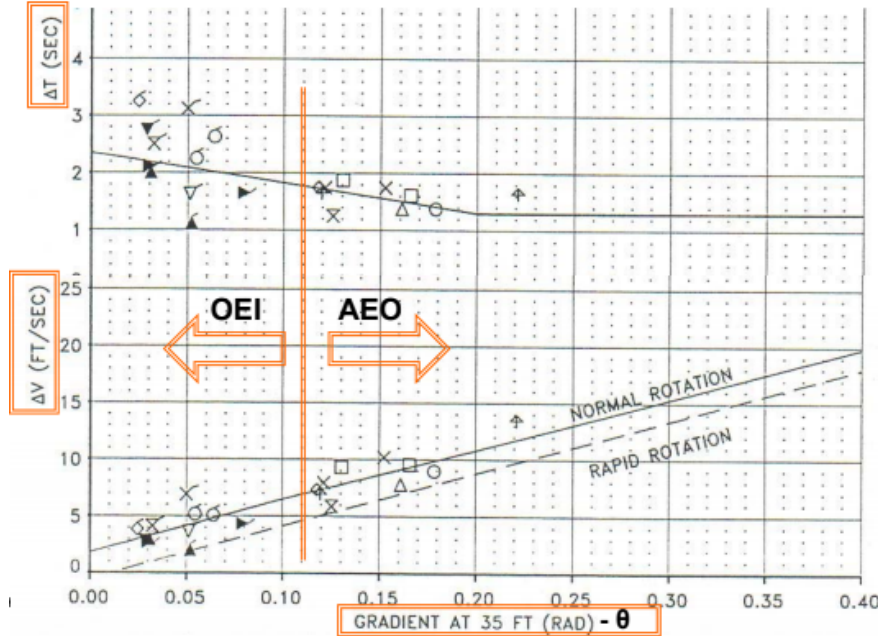


Figure G.0.4: VR-VLOF segment

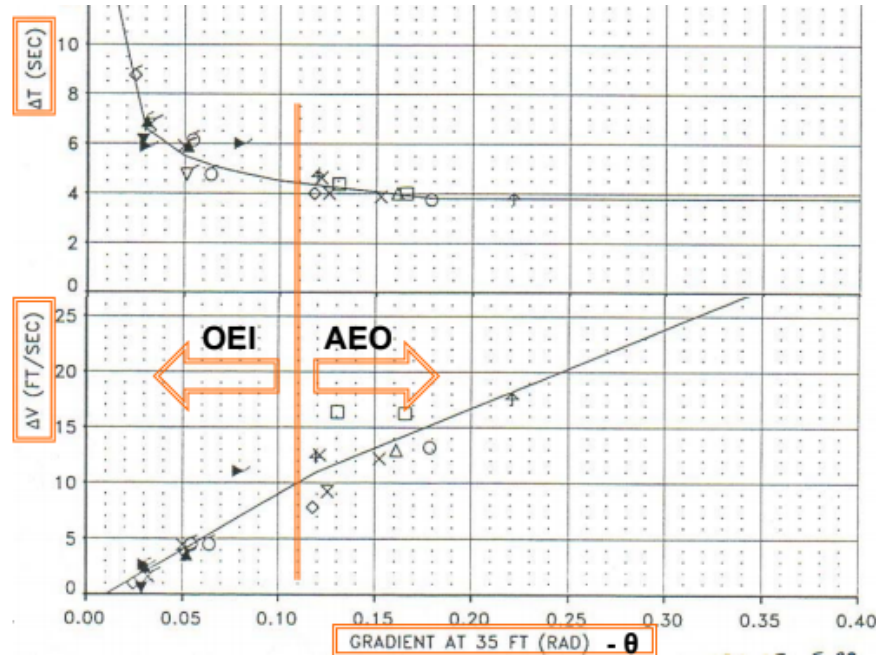


Figure G.0.5: VLOF-V2min segment

The rest of the necessary values are distance calculations from a combination of acceleration and time or from acceleration and speed increment. Shown in the digital appendix are the results at MTOW, sea level, standard atmosphere and on gravel with the OEI takeoff on the middle and AEO ASD on the right.

Takeoff BFL Calculation

Digital Appendix: AERO 490 > Report > Final report > Digital Appendix > Appendix AB > \Performance Calculation Tool.xlsx" > Sheet: Takeoff

A similar procedure was applied to the landing distance calculation, using segments defined in figure G.0.6 [81].

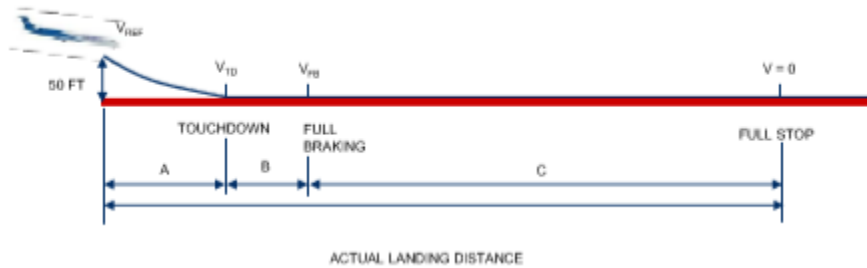


Figure G.0.6: Landing Distance definition

V_{ref} is found from equation G.3 [81], the glide path is assumed to be at 3.5° and the other speeds are taken as the minimum required values from FAR 25.125 [28]. The rest of the calculations are based on equation G.0.1 and on acceleration, velocity and distance relationship formulas, as in the takeoff calculations.

$$V_{ref} = \sqrt{\frac{295.37W}{C_{L,ap}S}} \quad (\text{G.3})$$

Where V_{ref} is the reference speed in knots, W is the aircraft weight in lb, $C_{L,ap}$ is the approach lift coefficient, S is the wing area in ft^2 .

Shown in the digital appendix are the accelerations, speeds, times and distances of each segment at MLW (38 000 lb), sea level, standard atmosphere and on gravel.

Digital Appendix: AERO 490 > Report > Final report > Digital Appendix >
Aircraft Performance Calculations > \Performance Calculation Tool.xlsx" >
Sheet: Landing

Digital Appendix: AERO 490 > Report > Final report > Digital Appendix >
Aircraft Performance Calculations > \Performance Calculation Tool.xlsx" >
Sheet: Cruise

H Electrical System

Electrical System Requirements (R) and Functions (F)

- R: The electrical system shall provide enough power to supply essential loads.
Rationale: The electrical system needs to provide enough power so that “essential loads” are never inoperative. Essential loads are: Engine ignition systems and other systems whose functioning is required for type certification. Conformity to 525.1310
F: Provide Electrical Power
- R: The failure of one power source shall not impair the ability of remaining sources to supply essential loads
Rationale: Any one power source should not, when it fails, cause the failure of other power sources. Conformity to 525.1351
F: none
- R: The electrical power sources shall be disconnectable from the system
Rationale: In case of failure, it is possible to disconnect electrical systems. Conformity to 525.1351 5(c).
F: Disconnect electrical power source
- R: The aircraft shall be safely operable in VFR for over 5 minutes with normal electrical power inoperative
Rationale: The aircraft shall be operable for some time, starting from its max cert. Altitude and with critical fuel. Electrical parts can stay on if they’re electrically and mechanically isolated from parts turned off, and if it can be proven that a single malfunction cannot cause the loss of two separate parts. Conformity to 525.1351 4(d)
F: none
- R: There shall be at least 2 independent sources of electrical power
Rationale: Redundancy and safety. Conformity to 525.1307
F: none
- R: In the event of the failure of one power source, another shall automatically be provided or manually selectable to maintain operation
Rationale: Ensure that the failure of one system can be mitigated by switching to another system. Confirmity to 525.1355 3(c)
F: automatically switch to functioning electrical source
- R: The generating systems shall protect against hazardous over-voltage and other malfunctioning
Rationale: Protect the system from over-voltages, which would result in further harm to the system. Conformity to 525.1357 2(b)
F: Protect against over-voltages
- R: There shall be sufficient electrical power for emergency procedures after an emergency landing or ditching.
Rationale: Ensure that, if electrical power is needed for post-emergency procedures, it can be provided by a suitable electrical supply which has a low risk of being damaged in emergencies. Conformity to 525.1362
F: Provide electrical power for emergency procedures
- R: Batteries shall provide enough electrical power to supply emergency electrical power to essential DC loads for at least 30 minutes

Rationale: Conformity to CAR 551.201

F: Provide emergency DC power

#	Functional Requirements	Importance Score	Variable Frequency 230VAC Generation	400 Hz AC Generation	28VDC Generation	270VDC Generation	Variable Frequency 115VAC Generation
1	Low Operating costs	10.3%	BASELINE	-	-	-	s
2	Low Component Costs	10.9%		-	-	-	-
3	Fault Recognition System	14.50%		s	s	s	s
4	Self-Sustenance	19.73%		s	s	s	s
5	System Reliability (MTBF)	19.73%		-	-	-	-
6	Ajusted to Northern Climates	13.96%		s	s	s	s
7	Low Component Weight	10.87%		-	-	+	-
			Total Plus	0	0	1	0
			Total Minus	0	0	0	0
			Weighted Score	-51.812	-51.812	-30.067	-41.477

Figure H.0.1: Electrical system power generation trade study

#	Functional Requirements	Importance Score	Ni-cd	Lipo	NiMH	Lead-Acid
1	Low Operating costs	10.34%	BASELINE	s	+	-
2	Low Component Costs	10.87%		-	-	+
3	Fault Recognition System	14.50%		s	s	-
4	Self-Sustenance	19.73%		s	s	s
5	System Reliability (MTBF)	19.73%		-	-	-
6	Ajusted to Northern Climates	13.96%		+	-	-
7	Low Component Weight	10.87%		+	+	-
			Total Plus	2	2	1
			Total Minus	0	0	0
			Weighted Score	-5.772	-23.356	-58.523

Figure H.0.2: Battery type trade study

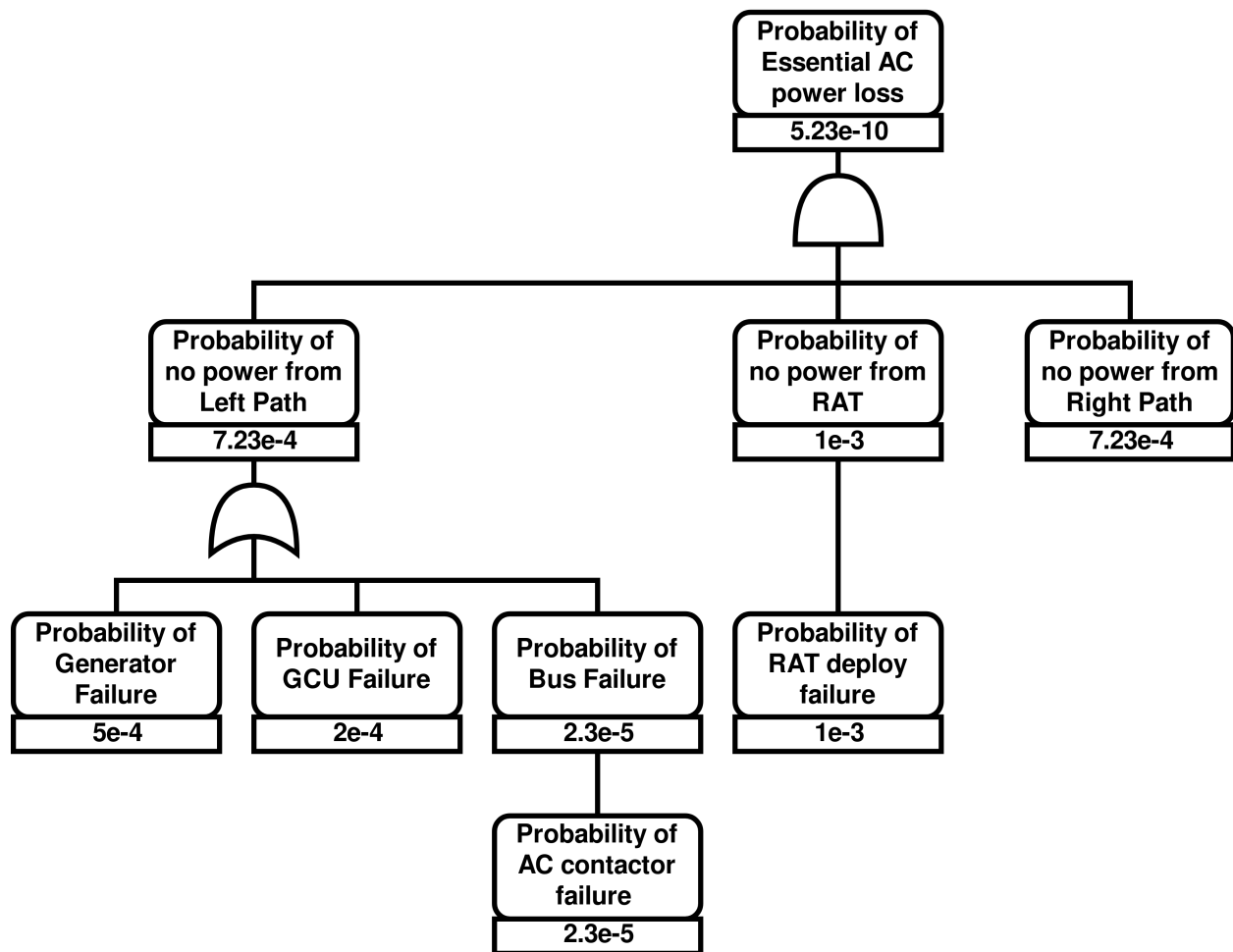


Figure H.0.3: Fault tree analysis for failure to provide power to essential AC loads

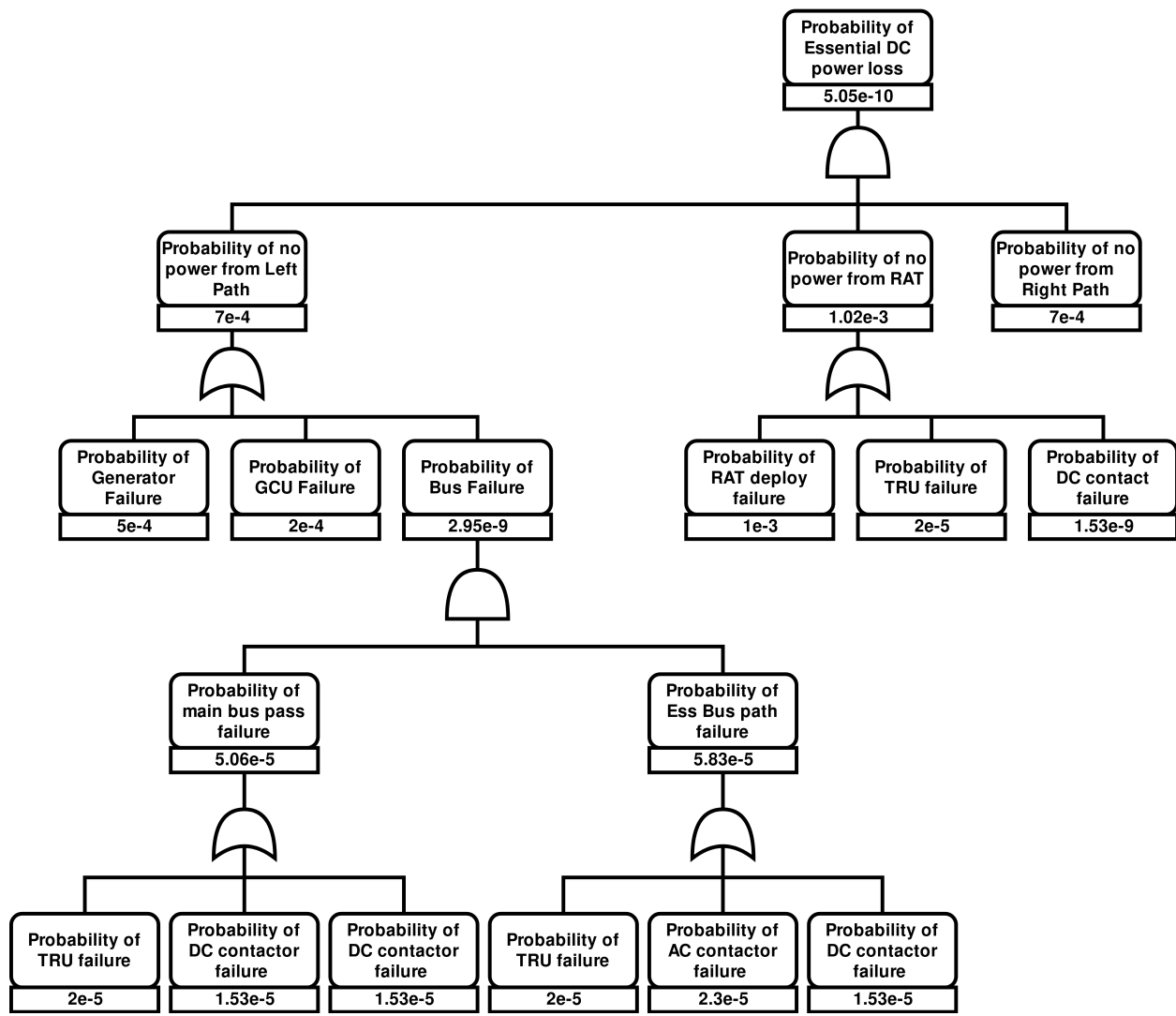


Figure H.0.4: Fault tree analysis for failure to provide power to essential DC loads

Electrical Load Analysis Calculations

To determine the power required for lighting the cargo bay, lighting the cockpit, exterior lighting, and heating the windshield, electrical load data for the DC-10 provided by [20, Part IV, Ch. 7] was used and applied to the Arctic Fox using sizing estimates. Sample calculations are presented for a single phase.

For the cargo bay lighting electrical load estimation, the floor area was estimated for the DC-10 and the Arctic Fox to use as a proportionality factor. The DC-10 cabin lighting power use during ground loading is 13400VA. The DC-10 floor area was estimated to be rectangular and proportional to the product of the fuselage length and width:

$$A_{floor,DC-10} = L_{DC-10} * W_{DC-10} = 182'3'' \cdot 19'9'' = 3600ft^2$$

Similarly, the Arctic Fox floor area was calculated to be:

$$A_{floor,AF} = L_{AF} * W_{AF} = 840'' * 92'' = 537ft^2$$

The Arctic Fox electrical load for interior lighting was calculated to be

$$P_{lighting,AF} = \frac{A_{floor,AF}}{A_{floor,DC-10}} * P_{lighting,DC-10} = \frac{537ft^2}{3600ft^2} * 13400VA = 1999VA$$

Since the interior lighting would only be active when the aircraft is on the ground, this load was equal to zero during flight.

For the cockpit lighting, the loads were determined based on the cockpit floor area. A triangular area was assumed based on the width and height of the cockpit area. For the DC-10, the cockpit length and width were estimated to be 4.04m, giving a floor area of $0.5 * 4.04^2 = 8.08m^2$. The Arctic Fox has a rectangular cockpit area of $4ft * 7.56ft = 30.24ft^2 = 2.8m^2$. During climb, the DC-10 uses 1200VA for cockpit lighting. The Arctic Fox climb power load was calculated to be 416VA during climb.

For the exterior lighting, it was assumed to be similar for the DC-10 and the Arctic Fox, so the same loads were used.

For the windshield heating, the width of the fuselage was used as the proportionality factor. For the DC-10, this is 237", and for the Arctic Fox it is 92". The DC-10 uses 6000VA for windshield heating during climb, so the Arctic Fox power usage was estimated to be

$$P_{windshield,AF} = \frac{Width_{AF}}{Width_{DC-10}} * P_{windshield,DC-10} = \frac{92}{237} * 6000VA = 2280VA$$

For the avionics power use, an estimation was made to determine the "conventional" avionics power use, and an autonomy factor was added to it in order to account for the extra avionics systems that would be required to permit autonomous flight.

To estimate the conventional avionics power usage, the weight of the avionics was estimated for the Arctic Fox and DC-10 using the NASA FLOPS method [82]. The weight is a function of the range, crew, and aircraft dimensions:

$$\begin{aligned} W_{conv,avionics,AF} &= 15.8 * Range^{0.1} * Crew^{0.7} * Fusearea^{0.43} \\ &= 15.8 * (460nm)^{0.1} * (2)^{0.7} * (536ft^2)^{0.43} = 707.01lb \end{aligned}$$

$$W_{avionics,DC-10} = 15.8 * (3500nm)^{0.1} * (3)^{0.7} * (899ft^2)^{0.43} = 2607.53lb$$

Using these weights as a proportionality factor, and using 7400VA for the DC-10 avionics during climb, the conventional Arctic Fox avionics power use was estimated to be

$$P_{conv,avionics,AF} = \frac{W_{conv,avionics,AF}}{W_{avionics,DC-10}} P_{avionics,DC-10} = \frac{707.01}{2607.53} * 7400VA = 2006VA$$

An "autonomous" avionics power use was determined from [63], which adds 1298VA to account for additional antennae, cameras, and data storage. Hence, the avionics power use during climb is 3304VA.

The engine starting load was estimated using a Casa C-295 aircraft model in X-Plane 11, which has a similar engine to the Arctic Fox, and determining the power draw for engine starting, which was estimated to be 5800W.

The rest of the loads were initially calculated, and finally provided by other teams. A summary of the electrical load analysis is presented below.

Load	Type	Unit	Cargo Load	Taxi	TO & Climb	Cruise	Descent
Int. Light	DC	W	1999	1999	0	0	0
Cockpit Light	DC	W	225	225	415	415	415
Ext. Light	DC	W	2800	2800	3850	200	3850
Windshield Heat	AC	VA	0	323	1938	2325.6	1938
Fuel Pumps	AC	VA	0	4000	4000	4000	4000
Hydraulics	AC	VA	0	0	527	0	527
Avionics	DC	W	0	2735	3305	3263.8	3304
Rudder EMAs	AC	VA	0	2204	2204	2204	2204
Ailerons EMAs	AC	VA	0	278	278	278	278
Elevator EMAs	AC	VA	0	4520	4520	4520	4520
ECS	AC	VA	0	3400	3400	3400	3400
Avionics Cooling	AC	VA	0	6000	6000	6000	6000

Table H.0.1: Electrical load analysis for the Arctic Fox

Functional Hazard Assessment

Digital Appendix: AERO 490 > Report > Final report > Digital Appendix > Electrical System > "Electrical System General" > Sheet: FHA

Electrical Load Analysis Data

Digital Appendix: AERO 490 > Report > Final report > Digital Appendix > Electrical System > "Electrical System General" > Sheet: Electrical Load Analysis

Electrical System Amesim Model (generic case)

Digital Appendix: AERO 490 > Report > Final report > Digital Appendix > Electrical System > "Arctic_Fox_Electrical_system_currentload.ame"

I Flight Control System

Flight Control System - Power Trade Study

Digital Appendix: AERO 490 > Report > Final report > Digital Appendix >
Flight Control System > Flight Control System Types Trade Study >
Sheet: Power Pugh Matrix

Flight Control System - Actuator Electrical Loads

Digital Appendix: AERO 490 > Report > Final report > Digital Appendix >
Flight Control System > EMA Electrical Loads

Flight Control System - Actuator Sizing

Digital Appendix: AERO 490 > Report > Final report > Digital Appendix >
Flight Control System > Actuator Sizing > Sheet: FCS Envelope and Load
Sizing & Linkage Geometry

Flight Control System - Airfoil for CFD Modelling

Digital Appendix: AERO 490 > Report > Final report > Digital Appendix >
Flight Control System > Airfoil Plots for CFD

Flight Control System - Aileron CFD Hinge Moment Calculations

Digital Appendix: AERO 490 > Report > Final report > Digital Appendix >
Flight Control System > CFD Data & Calcs > Aileron

Flight Control System - Elevator CFD Hinge Moment Calculations

Digital Appendix: AERO 490 > Report > Final report > Digital Appendix >
Flight Control System > CFD Data & Calcs > Elevator

Flight Control System - Rudder CFD Hinge Moment Calculations

Digital Appendix: AERO 490 > Report > Final report > Digital Appendix >
Flight Control System > CFD Data & Calcs > Rudder

I.1 Roll Control Summing Link Design

For roll control, a dual actuator system acting on each aileron over a summing lever was implemented. The lever's position corresponds with the sum of the positions of the actuators attached to it. Jamming of one of the actuators would result in the other actuator

compensating for the malfunctioning one in order to bring the flight control surface to a neutral position.

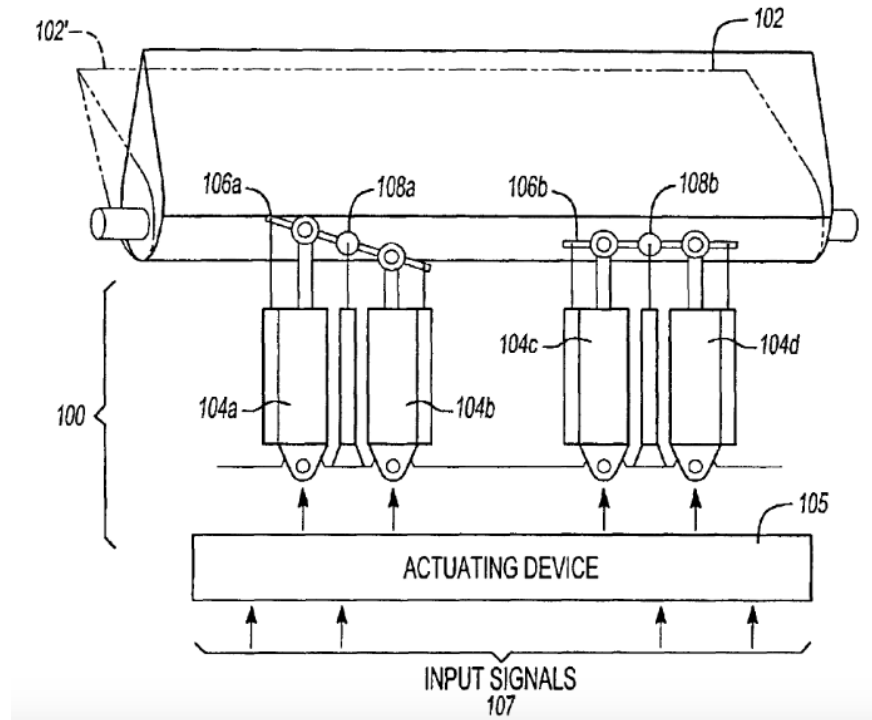


Figure I.1.1: Flight control surface actuation system [83]

J Landing Gear

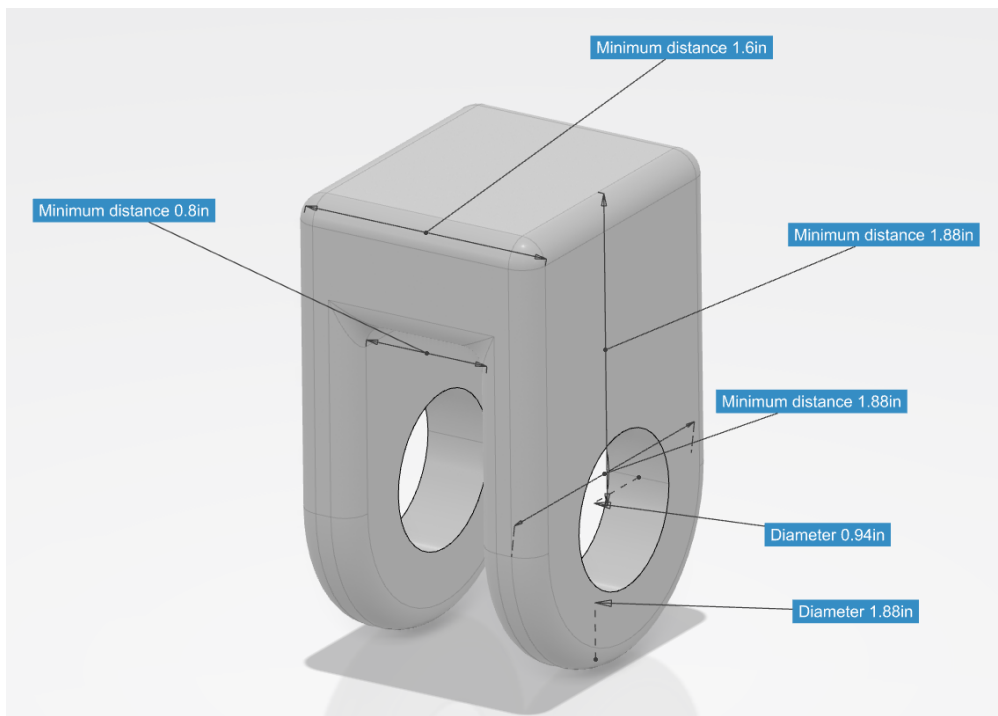


Figure J.0.1: Main Landing Gear Attachment Dimension

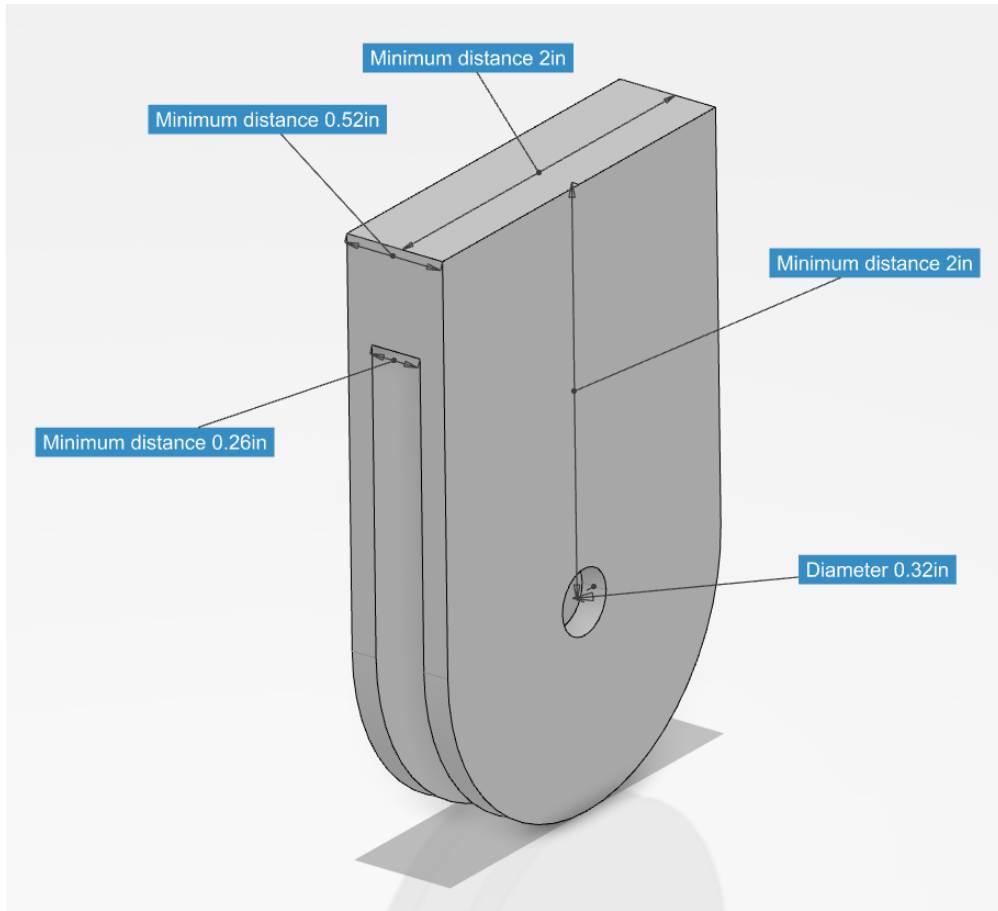


Figure J.0.2: Nose Landing Gear Attachment Dimension

Landing Gear Attachment Dimensions Results

Digital Appendix: AERO 490 > Report > Final report > Digital Appendix >
Landing Gear > \Landing Gear Lug Calculations" > Sheet: Final Results

Landing Gear Component Sizing

Digital Appendix: AERO 490 > Report > Final report > Digital Appendix >
Landing Gear > \Landing Gear Tool"

Main Landing Gear ANSYS Results

Digital Appendix: AERO 490 > Report > Final report > Digital Appendix >
Landing Gear > \ANSYS Folder"

K Overview

CAD files of the Arctic Fox can be viewed here:

Digital Appendix: Sign into the 3Dexperience Space > search '\Final Assembly" in the search tab on top of the page > The file will be the 3rd search result with Revision '\B.1" in the revision column

- To simply preview the file, left-click and click the preview button to the right of the page (look for a picture of an eye)
- NB: If working from a personal computer, opening the file would require downloading a 3Dexperience App which would take time and disk space so a preview is recommended instead. If working from an NCADE PC (or any public PC), the file can be opened by opening any 3Dexperience app, finding the file with the steps given above within the app space, right-clicking on the file and clicking "Open".

L Weights and CG Limits

Component weight estimations from Raymer [35]

Digital Appendix: AERO 490 > Report > Final report > Digital Appendix > Appendix AL > \Weight Estimation.xlsx" > Sheets: Structures Group, Equipment Group and Propulsion Group

The terminology used in the weight estimation equations in the previous digital appendix can be found in the following digital appendix.

Digital Appendix: AERO 490 > Report > Final report > Digital Appendix > Appendix AL > \Weight Estimation.xlsx" > Sheet: All Terminology

Some components weights were not found from the Raymer estimations, since actual data was available (i.e. engine and propeller). The complete list of the weights and positions used for the CG determination can be found in the following digital appendix, which also includes the MTOW of the aircraft highlighted in yellow at the bottom.

Components weight and positioning

Digital Appendix: AERO 490 > Report > Final report > Digital Appendix > Appendix AL > \Weight Estimation.xlsx" > Sheet: CG Inputs

Table L.0.1 illustrates the flight and ground CG limits, with respect to the leading edge of the wing, and the payload, fuel and crew combinations that cause them. The digital appendix refers to the full list of components and positions, where only the payload position and the payload, fuel and crew weights are changed for the different limits.

Limits	Payload (lb) (ft from datum)	Payload FS Position	Fuel (lb)	Crew (lb)	CG (% MAC)
Aft Flight	10,800	39.56	500	450	69.25%
Forward Flight	3,750	29.36	500	450	41.06%
Aft Ground	4,350	58.37	0	60	86.79%
Forward Ground	4,350	29.36	0	450	32.13%

Table L.0.1: CG limits

Flight most aft CG

Digital Appendix: AERO 490 > Report > Final report > Digital Appendix >
Appendix AL > \Weight Estimation.xlsx" > Sheet: Aft flight limit

Flight most forward CG

Digital Appendix: AERO 490 > Report > Final report > Digital Appendix >
Appendix AL > \Weight Estimation.xlsx" > Sheet: Fwd flight limit

Ground most aft CG

Digital Appendix: AERO 490 > Report > Final report > Digital Appendix >
Appendix AL > \Weight Estimation.xlsx" > Sheet: Aft ground limit

Ground most forward CG

Digital Appendix: AERO 490 > Report > Final report > Digital Appendix >
Appendix AL > \Weight Estimation.xlsx" > Sheet: Fwd ground limit

M Propeller Efficiency

The digital appendix shows the details of the propeller efficiency iterative calculations using the Rankine-Froude momentum theory described in Gudmundsson [32, Ch. 14]. The calculation uses inputs of drag coefficient, lift induced drag coefficient, weight (lb) and engine power (shp) in cruise conditions along with the propeller disc and wing areas (ft^2). The initial assumption of propeller efficiency used for the iterations is 0.85, while the viscous profile efficiency is assumed to be 0.85 as suggested in Gudmundsson [32, Ch. 14].

The left section of each iteration is used to determine the velocity of the aircraft with the inputs given, by equating thrust and drag with the same equation that was used to determine the cruise velocity in section 4.4.3. Using this V , equations M.1, M.2, M.3 and M.4 [32, Ch. 14] are used to calculate the new propeller efficiency iteratively.

$$T = \frac{550\eta_p P}{V} \quad (\text{M.1})$$

Where T is the thrust in lbf, η_p the propeller efficiency, P is the engine power in shp and V is the velocity in ft/s.

$$\omega = 0.5 \left[-V + \sqrt{V^2 + \frac{2T}{\rho A}} \right] \quad (\text{M.2})$$

Where ω is the induced velocity in ft/s, V is the velocity in ft/s, T is the thrust in lbf, ρ is the air density in slugs/ ft^3 and A is the propeller disc area in ft^2

$$\eta_i = \frac{1}{1 + \omega/V} \quad (\text{M.3})$$

Where η_i is the ideal propeller efficiency, ω is the induced velocity in ft/s and V is the velocity in ft/s.

$$\eta_p = \eta_v \eta_i \quad (\text{M.4})$$

Where η_p the propeller efficiency, η_v the viscous profile efficiency and η_i the ideal propeller efficiency.

The procedure was done with the Gudmundsson drag calculation and the OpenVSP [84] drag in cruise and the more conservative value was used in the design of the aircraft. The Gudmundsson method included iterations to find the velocity, where the OpenVSP method did not.

Propeller efficiency iterative calculation with Gudmundsson drag

Digital Appendix: AERO 490 > Report > Final report > Digital Appendix > Appendix AI > \Calculations Anthony.xlsx" > Sheet: Gudmundsson

Propeller efficiency iterative calculation with OpenVSP drag

Digital Appendix: AERO 490 > Report > Final report > Digital Appendix > Appendix AI > \Calculations Anthony.xlsx" > Sheet: OpenVSP

N Fuselage Structural Layout

Pitch axis bending moments

AERO 490 > Report > Final report > Digital Appendix >
Fuselage > \Bending moment.xlsx" > Sheet: Load diagram 3

Distributed Cargo Loads

AERO 490 > Report > Final report > Digital Appendix >
Fuselage > \Bending moment.xlsx" > Sheet: Floor beam sizing 2

Yaw axis bending moment

AERO 490 > Report > Final report > Digital Appendix >
Fuselage > \Bending moment.xlsx" > Sheet: Yaw Arrest

Roll axis torsional moment, ie roll arrest

AERO 490 > Report > Final report > Digital Appendix >
Fuselage > \Bending moment.xlsx" > Sheet: Roll Arrest

Longitudinal beams selection

AERO 490 > Report > Final report > Digital Appendix >
Fuselage > \Bending moment.xlsx" > Sheet: Longitudinal beams

Transversal beams selection

AERO 490 > Report > Final report > Digital Appendix >
Fuselage > \Bending moment.xlsx" > Sheet: Floor beam sizing 2

Strut selection

AERO 490 > Report > Final report > Digital Appendix >

Fuselage > \Bending moment.xlsx" > Sheet: Compression strut

Stringer selection

AERO 490 > Report > Final report > Digital Appendix >

Fuselage > \Bending moment.xlsx" > Sheet: Stringer sizing 3

Skin selection simplified

AERO 490 > Report > Final report > Digital Appendix >

Fuselage > \Bending moment.xlsx" > Sheet: All skin sizing

Skin selection Bruhn's method for curved panels

AERO 490 > Report > Final report > Digital Appendix >

Fuselage > \Bending moment.xlsx" > Sheet: Skin sizing corners

O Aft Fuselage and Cargo Door

Load summary

Digital Appendix: AERO 490 > Report > Final report > Digital Appendix >
Appendix Cargo Door + Aft Fuselage > \Loads.xlsx" > Sheet: Frame Loads

Cross-section analysis example

Digital Appendix: AERO 490 > Report > Final report > Digital Appendix > Appendix
Cargo Door + Aft Fuselage > \Loads.xlsx" > Sheet: Frame 6

Cargo door attachments Digital Appendix: AERO 490 > Report > Final report
> Digital Appendix >
Appendix Cargo Door + Aft Fuselage > \Loads.xlsx" > Sheet: Door

P Wing Structure

P.1 Wing Spar

REQUIREMENTS	Importance	T-beam	I-beam	Hollowed Square Beam	I-Beam (Spar Caps and web)	
I _x maximized to resist static and lift loads	1	4	2	3	1	
Manufacturability	3	2	3	4	1	
I _z to resist yawing moment	2	2	4	1	3	
Total		14	22	22	10	
Final Rank		2	3	3	1	

Figure P.1.1: Decision Matrix for spar cross-section

DECISION MATRIX FOR SPAR MATERIAL					
Selection Criteria	Rank	2024-T81	7075-T7	2224-T3	2324-T3
Elastic Modulus	5	2	1	4	3
Density	2	1	2	2	2
Fatigue strength	4	4	1	2	3
Fracture toughness	3	4	3	1	1
Environmental stability	6	4	3	1	2
Cost:Material and fabrication	1	1	4	2	3
Total		16	44	43	49
Material Properties of 2024-T81	NB: Changed to T81 for increased tensile yield strength				
Min Tensile yield strength	56000	psi			
Shear Strength	41000	psi			
Min compressive strength	57000	psi			
Elastic Modulus	10800000	psi			

Figure P.1.2: Decision Matrix for Spar Material Selection

Spar Materials			
	Front Spar	Mid spar	Rear spar
Web	2024 - T81	2024 - T81	2024 - T81
Spar cap	2024 - T81	2024 - T81	2024 - T81

Figure P.1.3: Material specification for the three spar components

P.1.0.1 Load and Moment distributions

[NB: The MATLAB codes used to create these loads were, unfortunately, lost due to a Hard-drive corruption.]

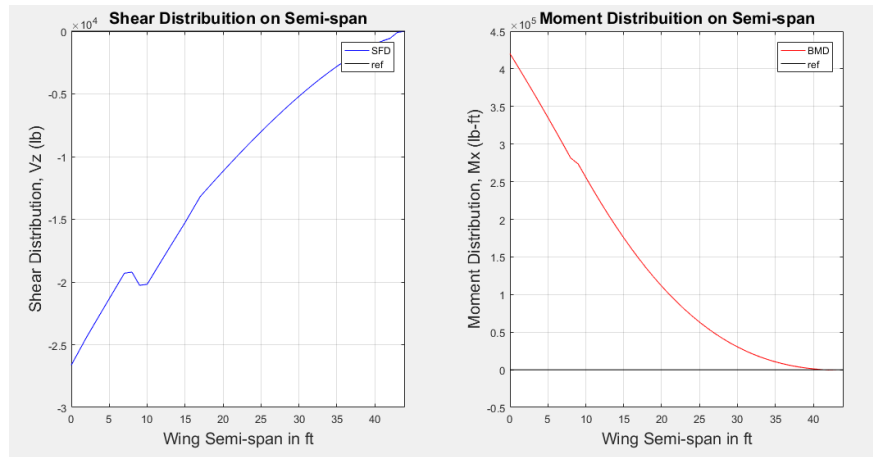


Figure P.1.4: Shear and Bending moment distribution about the fuselage station (M_x) of the Arctic Fox

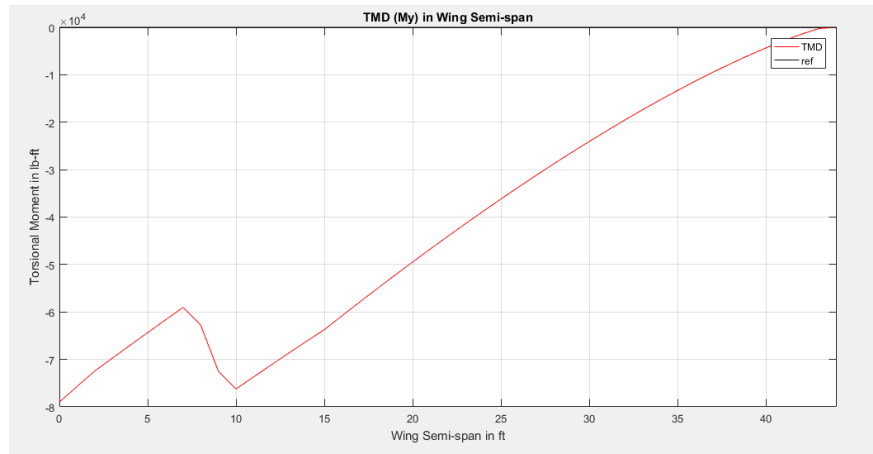


Figure P.1.5: Torsional moment (My) about buttline

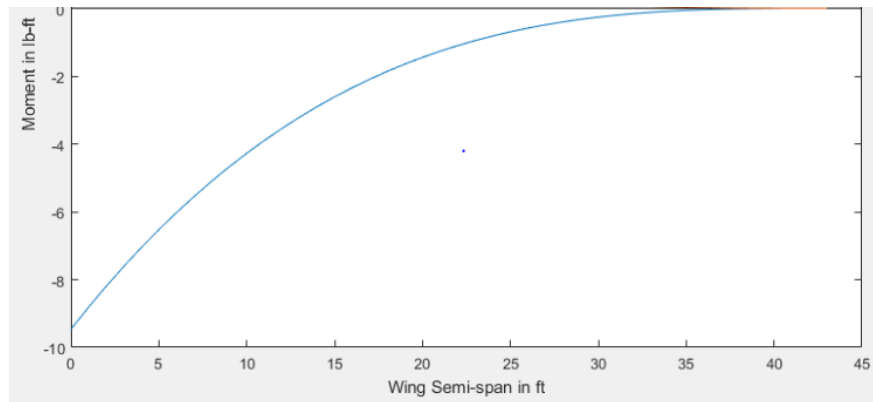


Figure P.1.6: Bending moment about waterline (M_z) (Reference at 50% of chord)

P.1.0.2 Load Envelopes

Digital Appendix: AERO 490 > Report > Final report > Digital Appendix >
Wing (Spar and Wing-fuselage attachment) > '\Loads.xlsx" >
Sheet: Load Envelopes

P.1.0.3 Load Cases Summary:

Digital Appendix: AERO 490 > Report > Final report > Digital Appendix >
Wing (Spar and Wing-fuselage attachment) > '\Loads.xlsx" >
Sheet: Load Summary

P.1.0.4 Spars

Digital Appendix: AERO 490 > Report > Final report > Digital Appendix >
Wing (Spar and Wing-fuselage attachment) > '\Loads.xlsx" > Sheet: Spars

P.1.0.5 Spar Optimization

Digital Appendix: AERO 490 > Report > Final report > Digital Appendix >
Wing (Spar and Wing-fuselage attachment) > '\Loads.xlsx" > Sheet: Spar Optimization

P.2 Lug Design Guidelines

- Important considerations
 - The design considers both the bolt or pin and the lug to be acting together since their structural integrity are dependent
 - The lugs be sized conservatively
 - A bushing is attached for rotational movement and transfer of loads
 - A minimum margin of safety of 20% for all lug sizing
- General

- Other guidelines are found in the digital appendix:

Digital Appendix: AERO 490 > Report > Final report >

Digital Appendix > Wing (Spar and Wing-fuselage attachment) >

\Loads.xlsx" > Sheet: Lugs Considerations

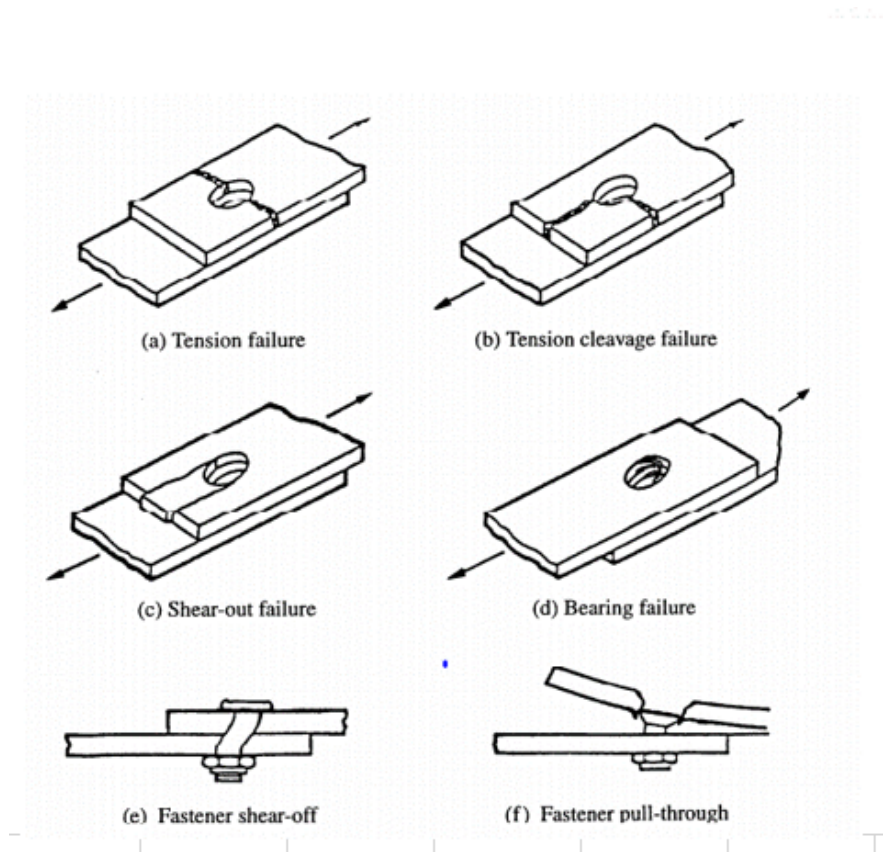


Figure P.2.1: Lug failure modes due to axial loading

P.3 Lug load cases, margin of safety for forward and aft-attachments

Aft Attach

- Digital Appendix: AERO 490 > Report > Final report >
- Digital Appendix > Wing (Spar and Wing-fuselage attachment) >
- \Loads.xlsx" > Sheet: Aft attach

Forward Attach

- Digital Appendix: AERO 490 > Report > Final report >
Digital Appendix > Wing (Spar and Wing-fuselage attachment) >
\Loads.xlsx" > Sheet: Forward attach

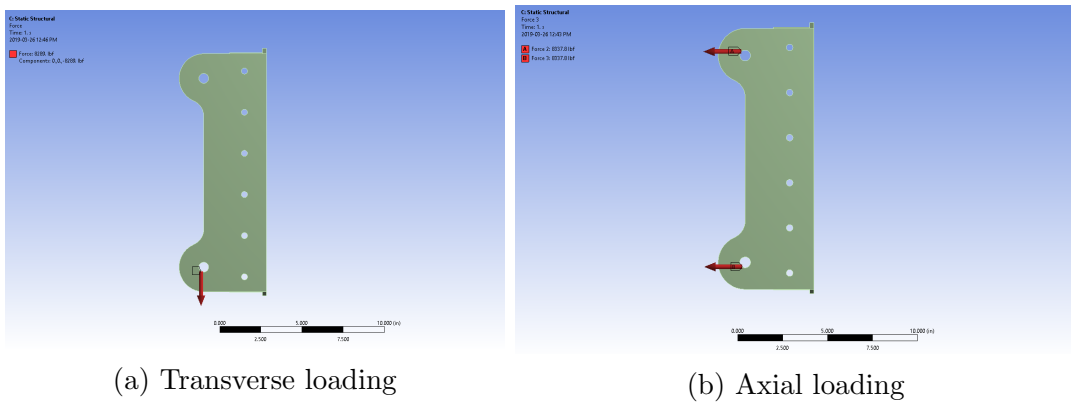


Figure P.3.1: Load Application on ANSYS

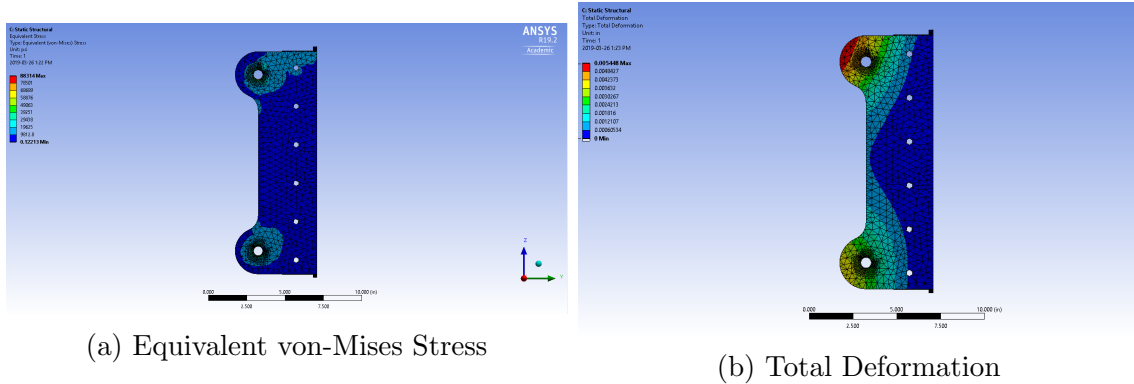


Figure P.3.2: ANSYS results for the Lug

P.4 Fasteners

Titanium Hi-Lok and Hi-shear fasteners were evaluated to be used for the lug attachments. The details of these evaluations can be found in the digital appendix.

Digital Appendix: AERO 490 > Report > Final report > Digital Appendix >
Wing (Spar and Wing-fuselage attachment) > \Loads.xlsx" >
Sheets: Hi Shear(Aft Attach), Hi Shear(Forward Attach)

P.5 Aileron Design

The ailerons must be designed for loads corresponding to airworthiness specifications as per CAR 525.349 [40]. Considerations such as the aileron effectiveness, aerodynamic and mass balancing, flap geometry, and maneuverability were taken into account. The flight phase category, aircraft class and the level of acceptability of the Arctic Fox are presented in the Digital Wing (Spar and Wing-fuselage attachment). The roll requirements of the aircraft were obtained and it defines that the Arctic Fox must achieve a bank angle of 30° in 1.8 seconds [21, ch. 12]. The main design constraints are the flap geometry and the location of the rear spar as these limit the aileron chord to 30%. This improves the structural integrity of the wings as both flaps and ailerons are held by the rear spar [21, p. 668]. After determining the aileron effectiveness, the rolling moment coefficient, and other design variables, the aileron position is at 67% to 97% of the wingspan. The maximum aileron deflection is at 20° and more design details can be found in the Digital Appendix.

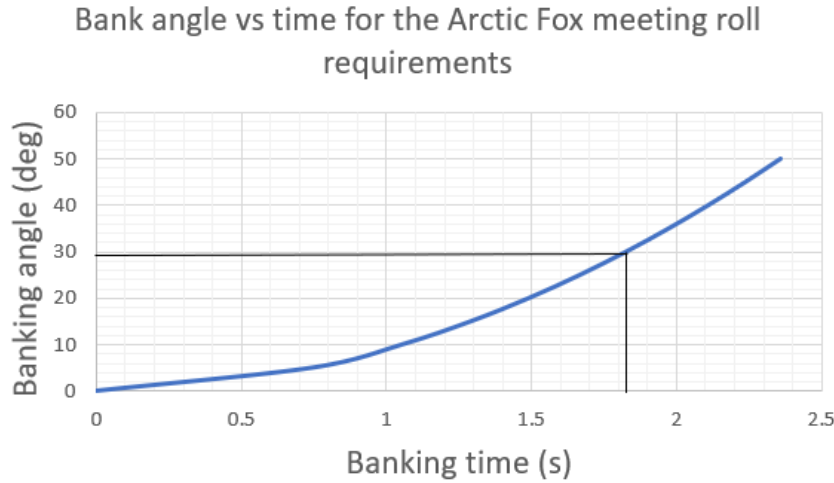


Figure P.5.1: Aileron Meeting roll requirement

More details of evaluation can be found in the design tool:

Digital appendix: AERO 490 > Report > Final report > Digital Appendix >
Wing (Spar and Wing-fuselage attachment) > Aileron

Q Wings (Ribs, skin and stringers)

**Rib and skin calculations using the method of buckling strength of flat sheet
in compression from Bruhn**

Digital Appendix: AERO 490 > Report > Final report > Digital Appendix >
Wing (Ribs, skin and stringers) > \Wing Box Calculations" >
Sheet: Ribs and Skin

Stringer spacing calculations

Digital Appendix: AERO 490 > Report > Final report > Digital Appendix >
Wing (Ribs, skin and stringers) > \Wing Box Calculations" >
Sheet: Stringers

Skin and stringers design validation calculations using the structural idealization method from Megson

Digital Appendix: AERO 490 > Report > Final report > Digital Appendix >
Wing (Ribs, skin and stringers) > \Wing Box Skin and Stringers" >
Sheet: Skin and Stringers

Rib cutouts design calculations

Digital Appendix: AERO 490 > Report > Final report > Digital Appendix >
Wing (Ribs, skin and stringers) > \Wing Box Skin and Stringers" >
Sheet: Cutouts

Stringers configuration trade study

Digital Appendix: AERO 490 > Report > Final report > Digital Appendix >
Wing (Ribs, skin and stringers) > \Wing Box Stringers Config" >
Sheet: Wing Box Stringers

R Center Wingbox

Load Summary

Digital Appendix: AERO 490 > Report > Final report > Digital Appendix >
Center wing-box>"wing-box" > Sheet: Load summary

Load Envelope

Digital Appendix:AERO 490 > Report > Final report > Digital Appendix >
Center wing-box>"wing-box" > Sheet: Load envelope

Spar Design

Digital Appendix:AERO 490 > Report > Final report > Digital Appendix >
Center wing-box>"wing-box" > Sheet: Spar Design

Skin and stringer design

Digital Appendix:AERO 490 > Report > Final report > Digital Appendix >
Center wing-box>"wing-box" > Sheet: Skin and Stringers

S Engine Mount Design

Load Type	Related Regulation	Load Factors
General	CAR 525.303	$n_{ultimate} = 1.5n_{limit}$
Maneuvering	CAR 525.337(b),(c)(1)	$n_{limit,positive} = +2.6$ $n_{limit,negative} = -1.0$
Side	CAR 525.363(a)(1)	$n_{limit,side} = 1.33$
Emergency landing (crash)	CAR 525.561(b)(3)	$n_{ultimate,upward} = 3.0$ $n_{ultimate,forward} = 9.0$ $n_{ultimate,sideward} = 3.0$ $n_{ultimate,downward} = 6.0$ $n_{ultimate,rearward} = 1.5$
Gust and Turbulence	CAR 525.333 CAR 525.341	$n_{ultimate,positive} = +4.41$ $n_{ultimate,negative} = -1.5$
Engine Torque	CAR 525.361(a)(2)	$n_{ultimate,torque} = 1.25$
Gyroscopic and Aerodynamic	CAR 25.371 CAR 25.331	-

Table S.0.1: Powerplant loads and airworthiness regulations [40]

Load Types and Related Regulations

Digital Appendix: AERO 490 > Report > Final report > Digital Appendix >
 Engine Mount > \Engine Mount Load Analysis" >
 Sheet: \Structure Requirements"

Parameters and Assumptions

Digital Appendix: AERO 490 > Report > Final report > Digital Appendix >
 Engine Mount > \Engine Mount Load Analysis" >
 Sheet: \Parameters/Assumptions"

Load Calculations

Digital Appendix: AERO 490 > Report > Final report > Digital Appendix >
 Engine Mount > \Engine Mount Load Analysis" >

Sheet: \Load Case Matrices"

FEA Results

Digital Appendix: AERO 490 > Report > Final report > Digital Appendix >
Engine Mount > \Engine Mount Load Analysis" >
Sheet: \FEA Results"

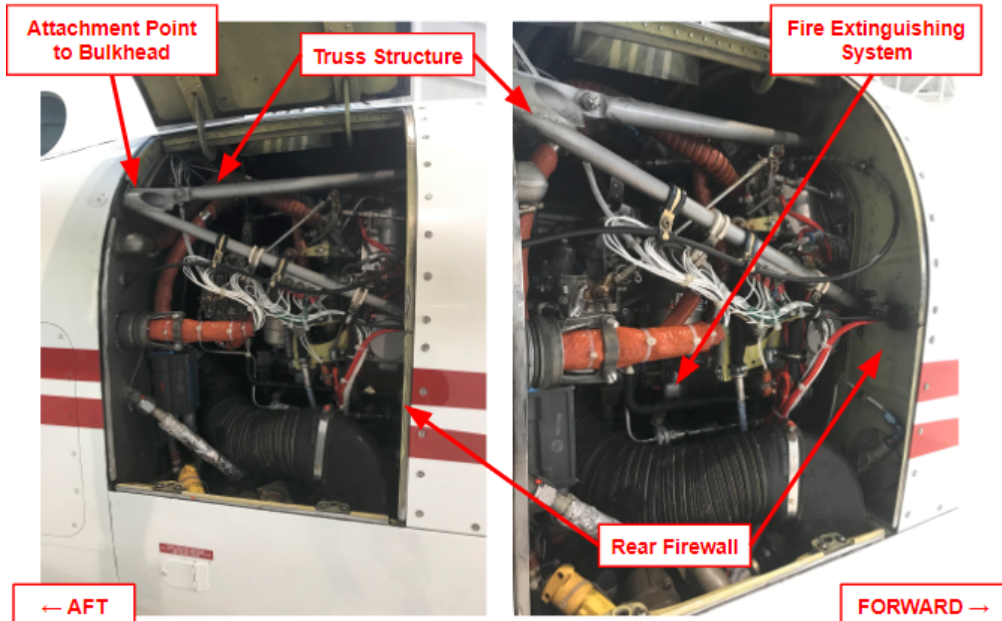


Figure S.0.1: Beechcraft King Air Engine Mount Survey

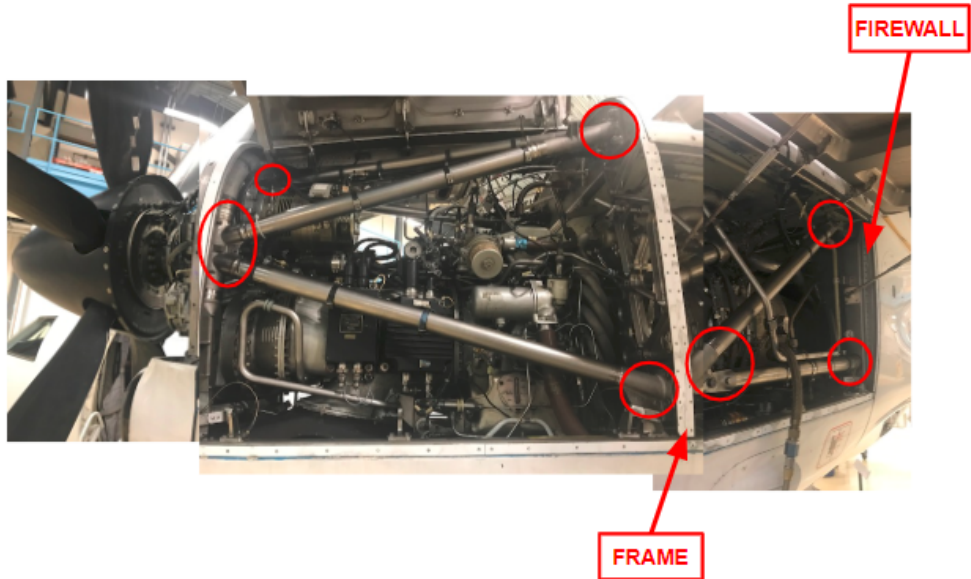


Figure S.0.2: Dornier 328 Engine Mount Survey

T Empennage

T.1 Vertical Tail

Vertical Tail Specifications	Value	Rudder Specification	Value
Root Chord [ft]	12.15	Root Chord Percentage [%]	25
Tip Chord [ft]	4.04	Tip Chord Percentage [%]	25
Span [ft]	12.36	Span Percentage [%]	90
Area [ft ²]	104	Rudder Area [ft ²]	22.87
Sweep Angle [deg]	33		

Table T.1.1: Vertical tail and rudder specifications

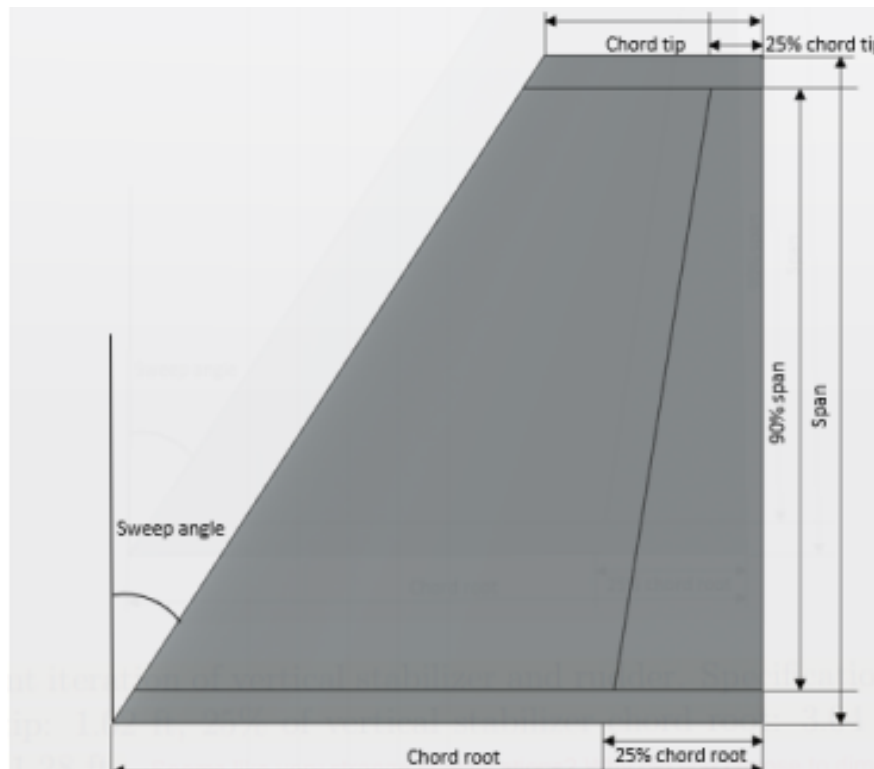


Figure T.1.1: Vertical Stabilizer

The area of the vertical tail was calculated after determining the appropriate moment arm was established with respect to the directional stability. Using equation T.1, and a

volume coefficient of 0.06, the vertical tail area was determined. More information and the sizing of the vertical tail and the volume coefficient is shown in Master sizing file.

$$C_{vt} = \frac{L_{vt}S_{vt}}{b_w S_w} \quad (\text{T.1})$$

The chord and span percentage of the rudder was using recommendations from a method outlined in *A conceptual Approach* by Daniel P.Raymer. The rudder sizing was also checked to meet the deflection requirements needed for the takeoff phase. More details on the deflection and how the rudder was analyzed for the take off phase is in the hinge moment rudder excel sheet.

T.2 Horizontal Tail

Horizontal Tail Specifications	Value	Elevator Specification	Value
Root Chord [ft]	6.35	Root Chord Percentage [%]	30
Tip Chord [ft]	5.73	Tip Chord Percentage [%]	30
Span [ft]	32	Span Percentage [%]	95
Area [ft ²]	190	Elevator Area [ft ²]	22.87
Sweep Angle [deg]	4		

Table T.2.1: Horizontal tail and elevator specifications

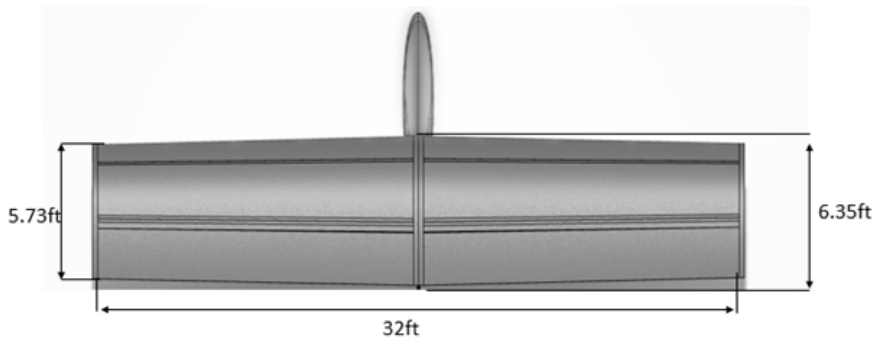


Figure T.2.1: Horizontal Stabilizer

The final revision was reached after the design review which concluded the problems of the 10th iteration. The main problem of the previous revision was that only the span was increased in order to obtain the span area requested by stability. A sanity check was

done with the DHC-7 that comparing the specs of our aircraft, the horizontal tail was still too small. With later research, it is found that tapering the stabilizer comes with trade offs between structural merit and resistance to tip stall. A large sweep angle is not needed as the effect of delaying the shockwaves and accompanying the aerodynamic drag rise caused by fluid compressibility only happens at supersonic speed. The aircraft will cruise at 0.4 Mach number meaning the sweep angle will not affect the drag which will not improve the performance expected from the horizontal stabilizer.

After the final change on the horizontal stabilizer, the elevators were sized similarly to the rudder in terms of percentage of chord and span. However, after checking with flight testing, it was suggested to increase the elevators chord percentage to 35 which increased the elevator authority. Improvement in takeoff distance was found as it was needed for short runways. The final design was checked with static stability in pitch.

T.3 T-Tail Trade Study

Customer Need	Rank	Functional Requirements
Operator Return on Investment	1	Low Maintenance Costs
Manufacturer Return on Investment	5	Low Manufacturing Costs
Development Time	1	Simplistic structural design
		Shall use TSO (technical standard order) aviation components
Operational Reliability/Safety	3	Provide stability
		Provide trim
		Structural reliability

Table T.3.1: Ranking Customer Needs

HOQ2	Low Maintenance Costs	Low Manufacturing Costs	Simple Structural Design	Stall recoverability	Provide stability	Provide trim	Provide control	Lightweight design
Operator Return on Investment	9	1	3	1	3	3	3	3
Manufacturer Return on Investment	0	9	3	1	3	3	3	3
Development Time	1	1	9	3	1	1	1	3
Operational Reliability/Safety	0	0	9	9	9	9	9	1
Total	10	47	54	36	46	46	46	24
Importance	3.2%	15.2%	17.5%	11.7%	14.9%	14.9%	14.9%	7.8%

Table T.3.2: HOQ2

#	Functional Requirements	Importance score	Conventional	T-tail	Cruciform	H-tail
1	Low Maintenance Costs	3.24%	BASELINE	-	-	-
2	Low Manufacturing Costs	15.21%		-	-	-
3	Simple Structural Design	17.48%		s	s	-
4	Stall recoverability	11.65%		s	s	s
5	Provide stability	14.89%		+	s	s
6	Provide control	14.89%		+	s	s
7	Provide trim	14.89%		s	s	s
8	Lightweight design	7.77%		-	-	-
		100.00%	Total Plus	2	0	0
			Total Minus	3	3	4
			Weighted Score	3.560	-26.214	-43.689

Table T.3.3: Pugh Matrix and Selecting T-Tail Configuration

T.4 Hinge FEA

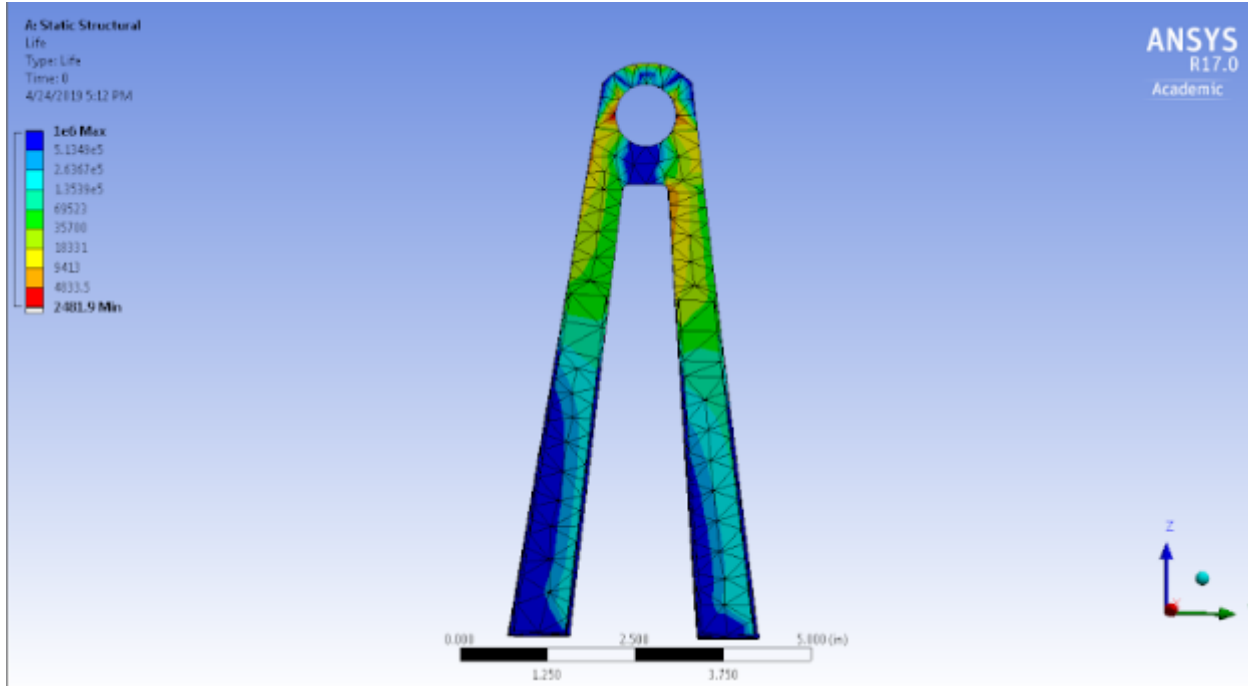


Figure T.4.1: Fatigue life of Hinge with 2666lbf load in tension

T.5 Digital Appendices

Empennage Dimensions and Justifications

Digital Appendix: AERO 490 > Report > Final report > Digital Appendix >
Empennage > \Empennage Specifications"

Lug Analysis and Margin of Safety

Digital Appendix: AERO 490 > Report > Final report > Digital Appendix >
Empennage > \Lug Analysis" > Sheet: Lug Analysis

Fatigue Analysis on Hinge

Digital Appendix: AERO 490 > Report > Final report > Digital Appendix >
Empennage > \Fatigue Analysis " > Sheet: Fatigue

Hinge moments and angle of deflection and Sideslip

Digital Appendix: AERO 490 > Report > Final report > Digital Appendix >
Empennage > \Hinge moment for Rudder " > Sheet: Asymmetric Thrust

Kinematic Simulation for the rudder

Digital Appendix: AERO 490 > Report > Final report > Digital Appendix >
Empennage > \Kinematic Simulation 1 "

Empennage Sizing Information

Digital Appendix: AERO 490 > Report > Final report > Digital Appendix >
Empennage > \Master Sizing File "

FEA model

Digital Appendix: AERO 490 > Report > Final report > Digital Appendix >
Empennage > "FEA HINGE V6"

U Wind Tunnel Testing

Wind tunnel procedure

Digital Appendix: AERO 490 > Report > Final report > Digital Appendix >
Wind Tunnel Testing > \Wind Tunnel Testing Procedure.pdf"

Wind tunnel icing test video

Digital Appendix: AERO 490 > Report > Final report > Digital Appendix >
Wind Tunnel Testing > \Wind Tunnel Complete Icing Test - Video"

V Nacelle Aerodynamics

In order to validate the nacelle aerodynamic profile in level cruise flight, CFD simulations of a full wing with and without nacelle were performed using ANSYS Fluent at different wing incidences to determine the effect of the nacelle on the lift of the wing. The results of the simulations along with the full wing with nacelle calculations are illustrated in Table V.0.1.

Wing incidence (degree)	C_L full wing without nacelle (simulated)	C_L inboard wing without nacelle (simulated)	C_L inboard wing with nacelle (simulated)	C_L full wing with nacelle (calculated)
0	0.370	0.427	0.338	0.321
1	0.444	0.506	0.429	0.402

Table V.0.1: CFD Results

All simulations were made with inviscid air at a velocity of 397 ft/s, density of 0.001756 slugs/ft³ and temperature of 238.25°K, which are the cruising conditions in standard atmospheric conditions. The mesh size was set to “fine” for all simulations with an added condition of 0.01 ft element size on every surfaces of the wing and nacelle. The use of the inviscid assumption and the specified mesh size were validated for low angle of attack from the wind tunnel wing testing presented in section 5.5.2.

Due to a lack of computing power, the full wing with a nacelle was not simulated, only the inboard portion of 20 feet where the nacelle is situated. The entire wing simulations showed the expected elliptical lift distribution and the inboard wing simulations showed a constant lift distribution along the span. In order to determine the full wing lift with a nacelle, simulations of the inboard wing section were created with and without the nacelle to allow for a substitution of the lift contribution of the inboard wing on the full wing lift.

The drag effect of the nacelle on the wing was not computed, since the main drag contributor on a turboprop aircraft wing is the propeller, whereas the lift contribution by the propeller is limited to a change of less than 5% [84]. Simulations with the propeller were not made during the preliminary design, but would be the next step in the nacelle aerodynamic design. The simulation of the nacelle without a propeller still showed the effect of the 1 foot

diameter stagnation point on the flow around the nacelle, as illustrated by the streamlines aft of the nacelle in the figure below.

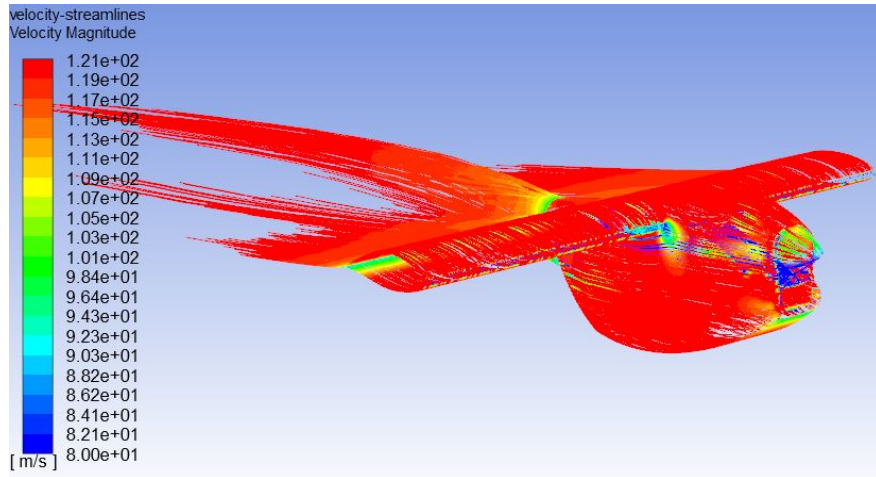


Figure V.0.1: Flow around the Nacelle

Pictures of simulation results are available in the digital appendix.

ANSYS Fluent Full Wing Results

Digital Appendix: AERO 490 > Report > Final report > Digital Appendix >
Nacelle Aerodynamics > Full wing CFD

ANSYS Fluent Inboard Wing Results

Digital Appendix: AERO 490 > Report > Final report > Digital Appendix >
Nacelle Aerodynamics > Inboard wing CFD

ANSYS Fluent Nacelle Results

Digital Appendix: AERO 490 > Report > Final report > Digital Appendix >
Nacelle Aerodynamics > Nacelle CFD[

W Anti-Icing

W.1 Wind Tunnel Testing

Wind tunnel specimen NACA 0018

➤ Airfoil thickness	0.262 ft
➤ Airfoil chord	1.458 ft
➤ Span	3.000 ft
➤ Heated area	1.601 ft ²



Figure W.1.1: Wind Tunnel Testing Specimen

Icing wind tunnel testing conditions:

- Temperature: -10°C
- Flowstream velocity: 18.4 m/s
- Nozzles
 - Water pressure at the nozzle: 114.3 psi
 - Number of nozzles: 4
 - Distance between nozzles: 0.9 m
 - Distance from Airfoil: 4.55 m
 - Spray angle: 90°

Pressure (psi)	30	40	60	100	200	300	500	700	1000
Flow rate (gallons/hour)	6.9	8.0	9.8	12.6	17.9	22	28	33	40

Table W.1.1: Nozzle Flow rate

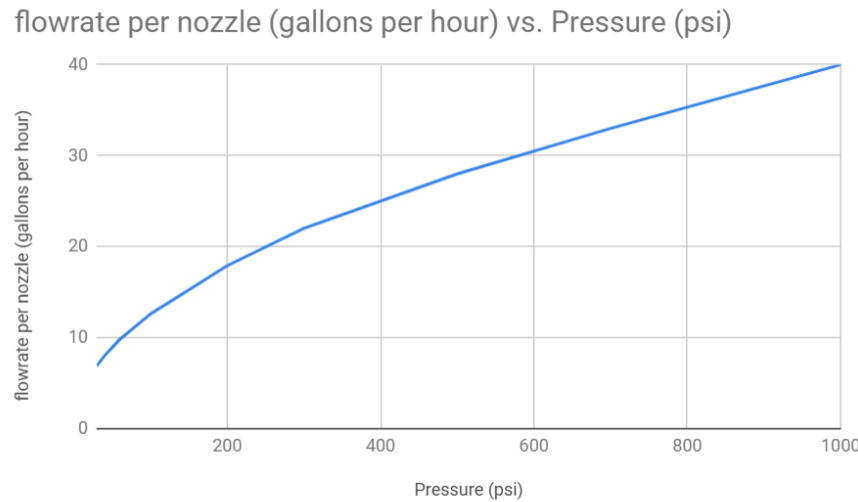


Figure W.1.2: Nozzle Flow rate graph

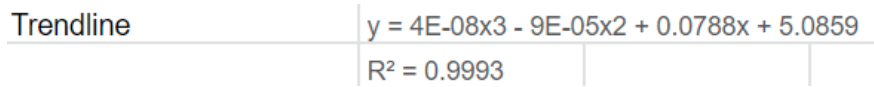


Figure W.1.3: Nozzle Flow rate trendline

Interpolated flow rate at 114.3 psi is 12.92 gallons/hour/nozzle which is equivalent to 0.0136 Kg/s/nozzle, or a total of 0.05425 Kg/s.

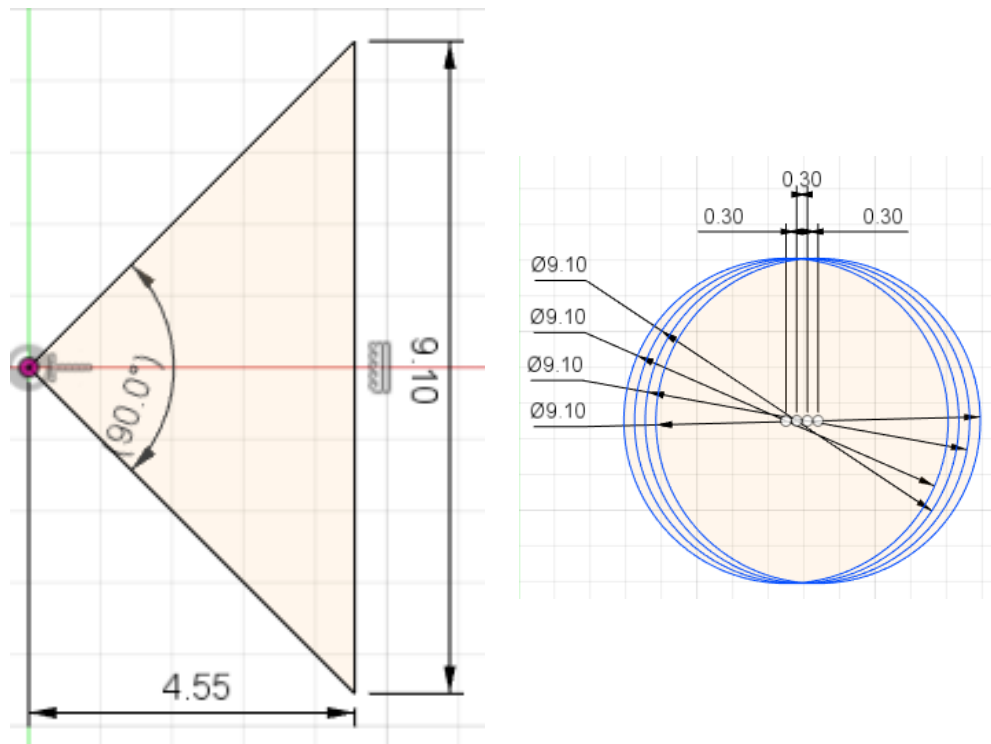


Figure W.1.4: Nozzle Spray Area

The total spray area at 4.55 m away from the nozzles is 39.59 m². The total frontal area of the airfoil is 0.406 m². Therefore, only 1.02% of the water flowing out of the nozzles actually intersects the airfoil. The total water catch rate is 0.0005569 Kg/s.

W.2 Convective heat transfer coefficient determination

To estimate the convective heat transfer coefficient, the Nusselt number is required. $Nu = h \frac{L}{k}$. However, the Nusselt number is still unknown. The Churchill-Bernstein equation can be used to find the Nusselt number for a cylinder with its axis perpendicular to the flow. The leading edge is assumed to be a cylinder. Although this may introduce some error in the determination of the convective heat transfer coefficient, wind tunnel testing will determine if this method is feasible.

$$Nu = 0.3 + \frac{\left(0.62 \cdot Re_d^{(\frac{1}{2})} \right) \cdot Pr^{(\frac{1}{3})}}{\left(1 + \left(\frac{0.4}{Pr}\right)^{(\frac{2}{3})}\right)^{(\frac{1}{4})}} \cdot \left(1 + \left(\frac{Re_d}{282000}\right)^{(\frac{5}{8})}\right)^{(\frac{4}{5})}$$

Figure W.2.1: Churchill-Bernstein equation

Using the two previous equations, the convective heat transfer transfer coefficient can be estimated.

W.3 Total water catch rate determination

The total amount of water caught by the airfoil can be determined using the following equation from AGARD advisory report No. 127

$$W_c = 0.38 V (\cos \Lambda) E_m (H/C) (C) \omega$$

Figure W.3.1: Water catch rate equation

where:

- W_c : Total water catch rate (lb/hr*ft*span)
- V : Free stream velocity (knots)
- Λ : Airfoil sweep angle (degrees)
- E_m : Total water catch efficiency
- H : airfoil projected height (ft)
- C : Chord (ft)
- ω : Cloud liquid water content (g/m^3)

From the same document, E_m is estimated to be 0.8 along the wing and reducing to lower than 0.5 when getting closer to the root. For our wind tunnel test, we had no root, just a section of wing and assumed the value of 0.8 throughout.

Anti icing heat transfer model

Digital Appendix: AERO 490 > Report > Final report > Digital Appendix >
Anti-icing > \Anti icing heat transfer model"

X Environmental Control System

X.1 Regulations for oxygen concentration for unpressurized aircraft

- CAR 605.31
- CAR 605.32
- FAR 25

X.2 Regulations for the use of refrigerants on aircraft

Federal Halocarbon Regulation, 2003; Installation, Servicing, Leak Testing and Charging
(16)

Digital Appendix: AERO 490 > Report > Final report > Digital Appendix >
ECS > SOR-2003-289

Digital Appendix: AERO 490 > Report > Final report > Digital Appendix >
ECS > Canada Gazette Part 2

X.3 Weather conditions in summer

- Rankin Inlet
 - Average high : 20°C
 - Average low: 7°C
 - Wind speed: 40 to 70 km/h
- Arviat
 - Average high : 24°C
 - Average low: 7°C
 - Wind speed: 35 to 58 km/h
- Iqaluit
 - Average high : 19°C
 - Average low: 0°C
 - Wind speed: less than 31km/h
- Arctic Bay
 - Average high : 4°C

- Average low: -0.5°C
- Wind speed: less than 31km/h

X.4 Weather conditions in winter

- Rankin Inlet
 - Average high : -28.2°C
 - Average low: -35.5°C
 - Wind speed: 40 to 70 km/h
- Arviat
 - Average high : -26°C
 - Average low: -34°C
 - Wind speed: 35 to 58 km/h
- Iqaluit
 - Average high : -24°C
 - Average low: -32°C
 - Wind speed: less than 31km/h
- Arctic Bay
 - Average high : -32°C
 - Average low: -41°C
 - Wind speed: less than 31km/h

X.5 Assumptions

- Fuselage modeled as flat plate
- Isothermal flow over fuselage
- Aircraft cruise speed is below the compressibility of air, $Ma = 0.3$
- Specific heat of air is at ambient temperature
- No passengers on board, recirculation permitted for cargo bay and avionics.

X.6 Heat Transfer

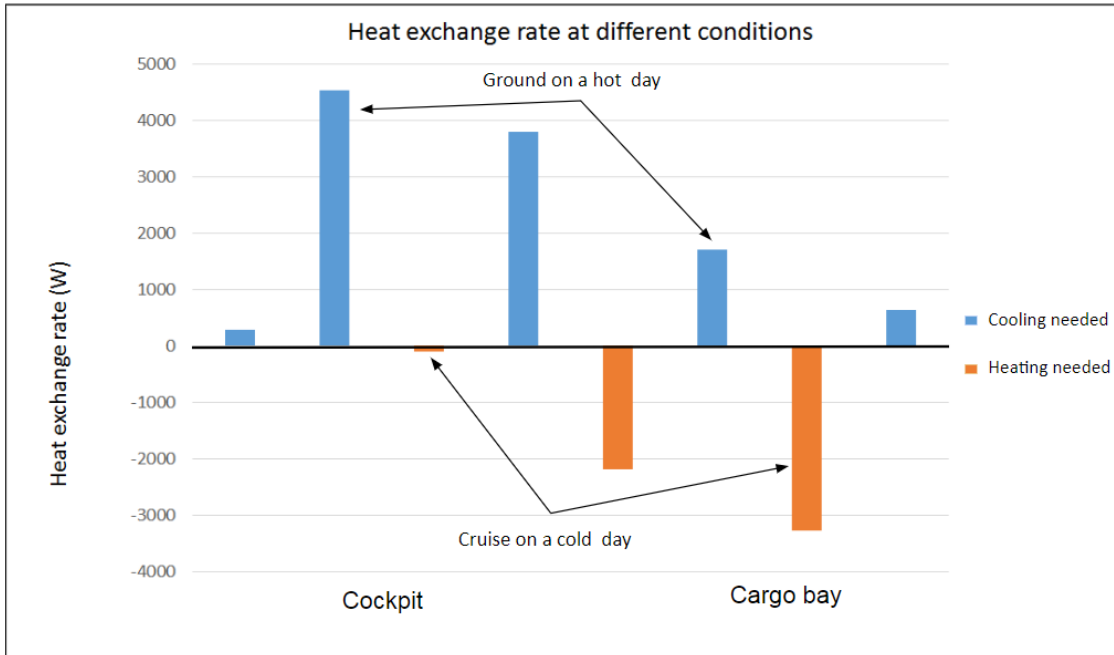


Figure X.6.1: Bar diagram demonstrating the heat transfer loads at different operating conditions

Heat Transfer loads

Digital Appendix: AERO 490 > Report > Final report > Digital Appendix > ECS > ECS.xlsx

ACM sheet is the air cycle machine calculation for the required work input to the compressor if using ambient air.

X.7 Heating with resistive electric elements:

When trying to keep the cargo bay or cockpit at a steady temperature, it is more efficient to simply maintain the temperature with small addition or removal of heat energy. Therefore, according to the critical heating conditions determined, shown in the bar diagram of the heat transfer loads, to maintain the cargo bay at constant temperature of 4 degree Celsius, the resistive electric element required is 3 kW. However, the cockpit requires heating as well, which would require a second heating element of 3 kW since these are the lowest standard heating elements.

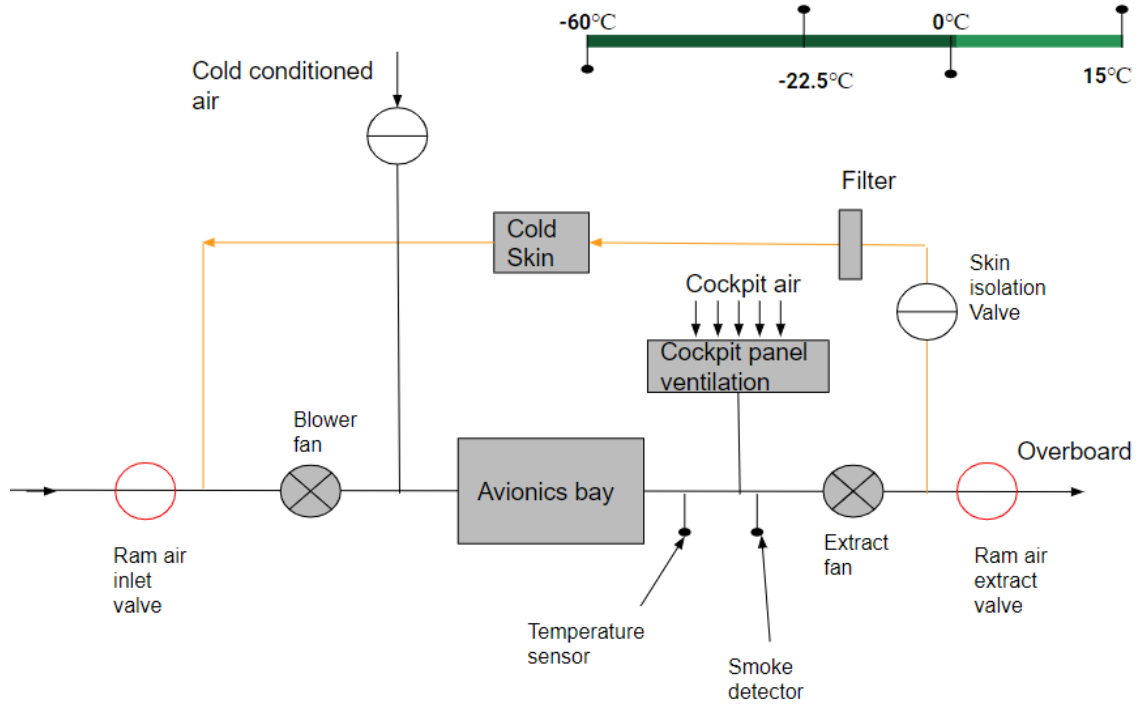


Figure X.7.1: Thermal management diagram of the avionics bay for the Arctic Fox

Y Hydraulic System

REGULATIONS USED

Canadian Aviation Regulations, 5 C.A.R. 525.735 (2019)

Canadian Aviation Regulations, 5 C.A.R. 525.1435 (2019)

FEARED EVENTS AND FAILURE RATES IN ACTUATION

Digital Appendix: AERO 490 > Report > Final report > Digital Appendix >
Hydraulic System > F.E&F.R.A

HYDRAULIC SYSTEM COMPONENTS & SKYDROL PROPERTIES

Digital Appendix: AERO 490 > Report > Final report > Digital Appendix >
Hydraulic System > H&S

LANDING DISTANCE RESULTS (Braking Distance with Brakes Vs. No Brakes)

Digital Appendix: AERO 490 > Report > Final report > Digital Appendix >
Landing Performance > LDR

FHO DEVELOPMENT AND EMERGENCY PROCEDURE

Digital Appendix: AERO 490 > Report > Final report > Digital Appendix >
Hydraulic System > FHO

Z Fuel System

Fuel level sensor datasheet

Digital Appendix: AERO 490 > Report > Final report > Digital Appendix >
Fuel System > \Fuel_Level_EN"

Fuel transfer pump datasheet

Digital Appendix: AERO 490 > Report > Final report > Digital Appendix >
Fuel System > \DS600-24A Type 6902 Fuel Transfer Pump Jaguar"

Fuel boost pump datasheet

Digital Appendix: AERO 490 > Report > Final report > Digital Appendix >
Fuel System > \DS600-9A_Type8810 Fuel Boost Pump A330 340"

AA Avionics



Figure AA.0.1: Arctic Fox instrument panel

Number	Name	Function
(1)	Primary Flight Display	Display flight data, i.e.: altitude, airspeed, vertical speed etc.
(2)	Multi-Function Display	Display external information, i.e.: weather information, map detail, obstacles with above ground level (AGL) and mean sea level (MEL)
(3)	Multi-Function Display	Display information on aircraft performance, i.e.: engine instrument, fuel capacity, etc.
(4)	Transponder	Receive and transfer radio signal with ADS-B
(5)	Power Panel	Power control panel for the electrical system on board
(6)	Annunciator Panel	Warning system
(7)	Traffic Collision Avoidance System	Avoid collision
(8)	Autopilot	Autopilot control panel
(9)	Radar Altimeter	Backup altimeter
(10)	Throttle	Throttle control
(11)	Compass	Backup magnetic compass
(12) (From top to bottom)		
	Aileron Trim Indicator	Give indication of the servo output shaft position
	Rudder Trim Indicator	Give indication of the servo output shaft position

Number	Name	Function
(13) (From top to bottom, left to right)		
	Fuel Gauge	Backup fuel gauge
	Elevator Trim Indicator	Give indication of the servo output shaft position
	Light/Diode	Landing gear warning light
	Landing Gear Up Switch	Switch to retract landing gear
	Landing Gera Down Switch	Switch to lower the landing gear
	Flap Control	Flap control switch
	Elevator Trim	Elevator control
	Aileron Trim	Aileron control
(14) (From top to bottom)		
	Airspeed Indicator	Backup airspeed indicator
	Attitude Indicator	Backup attitude indicator
	Altimeter	Backup altimeter
(15) (From top to bottom)		
	Directional Gyro	Backup gyro
	Turn Coordinator	Backup turn coordinator
	VOR/LOC Indicator	Backup VOR indicator
	Vertical Speed Indicator	Backup vertical speed indicator
(16) (From top to bottom, left to right)		
	Outside Air Temperature	Backup outside air temperature indicator
	Cockpit Voice Recorder	Cockpit voice recorder
	Gyro Vacuum/Suction	Backup gyro vacuum
	Flight Data Recorder	Flight data recorder
	Rudder Trim	Rudder control

Table AA.0.1: Arctic Fox panel, instrument list

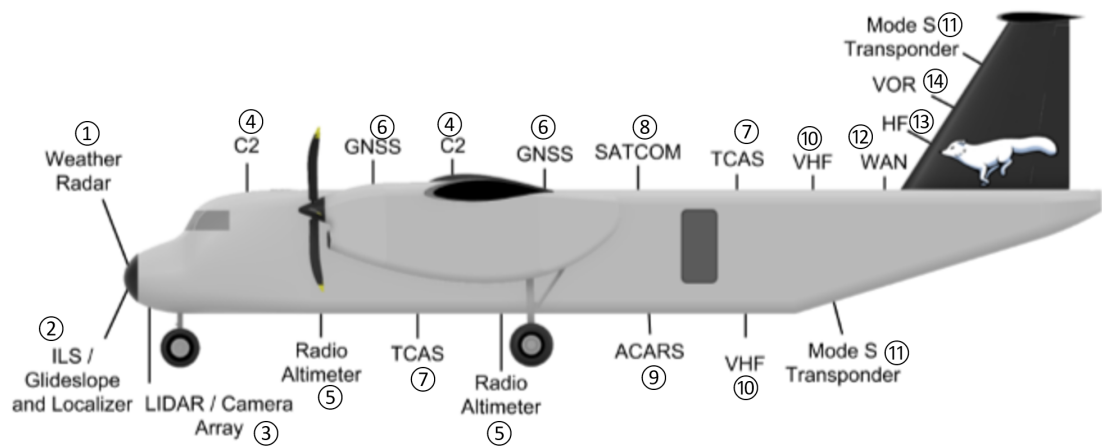


Figure AA.0.2: Arctic Fox installed antennas

Number	Name	Function
①	Weather Radar	Detect weather condition in the way
②	ILS Glideslope and Localizer	Detect runway location in the airport
③	Lidar/Camera Array	Detect wind, turbulence, model terrain
④	Command and Control	A type of the air traffic control radar beacon system (ATCRBS), communicating with the ATC to enhance surveillance radar monitoring and separation of air traffic.C2 use Gray code to encode the altitude information. The altitude transmitted is pressure altitude, and corrected for altimeter setting at the ATC facility. If no encoder is attached, the transponder may optionally transmit only framing pulses
⑤	Radio Altimeter	Measures altitude above the terrain
⑥	Global Navigation Satellite System	Detect aircraft location(latitude, longitude and altitude)
⑦	Traffic Collision Avoidance System	Monitor the airspace around the aircraft, to reduce the incidence of mid-air collisions between aircraft
⑧	Satellite Communications	Serve as a communication channel to transmit and receive telecommunications signals along with the amplifies radio
⑨	Aircraft Communications Addressing and Reporting System	A digital data-link system for transmission of short messages between aircraft and ground stations via Airband radio or satellite
⑩	Very High Frequency Radio	Short range communicate with air traffic control and aid to locate the location of the receiving station
⑪	Mode S Transponder	Transmit and receive device, facilitates TCAS, reducing channel congestion by ignoring interrogations not addressed with their unique identity code
⑫	Wide Area Network	Telecommunications network for computer networking
⑬	High Frequency Radio	Long-distance communicate with air traffic control and aid to locate the location of the receiving station
⑭	VHF Omnidirectional Range	Short-range radio navigation system, enabling aircraft with a receiving unit to determine its position and stay on course by receiving radio signals transmitted by a network of fixed ground radio beacons

Table AA.0.2: Arctic Fox list of installed antennas

AB Autonomous Route Revision system for Icing Avoidance



Figure AB.0.1: X-Plane Simulation: One waypoint - enough fuel - low icing severity



Figure AB.0.2: X-Plane Simulation: Two waypoints - enough fuel - high icing severity

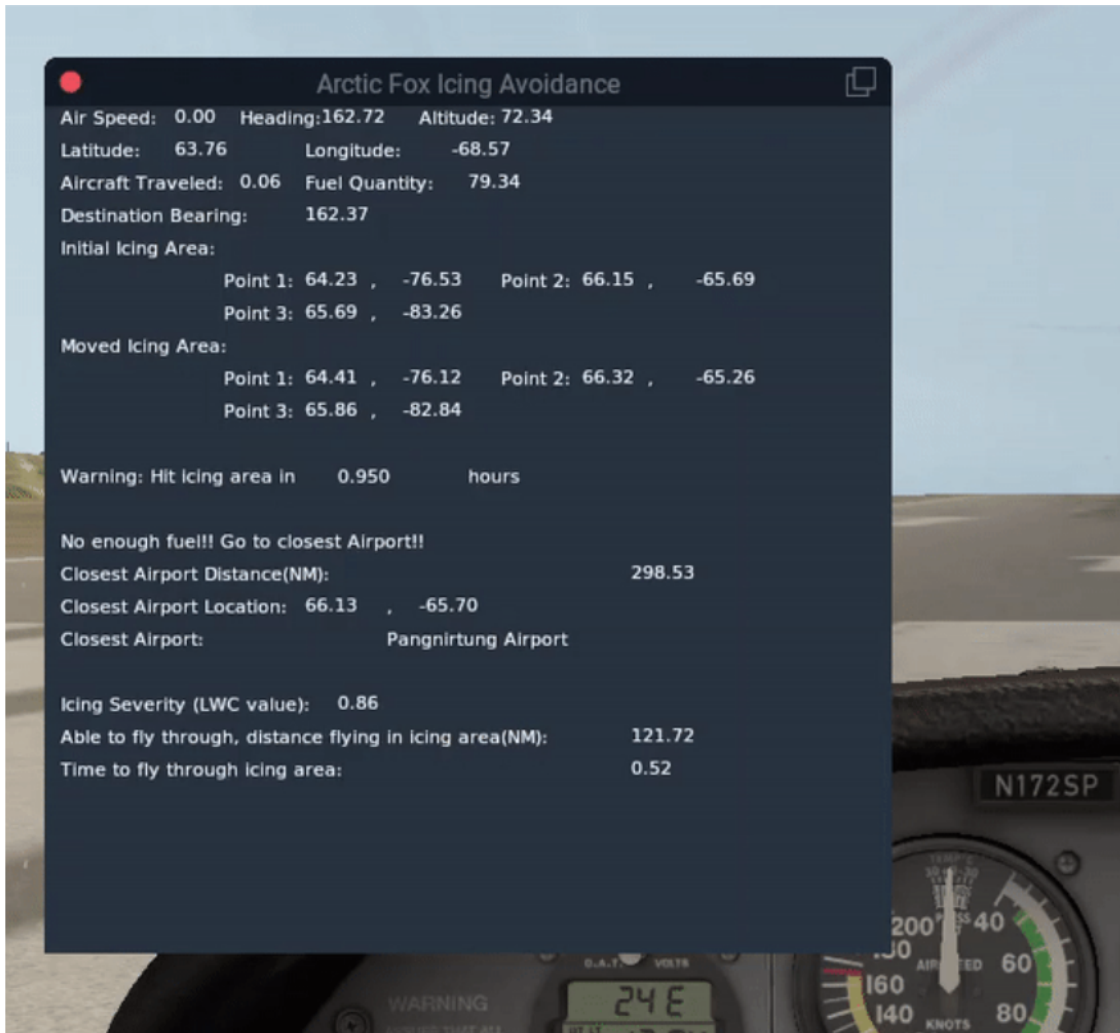


Figure AB.0.3: X-Plane Simulation: Not enough fuel

Video demonstration on X-Plane

Digital Appendix: AERO 490 > Report > Final report > Digital Appendix >
Icing Avoidance >X-Plane demonstration

Code for X-Plane plugin (The scenario in the provided source code is two waypoint generation with high icing severity.)

Digital Appendix: AERO 490 > Report > Final report > Digital Appendix >
Icing Avoidance >Software source code

AC Stability

$$\begin{bmatrix} X_u & X_w & 0 & -g \\ Z_u & Z_w & u_0 & 0 \\ M_u + M_{\dot{w}}Z_u & M_w + M_{\dot{w}}Z_w & M_q + M_{\dot{w}}u_0 & 0 \\ 0 & 0 & 1 & 0 \end{bmatrix}$$

Figure AC.0.1: State-Space Longitudinal Motion Matrix

The related characteristic equation is

$$\lambda^4 + 5.05\lambda^3 + 13.2\lambda^2 + 0.67\lambda + 0.15 = 0$$

Resulting in 2 set of answers (short period and phugoid) in the following form:

$$\lambda = \text{real part} \pm \text{imaginary part}$$

$$\text{Damping ratio} = \text{real}/(\text{real}^2 + \text{imaginary}^2)^{1/2}$$

$$\text{Undamped natural freq.} = (\text{real}^2 + \text{imaginary}^2)^{1/2}$$

(solved using exact method with MATLAB)

where,

Longitudinal Derivatives:

u_0 = cruise speed, 395 ft./s

$$Q = \frac{1}{2} \rho u_0^2$$

$$X_u = -(2C_{D0}) \cdot \frac{QS}{mu_0}$$

$$X_w = -(C_{D\alpha} - C_L) \cdot \frac{QS}{mu_0}$$

$$Z_u = C_{zu} \cdot \frac{QS}{mu_0}$$

$$Z_w = -(C_{L\alpha} + C_{D0}) \cdot \frac{QS}{mu_0}$$

$$Z_\alpha = u_0 \cdot Z_w$$

M_u is assumed 0 for small change

$$M_q = u_0 \cdot M_w$$

$$M_w = C_{m\alpha} \cdot \frac{QS}{u_0 I_y} \cdot \text{wing chord}$$

$$M_{\dot{w}} = C_{m\alpha} \cdot \frac{QS}{2u_0^2 I_y} \cdot \text{wing chord}^2$$

Approximate method to evaluate the undamped natural frequency and damping ratio:

Short Period:

$$\text{Undamped nat. freq.} = (Z_w M_q - u_0 M_w)^{1/2}$$

$$\text{Damping ratio} = M_q + u_0 M_{\dot{w}} + Z_w$$

Longitudinal Stability Coefficients:

$$C_{D0} = \frac{T}{W} - \frac{\frac{2KW}{\rho \sigma V_{cruise}^2 S}}{\rho_0 V_{cruise}^2 \frac{S}{2W}}$$

$$K = \frac{1}{\pi e A R}$$

$$C_{D\alpha} = 2K C_L C_{L\alpha}$$

$$C_{zu} = -(M^2/1 - M^2) CL_0 - 2C_{L0}$$

$$C_{L\alpha} = \text{wing airfoil lift curve, } 5.4[1/rad]$$

$$C_{L\alpha t} = \text{tail airfoil lift curve, } 4.8[1/rad]$$

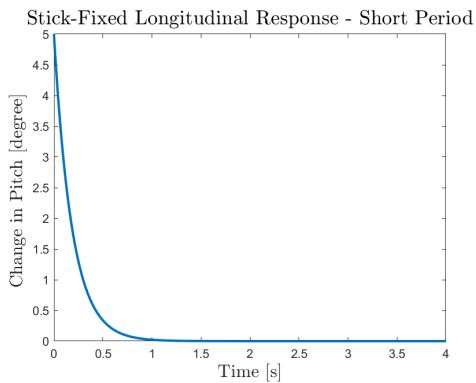
$$C_{zq} = -2C_{L\alpha t} V_H$$

$$C_{m\alpha} = C_{L\alpha} \frac{(X_{cg} - X_{ac})}{\text{chord}} + C_{m,fus} - V_H C_{L\alpha t} (1 - \frac{d\epsilon}{d\alpha})$$

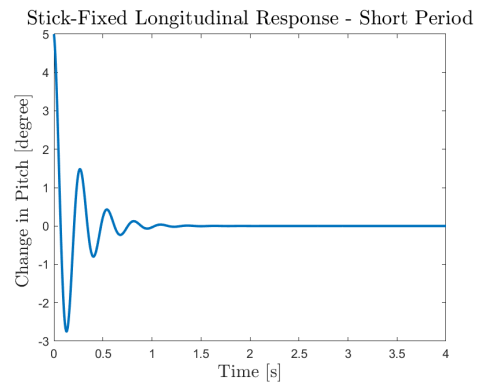
$$C_{m\alpha} = \frac{(-2C_{\alpha t} V_H l_t)}{\text{chord}} \cdot \frac{d\epsilon}{d\alpha}$$

$$\frac{d\epsilon}{d\alpha} = 0.381, \text{ from downwash analysis done in}$$

the first semester using [22, Chap 4.5]



(a) Forward CG



(b) Aft CG

AD X-Plane Simulation



Figure AD.0.1: Example screenshot of flight-testing plugin

Figure AD.0.1 shows a screenshot of the X-Plane flight simulator with the flight-testing plugin running. The top left and top right corners show some of the flight model data calculated by X-Plane. The middle left section shows a window with multiple graphs recording the parameters of interest over time. The bottom left corner shows a window with a plugin called DataRefEditor used to manually edit the simulator variables. The bottom right shows the built in Garmin G1000 interface. The middle right shows a control panel for the flight-testing plugin that allows the user to activate the automatic take off, phugoid test, or automatic trim modes.

The flight-testing plugin was written in Lua. Some excerpts of the code are included below. The following segment is a function that is called every frame of the simulation. The function runs different commands depending on the current autonomous flight phase that is set.

```

|| function update_every_frame()
||   if af.fmc.data.auto_flight_phase == "TAKEOFF_START" then
||     af.fmc.maintainHeadingDuringTakeoffStartPhase()

```

```

    end
    if af.fmc.data.auto_flight_phase == "ROTATE" then
        af.fmc.doRotateFlightPhase()
    end
    if af.fmc.data.auto_flight_phase == "CLIMB" then
        af.fmc.doClimbPhase()
    end
    if af.fmc.data.auto_flight_phase == "CRUISE" then
        af.fmc.doCruisePhase()
    end
    if af.fmc.data.auto_trimming ~= 0 then
        -- keep trimming until trimmed for more than 5 seconds
        af.fmc.trim_pitch()
        af.fmc.trim_sideslip()
        af.fmc.trim_roll()
        if slip_deg >= -0.015 and slip_deg <= 0.015 and
            vvi_fpm_pilot >= -15 and vvi_fpm_pilot <= 15 and
            AHARS_roll_deg >= -0.015 and AHARS_roll_deg <= 0.015 then
            if af.fmc.data.trim_start_time == 0 then
                -- aircraft trimmed, start the clock
                af.fmc.data.trim_start_time = os.clock()
            end
        else
            -- aircraft not trimmed reset the clock
            af.fmc.data.trim_start_time = 0
        end
        if af.fmc.data.trim_start_time ~= 0 and
            os.clock() - af.fmc.data.trim_start_time > 5 then
            -- if trimmed for more than 5 seconds, stop trimming
            af.fmc.data.auto_trimming = 0
        end
    end
    if af.fmc.data.auto_flight_phase == "PHUGOID_TEST_START" then
        -- begin phugoid test by abrupt pitch up to 5 degrees
        af.fmc.trim_roll()
        if math.abs(AHARS_pitch_deg - 5) > 0.005 then
            af.fmc.maintain_pitch(5)
        else
            af.fmc.data.auto_flight_phase = "PHUGOID_TEST"
        end
    end
    if af.fmc.data.auto_flight_phase == "PHUGOID_TEST" then
        -- maintain roll during phugoid test
        af.fmc.trim_roll()
    end
end

```

The next segment shows the functions that execute during the different autonomous flight phases

```

local function maintain_pitch(desired_angle)
    -- uses PID control to maintain desired pitch angle
    local pitch_diff = desired_angle - AHARS_pitch_deg
    if math.abs(pitch_diff) > 0.01 then
        yoke_pitch_ratio = yoke_pitch_ratio + utils.PID_control(
            pitch_diff,
            data.pitch_error_values,
            AHARS_pitch_deg,
            data.AHARS_pitch_values,
            (1 / 180),
            (1 / 900),
            (1 / 720)
        )
    end

```

```

    end
end

local function maintain_roll(desired_angle)
    -- uses PID control to maintain desired roll angle
    local roll_diff = desired_angle - AHARS_roll_deg
    data.roll_diff = roll_diff
    if math.abs(roll_diff) > 0.01 then
        yoke_roll_ratio = yoke_roll_ratio + utils.PID_control(
            roll_diff,
            data.roll_error_values,
            AHARS_roll_deg,
            data.AHARS_roll_values,
            (1 / 4000),
            (1 / 1080),
            (1 / 1080)
        )
    end
end

local function trim_sideslip()
    -- use the rudder to trim side slip angle to 0
    local error = 0 - slip_deg
    if math.abs(error) > 0.015 then
        rudder_trim = rudder_trim + utils.PID_control(
            error,
            data.sideslip_error_values,
            slip_deg,
            data.sideslip_values,
            (1 / 700),
            (0),
            (1 / 3500)
        )
    end
end

local function trim_pitch()
    -- use the elevator to trim pitch for 0 vertical speed
    local error = 0 - vvi_fpm_pilot
    if math.abs(error) > 10 then
        local new_elevator_trim = elevator_trim + utils.PID_control(
            error,
            data.pitch_trim_error_values,
            vvi_fpm_pilot,
            data.pitch_trim_values,
            (1 / 10000000),
            (1 / 350000),
            (1 / 500000)
        )
        if new_elevator_trim >= 0 then
            elevator_trim = math.min(new_elevator_trim, 1)
        else
            elevator_trim = math.max(new_elevator_trim, -1)
        end
    end
end

local function trim_roll()
    -- use the elevator to trim pitch for level flight
    local error = 0 - AHARS_roll_deg
    if math.abs(error) > 0.0005 then
        aileron_trim = aileron_trim + utils.PID_control(
            error,
            data.roll_trim_error_values,

```

```

        AHARS_roll_deg,
        data.roll_trim_values,
        (1 / 20000),
        (1 / 1080),
        (1 / 1080)
    )
end
end

local function autoTrim()
    data.auto_trimming = 1
end

local function maintainHeadingDuringTakeoffStartPhase()
    -- uses PID control to maintain desired heading on takeoff using the
    rudder
    -- and nose wheel steering. Begins the rotate phase when airspeed
    reaches Vr
    --local heading_diff = AHARS_mag_heading - data.hdg_to_maintain
    local heading_diff = data.hdg_to_maintain - true_heading
    data.heading_diff = heading_diff
    if math.abs(heading_diff) > 0.01 then
        yoke_heading_ratio = utils.PID_control(
            heading_diff,
            data.heading_error_values,
            true_heading,
            data.true_heading_values,
            (1 / 3),
            (1),
            (1 / 30)
        )
    end
    if indicated_airspeed > v_rotate then
        -- initiate rotate phase
        data.auto_flight_phase = "ROTATE"
        XPLMSpeakString("rotate")
        yoke_heading_ratio = 0
        command_once("sim/autopilot/heading")
        --command_once("sim/autopilot/NAV")
        autopilot_mode = 1 -- turn on flight director
        override_flightdir_ptch = 1
    end
end

local function doRotateFlightPhase()
    -- increases the pitch to 10 degrees as long as aircraft is
    accelerating
    if AHARS_pitch_deg < 10 and airspeed_acceleration_kts_sec_pilot > 0
    then
        flight_director_pitch = math.min(10, AHARS_pitch_deg + 1.5)
    else
        flight_director_pitch = 10
    end
    maintain_pitch(flight_director_pitch)
    -- maintain roll when off the ground
    if radio_alt > 0 then
        maintain_roll(flight_director_roll_deg)
    end
    -- begin climb phase 25ft AGL
    if radio_alt > 25 then -- climb and maintain heading
        XPLMSpeakString( "positive climb" )
        data.auto_flight_phase = "CLIMB"
        autopilot_airspeed_knots = indicated_airspeed
        command_once("sim/autopilot/level_change")
    end
end

```

```

    end
end

local function doClimbPhase()
    -- keep increasing autopilot airspeed up to climb speed
    if indicated_airspeed < v_climb then
        if indicated_airspeed > autopilot_airspeed_knots then
            -- maintain airspeed
            autopilot_airspeed_knots = indicated_airspeed
        else
            -- increase airspeed gradually
            autopilot_airspeed_knots = math.min(v_climb, indicated_airspeed +
                2)
        end
    else
        autopilot_airspeed_knots = v_climb
    end
    -- retract landing gear above 250 ft
    if radio_alt > 250 and gear_deploy_ratio == 1 then
        XPLMSpeakString("retracting landing gear")
        command_once("sim/flight_controls/landing_gear_up")
    end
    -- smooth transition of flight director override from rotate phase
    if AHARS_pitch_deg >= flight_director_pitch - 0.1 and
        AHARS_pitch_deg <= flight_director_pitch + 0.1 then
        override_flightdir_ptch = 0
    end
    maintain_pitch(flight_director_pitch)
    maintain_roll(flight_director_roll_deg)
    -- begin cruise phase at cruise altitude
    if baro_altitude_ft_pilot > cruise_alt then
        XPLMSpeakString( "beginning cruise" )
        data.auto_flight_phase = "CRUISE"
        altitude_setting = cruise_alt
        command_once("sim/autopilot/altitude_hold")
        --command_once("sim/autopilot/FMS")
    end
end

local function doCruisePhase()
    maintain_pitch(flight_director_pitch)
    maintain_roll(flight_director_roll_deg)
    trim_sideslip()
    local nearest_airport_ref = XPLMFindNavAid(nil, nil, latitude,
        longitude, nil, 1)
    local outType, outLatitude, outLongitude, outHeight, outFrequency,
        outHeading, outID, outName = XPLMGetNavAidInfo(
            nearest_airport_ref )
    nearest_airport_name = outName
end

```

The proportional, integral, and derivative (PID) controller was created using the following functions to approximate the discrete first order integral and derivative.

```

local function integral(valueArray)
    -- returns the discrete sum of valueArray multiplied by the
    -- frame_period
    return table.sum(valueArray) * frame_period
end

local function derivative(valueArray)
    -- first order approximation of the derivative of valueArray values
    -- with respect

```

```

    -- to frame_period
    return (valueArray[#valueArray] - valueArray[#valueArray - 1]) /
        frame_period
end

-- returns a value based on provided error, value, and PID gains
local function PID_control(error, errorArray, value, valueArray, p_gain
    , i_gain, d_gain)
    -- truncate arrays to 10 items and insert new values
    if #errorArray > 10 then
        table.remove(errorArray, 1)
    end
    table.insert(errorArray, error)
    if #valueArray > 10 then
        table.remove(valueArray, 1)
    end
    table.insert(valueArray, value)
    return p_gain * error
        + i_gain * integral(errorArray)
        + - 1 * d_gain * derivative(valueArray)
end

```

The graphical user interface (GUI) was created using an immediate mode GUI library with Lua bindings.

```

local function af_fmc_build(wnd, x, y)
    -- this function builds the imgui window

    -- get window width and height
    local win_width = imgui.GetWindowWidth()
    local win_height = imgui.GetWindowHeight()

    -- display FMC title at top of window
    local title = "Arctic Fox FMC"
    local title_width, title_height = imgui.CalcTextSize(title)
    imgui.SetCursorPos(win_width / 2 - title_width / 2,
        imgui.GetCursorPosY())
    imgui.TextUnformatted(title)

    imgui.Columns(3)

    -- make plots
    for k, v in ipairs(data.plots) do
        imgui.PlotLines("", v.values, #v.values, 0, v.label, 0, FLT_MAX,
            imgui.GetContentRegionAvail(), 100)
        imgui.TextUnformatted(v.label .. ":" .. string.format("%g", _G[
            v.value]) .. " " .. v.unit)
        imgui.NextColumn()
    end

    imgui.Columns(1)

    -- reset graphs button
    if imgui.Button("Reset Graphs") then
        reset_graphs()
    end
end

local function createWindow()
    -- create imgui window
    af_fmc_wnd = float_wnd_create(600, 425, 1, true)
    float_wnd_set_title(af_fmc_wnd, "Arctic Fox FMC")

```

```
    || end float_wnd_set_imgui_builder(af_fmc_wnd , af_fmc_build)
```

While this code is sufficient for the purposes of the simulated flight testing, in reality, the code would need to be developed to be more robust and include automated self-tests and documentation as per requirements specified in guidance material document DO-178C.

AE Takeoff Performance Test Plan

Test Title: Speed Test

Test Objectives

1. Establish VR, wing flaps in the take-off position (20 degrees)
2. Establish V1, wing flaps in the take-off position (20 degrees)
3. Establish V2, wing flaps in the take-off position (20 degrees)

Certification Basis

The following document has been used as reference for demonstrating means of compliance:

FAA AC 25-7D Flight Test Guide for Certification of Transport Category Airplanes

Test Configuration

- Take-off performed at MTOW
- Wing flaps in the take-off position: 20 degrees
- Zero wind

Test Pre-conditions

- Aircraft (model) is built
- Aircraft (model) is safe and ready for flight

Special comments

- Distances will be recorded only on dry surfaced runway since braking with thrust reversers can't be taken for credit for certification on dry surfaced runway and longer distances are more relevant for this test as we are only interested in critical cases
- During the accelerate/stop distance test to establish V1, always brake at V1
- During the take-off with one engine inoperative test to establish V1, engine failure will be set to occur 2 seconds before V1 81 knots is the initial assumption for VR based on theoretical calculations
- Beware of any time delay between an airspeed indication and the speed at which the aircraft is accelerating on the runway

Special Equipment/Facilities Required

- Flight test entirely performed at Telluride Regional Airport

Checklist (To be followed prior to the test)

- Parking brake must be ON
- Extend flaps to 20 degrees
- Turn the yoke on the right and left to make sure ailerons are responding correctly
- Pull and push the yoke to make sure the elevators are responding correctly
- Push on the left and right pedal separately to make sure the rudder is responding correctly

Test Procedure

- Begin with aircraft in test configuration
- Get VR first
- Parking brake must always be OFF when test has started
- Full thrust applied
- Once 81 knots is reached, try to rotate the nose of the aircraft
- Record the speed at which rotation is feasible
- Repeat the above steps to make sure of that the speed obtained is reliable
- To get the optimum V1 speed, conduct an accelerate/stop distance (ASD) test for 4 different V1: 80, 87, 93 and 100% of VR and do the exact same for the take-off with one engine inoperative (OEI)
- During the accelerate/stop distance test, full thrust will be applied and once V1 (80% of VR) is reached, apply brakes by pushing on both pedals at the same time and idling the engines
- Repeat the above step for the next 3 V1 (87, 93 and 100% of VR)
- During the take-off with one engine inoperative test, an engine failure is set in X-Plane to occur 2 seconds before V1 is reached

- Once the engine failure occurs 2 seconds before the first V1 (80% of VR), the rudder must be used to keep the aircraft centered on the runway as much as possible until VR can be reached
- After VR, use the ailerons and the rudder together during the climb to compensate for the engine loss and keep the aircraft stable
- Repeat the above steps for the next 3 V1 (87, 93 and 100% of VR)
- V2 is obtained by recording the speed at a height of 35 ft above the runway surface

Hazard Identification

- Potential loss of control over the aircraft on the runway after the engine failure if the rudder is not being used efficiently

Relevant Environmental Parameters

- Weather: no wind or clouds; clear sky
- Runway surface type: asphalt & dry
- Runway airport distance: 7111 ft

Test Matrix

V1 [kt]	80% of VR	87% of VR	93% of VR	100% of VR
ASD [ft]	1674	2042	2378	2839
Take-off OEI [ft]	3130	2791	2516	2204

Table AE.0.1: Takeoff performance test matrix

AF Stall Performance Test Plan

Acronyms

The following acronyms are used in this section

AC – Advisory Circular

AGL – Above Ground Level

ALT – Altitude

ASL – Above Sea Level

AOA – Angle of Attack

CAR – Canadian Aviation Regulations

CFR – Code of Federal Regulations

CG – Center of Gravity

CL_{max} – Maximum Lift Coefficient

DEG – Degrees

FAA – Federal Aviation Administration

FT – Feet

FT/S – Feet Per Second

KIAS – Knots Indicated Air Speed

LB – Pounds Force

RPM – Revolutions Per Minute

TCCA – Transport Canada Civil Aviation

TLF – Thrust for Level Flight

TO – Take Off

V_{SR} – Reference Stall Speed for given configuration

V_{SRI} – Reference Stall Speed at maximum landing weight, flaps in approach position, and landing gear retracted

Introduction

Test objectives

1. Establish reference stall speed V_{SR1} . CAR 525.201
2. Establish thrust for level flight (TLF) CAR 525.201
3. Establish reference stall speeds for various aircraft configurations CAR 525.103, 525.201(a), 525.201(b), AC 525-020, AC 25-7D chapter 8
4. Establish stall warning AOA CAR 525.207
5. Evaluate wings level stall performance CAR 525.203
6. Evaluate turning flight stall performance CAR 525.203

Certification Basis

The following regulations of the Arctic Fox's certification basis are relevant to the proposed flight test.

TCCA Part V Chapter 525

14 CFR Part 25

The following documents were used as a reference for demonstrating means of compliance

TCCA AC 525-020 Stall, Compliance

FAA AC 25-7D Flight Test Guide for Certification of Transport Category Airplanes

Test configuration

Paragraph 525.21(c) requires stall characteristics demonstrated for each altitude up to the maximum expected in operation. Compliance is typically shown at 75% of the maximum altitude. – 7500 ft ASL

Paragraph 525.103(b)

- Engines idle or zero thrust
- Propeller pitch at TO position
- CG position that gives highest stall speed V_{SR}
- Aircraft trimmed for level flight between 1.13 and 1.3 V_{SR}

Paragraph 525.201

- Each configuration tested in level flight and in 30-degree banked turn
- Each configuration tested with power off and with power necessary for 1.5 V_{SR1}
- Flaps / landing gear in any likely combination
- Weight in the range for which certification is requested
- Most adverse CG for recovery

Most adverse condition for stall speed:

Forward CG

Gear down

Flaps up

Max landing weight

Idle thrust

Additional conditions

- One engine inoperative
- Flaps down
- Gear up
- Aft CG

Test pre-conditions

Aircraft (model) is built

Aircraft (model) is safe and ready for flight

Special comments

Due to T-tail design it is imperative the aircraft is shown to not be susceptible to deep stall.

Minimum stall entry altitude 7000 ft AGL

Paragraph 525.201(d) – Acceptable indications of stall

- Nose down pitch that cannot be easily recovered
- Severe buffeting
- Pitch control reaches aft stop and no further increase in pitch occurs for a short time

Special test equipment / facilities required

Flight testing airspace and runway.

Test Procedures

Pitch up stall

1. Trim aircraft and establish thrust for level flight (TLF) at speed of $1.3 V_{SR}$
2. Use pitch control to decelerate aircraft at a rate of 1ft/s until aircraft stalls
3. Recover using standard stall recovery technique

Turning flight and accelerated stalls

1. Trim aircraft and establish TLF at speed of $1.5 V_{SR1}$
2. Perform 30-degree banking turn decelerating aircraft at a rate of 1ft/s until aircraft stalls
3. Recover using standard stall recovery technique
4. Repeat steps 1-3 with power off
5. Repeat steps 1-4 with a deceleration rate of 3ft/s

Test Results

Configuration

Results

Test number: 1									
Alt (ft)	Weight (lb)	RPM	Gear	Flaps (deg)	Bank Angle (deg)	CLmax	Stall Speed (KIAS)	Stall AOA (deg)	
7420	38140	660	up	0	0	1.268	86	17	
Behavior: plane started to fall slowly, nose dropped, recovery was easy					Test passed				

Test number: 2									
Alt (ft)	Weight (lb)	RPM	Gear	Flaps (deg)	Bank Angle (deg)	CLmax	Stall Speed (KIAS)	Stall AOA (deg)	
7250	38115	670	up	0	30	1.254	91	16.3	
Behavior: plane held bank angle while falling, nose dropped, recovery was easy					Test passed				

Test number: 3									
Alt (ft)	Weight (lb)	RPM	Gear	Flaps (deg)	Bank Angle (deg)	CLmax	Stall Speed (KIAS)	Stall AOA (deg)	
7040	38102	670	up	0	-30	1.271	95	16.5	
Behavior: plane held bank angle while falling, nose dropped, recovery was easy					Test passed				

Test number: 4									
Alt (ft)	Weight (lb)	RPM	Gear	Flaps (deg)	Bank Angle (deg)	CLmax	Stall Speed (KIAS)	Stall AOA (deg)	
7600	38079	660	down	0	0	1.26	86	16.7	

Behavior: plane started to fall slowly, nose dropped, recovery was easy	Test passed
---	-------------

Test number: 5								
Alt (ft)	Weight (lb)	RPM	Gear	Flaps (deg)	Bank Angle (deg)	CLmax	Stall Speed (KIAS)	Stall AOA (deg)
7250	38070	670	down	0	30	1.24	91	16
Behavior: plane held bank angle while falling, nose dropped, recovery was easy				Test passed				

Test number: 6								
Alt (ft)	Weight (lb)	RPM	Gear	Flaps (deg)	Bank Angle (deg)	CLmax	Stall Speed (KIAS)	Stall AOA (deg)
7700	38057	670	down	0	-30	1.24	92	16.1
Behavior: plane held bank angle while falling, nose dropped, recovery was easy				Test passed				

Test number: 7								
Alt (ft)	Weight (lb)	RPM	Gear	Flaps (deg)	Bank Angle (deg)	CLmax	Stall Speed (KIAS)	Stall AOA (deg)
7420	38042	670	down	20	0	1.435	73	17.3
Behavior: aircraft rolled to -50 deg while falling, nose dropped, recovery was easy				Test failed: excessive roll during recovery				

Test number: 8								
Alt (ft)	Weight (lb)	RPM	Gear	Flaps (deg)	Bank Angle (deg)	CLmax	Stall Speed (KIAS)	Stall AOA (deg)
7800	38021	660	down	20	30	1.426	82	16.1

Behavior: aircraft rolled to 70 deg while falling, nose dropped, recovery was easy	Test passed
--	-------------

Test number: 9								
Alt (ft)	Weight (lb)	RPM	Gear	Flaps (deg)	Bank Angle (deg)	CLmax	Stall Speed (KIAS)	Stall AOA (deg)
7400	38014	670	down	20	-30	1.532	80	16
Behavior: aircraft rolled to -83 deg while falling, nose dropped, recovery was easy				Test passed				

Test number: 10								
Alt (ft)	Weight (lb)	RPM	Gear	Flaps (deg)	Bank Angle (deg)	CLmax	Stall Speed (KIAS)	Stall AOA (deg)
7650	37950	670	up	20	0	1.435	74	17.2
Behavior: aircraft rolled slightly side to side then to -50 deg, nose dropped, recovery was easy				Test failed: excessive roll during recovery				

Test number: 11								
Alt (ft)	Weight (lb)	RPM	Gear	Flaps (deg)	Bank Angle (deg)	CLmax	Stall Speed (KIAS)	Stall AOA (deg)
7550	37938	600	up	20	30	1.506	81.7	15.9
Behavior: aircraft rolled to 50 deg while falling, nose dropped, recovery was easy				Test passed				

Test number: 12								
Alt (ft)	Weight (lb)	RPM	Gear	Flaps (deg)	Bank Angle (deg)	CLmax	Stall Speed (KIAS)	Stall AOA (deg)
7400	37929	680	up	20	-30	1.435	81.3	15.9

Behavior: aircraft rolled to -79 deg while falling, nose dropped, recovery was easy	Test passed
---	-------------

Test number: 13								
Alt (ft)	Weight (lb)	RPM	Gear	Flaps (deg)	Bank Angle (deg)	CLmax	Stall Speed (KIAS)	Stall AOA (deg)
7530	37917	490	up	0	0	1.211	84	17.4
Behavior: plane started to fall slowly, nose dropped, recovery was easy					Test passed			

Test number: 14								
Alt (ft)	Weight (lb)	RPM	Gear	Flaps (deg)	Bank Angle (deg)	CLmax	Stall Speed (KIAS)	Stall AOA (deg)
7650	37912	500	up	0	30	1.227	94.5	16.3
Behavior: plane held bank angle while falling, nose dropped, recovery was easy								

Test number: 15								
Alt (ft)	Weight (lb)	RPM	Gear	Flaps (deg)	Bank Angle (deg)	CLmax	Stall Speed (KIAS)	Stall AOA (deg)
7320	37905	490	up	0	-30	1.226	95	16.2
Behavior: plane held bank angle while falling, nose dropped, recovery was easy					Test passed			

Test number: 16								
Alt (ft)	Weight (lb)	RPM	Gear	Flaps (deg)	Bank Angle (deg)	CLmax	Stall Speed (KIAS)	Stall AOA (deg)
7800	37894	490	down	0	0	1.235	87.5	16.8

Behavior: plane started to fall slowly, nose dropped, recovery was easy	Test passed
---	-------------

Test number: 17								
Alt (ft)	Weight (lb)	RPM	Gear	Flaps (deg)	Bank Angle (deg)	CLmax	Stall Speed (KIAS)	Stall AOA (deg)
7580	37889	490	down	0	-30	1.224	96.6	16
Behavior: plane held bank angle while falling slowly, nose dropped, recovery was easy					Test passed			

Test number: 18								
Alt (ft)	Weight (lb)	RPM	Gear	Flaps (deg)	Bank Angle (deg)	CLmax	Stall Speed (KIAS)	Stall AOA (deg)
7600	37885	490	down	0	30	1.227	89.1	16.5
Behavior: plane held bank angle while falling slowly, nose dropped, recovery was easy					Test passed			

Test number: 19								
Alt (ft)	Weight (lb)	RPM	Gear	Flaps (deg)	Bank Angle (deg)	CLmax	Stall Speed (KIAS)	Stall AOA (deg)
7750	37879	490	down	20	0	1.434	77.6	15.9
Behavior: aircraft rolled slightly side to side then to 30 deg, nose dropped, recovery was easy					Test failed: excessive roll during recovery			

Test number: 20								
Alt (ft)	Weight (lb)	RPM	Gear	Flaps (deg)	Bank Angle (deg)	CLmax	Stall Speed (KIAS)	Stall AOA (deg)
7650	37872	490	down	20	-30	1.478	86	15.8

Behavior: aircraft rolled to -83 deg while falling, nose dropped, recovery was easy	Test passed
---	-------------

Test number: 21								
Alt (ft)	Weight (lb)	RPM	Gear	Flaps (deg)	Bank Angle (deg)	CLmax	Stall Speed (KIAS)	Stall AOA (deg)
7600	37867	490	down	20	30	1.335	83	16
Behavior: aircraft rolled to 66 deg while falling, nose dropped, recovery was easy				Test passed				

Test number: 22								
Alt (ft)	Weight (lb)	RPM	Gear	Flaps (deg)	Bank Angle (deg)	CLmax	Stall Speed (KIAS)	Stall AOA (deg)
7420	37857	490	up	20	0	1.356	74.9	17.4
Behavior: aircraft rolled slightly side to side then to -20 deg, nose dropped, recovery was easy				Test passed marginally: allowable roll limit reached during recovery				

Test number: 23								
Alt (ft)	Weight (lb)	RPM	Gear	Flaps (deg)	Bank Angle (deg)	CLmax	Stall Speed (KIAS)	Stall AOA (deg)
7360	37851	490	up	20	-30	1.336	85.2	16.6
Behavior: aircraft rolled to -75 deg while falling, nose dropped, recovery was easy				Test passed				

Test number: 24								
Alt (ft)	Weight (lb)	RPM	Gear	Flaps (deg)	Bank Angle (deg)	CLmax	Stall Speed (KIAS)	Stall AOA (deg)
7650	37848	500	up	20	30	1.484	88.6	15.2

Behavior: aircraft rolled to 61 deg while falling,
nose dropped, recovery was easy

Test passed

AG Human Factors

Experiment Protocol

Digital Appendix: AERO 490 > Report > Final report > Digital Appendix >
Human Factors > \AppendixBN1.docx"

NASA - Task Load Index

Digital Appendix: AERO 490 > Report > Final report > Digital Appendix >
Human Factors > \AppendixBN2.pdf"

Graphical data analysis of approach path deviation, airspeed deviation, heading deviation and perceived workload

Digital Appendix: AERO 490 > Report > Final report > Digital Appendix >
Human Factors > \AppendixBN3.docx"

AH Autonomous Emergency Checklist

Checklist

Digital Appendix: AERO 490 > Report > Final report > Digital Appendix >
Autonomous Emergency Checklist > \EMERGENCY PROCEDURES.PDF"

LUA Source Code Description

Digital Appendix: AERO 490 > Report > Final report > Digital Appendix >
Autonomous Emergency Checklist > \AEP - Version 2.lua"

The Autonomous Emergency Procedure (AEP) begins to run once the system understands that the pilot has taken the appropriate actions to maintain safe flight in the event of an emergency. For the checklist defined for the human factors experiment, the pilot must idle the affected engine, feather the propeller of the affected engine and bring the mixture/-condition lever of the affected engine to the stop position. The script recognizes which engine is affected, and takes appropriate actions. Once these vital items have been completed, the AEP begins to action the non-vital checklist items. Each item is actioned individually and in order. The checked items appear on the screen in the line of sight of the pilot. There is a 0.5-second time delay between each actionned item so the pilot can visually affirm the completion of a step before the next one is completed. Once the AEP has completed the engine fire checklist, a voice announces through an audio system, "Engine fire checklist complete", as well as displaying it on the computer screen. A full procedure of the AEP in action can be seen in Figures AH.0.1 through AH.0.6



Figure AH.0.1: Aircraft before the emergency with the AEP running

```

FlyWithLua: User forced a script reload.
FlyWithLua Info: Load exit file.
FlyWithLua Info: Lua engine has restarted. LUA_RUN = 7, SDK_VERSION = 302, XPLANE_VERSION = 11320, XPLANE_LANGUAGE = English and XPLANE_HOSTID = 1
FlyWithLua Info: HD access initialized.
FlyWithLua Info: FlyWithLua.ini full path: C:/Users/Simulator/Desktop/X-Plane 11/Resources/plugins/FlyWithLua/Internal/FlyWithLua.ini
FlyWithLua Info: Discoverd 9 HD devices.
FlyWithLua Info: Load ini file.
FlyWithLua Info: Searching for Lua script files.
FlyWithLua Info: Sorting Lua script files.
FlyWithLua Info: Start loading script file C:/Users/Simulator/Desktop/X-Plane 11/Resources/plugins/FlyWithLua/Scripts/AEP - Version 2.lua
FlyWithLua Info: Finished loading script file C:/Users/Simulator/Desktop/X-Plane 11/Resources/plugins/FlyWithLua/Scripts/AEP - Version 2.lua
FlyWithLua Info: All script files loaded successfully.
FlyWithLua Info: Loading time for all scripts is 0.071 sec.

```

Figure AH.0.2: Aircraft before the emergency with the AEP running (blue text at the bottom)



Figure AH.0.3: Left engine fire occurred. AEP waiting for pilot to action the vital checklist items



Figure AH.0.4: Vital checklist items completed, AEP system on and actionned the non-vital checklist items

right fuel tank selected
left fuel pump off
left fire extinguisher triggered
prop sync off
cross tie off
engine fire checklist complete

Figure AH.0.5: Vital checklist items completed, AEP system on and actionned the non-vital checklist items. (blue text at the bottom)



Figure AH.0.6: AEP system announces “Engine fire checklist complete” and emergency has been averted

X-Plane Simulation Video

Digital Appendix: AERO 490 > Report > Final report > Digital Appendix >
Autonomous Emergency Checklist > \AEP.mov"

AI Identity Access Management System

Software requirements specification document

Digital Appendix: AERO 490 > Report > Final report > Digital Appendix >
Identity Access Management System > IAM SRS

AJ Cost Analysis

AJ.1 Program Cost Analysis

To complete the program cost, a modified DAPCA¹ IV cost model from Raymer method is used. The method used was developed in 2012. A inflation rate of 3% per year until 2019 was added to the formulas. Assumptions, the tool used and the formulas can be found below [35, p. 46-49] :

Assumptions:

Autonomy Factor

30% * Eng. hours + Tooling hours + Development support cost + Flight test cost + Avionic cost

Most determining input parameters:

- Arctic Fox empty weight
- Maximum aircraft speed
- Production quantity
- Avionic Costs = 3,000,000 USD
- Engineering hour rate = 115 USD
- Tooling hour rate = 118 USD
- Quality control rate = 108 USD
- Manufacturing rate = 98 USD

USD Inflation included = 1.21(3% over 7 years) Assumed that manufacturing complexity reduced since alumunium is used. Manufacturing complexity Factor (ranging from 1 to 2) assumed to be 1. The DAPCA tool is presented in figure AJ.1.1 and more details can be found in:

Digital Appendix: AERO 490 > Report > Final report > Digital Appendix > Cost Analysis > \Cost Analysis .xlsx" > Sheet: RDT&E + Production

¹DAPCA: Development And Procurement Cost of Aircraft

Modified DAPCA IV Cost Model		
Eng. hours (H_E)	\$1,933,717.46	
Tooling hours (H_T)	\$805,196.25	
Manufacturing hours (H_M)	\$477,410.45	
Quality Control hours (H_Q)	\$76,829.66	
Devel support cost (C_D)	\$76,810,271.25	
Flight test cost (C_F)	\$62,522,452.42	
Manufacturing materials cost (C_M)	\$8,364,503.40	
Eng. Production cost (C_eng)	-\$436,864.33	
Avionics Cost (USD)	\$3,630,000.00	
Additional Costs (USD)	\$0.00	
Autonomy Factor	\$138,106,016.79	
RDT&E + flyaway cost (USD)	\$661,034,009.08	
Cost per Aircraft	\$661,034,009.08	
Terminology	Explanation	Value
We	empty weight (lb)	23000
V	maximum velocity (knots)	240
Q	production quantity	1
FTA	number of flight test aircraft (typically 2-6)	6
N_eng	total production quantity times number of engines per aircraft	2
T_max	engine maximum thrust (lb)	2750
M_max	engine maximum Mach number	0.5
T_turbine inlet	turbine inlet temperature (Rankine)	1932
C_avionics	avionics cost (USD)	\$3,000,000.00
R_E	Engineering hour Wrap rate (USD)	\$115.00
R_T	Tooling hour Wrap rate (USD)	\$118.00
R_Q	Quality Control Wrap rate (USD)	\$108.00
R_M	Manufacturing Wrap rate (USD)	\$98.00
USDinfl	USD inflation Cost	1.21

Table AJ.1.1: Modified DAPCA Cost model tool for Arctic Fox

Formula used:

$$H_E = 4.86 \times We^{777} \times V^{894} \times Q^{163} \times USDinflation$$

$$H_T = 5.99 \times W_e^{-777} \times V^{696} \times Q^{263} \times USDinflation$$

$$H_M = 7.37 \times W_e^{82} \times V^{484} \times Q^{641} \times USDinflation$$

$$H_E = 0.133 \times H_M \times USD \text{ Inflation}$$

$$C_D = 91.3 \times W_E^{63} \times V^{1.3} \times USDinflation$$

$$C_F = 2498 \times W_E^{325} \times V^{822} \times FTA^{1.21} \times USDinflation$$

$$C_M = 22.1 \times W_E^{921} \times V^{621} \times Q^{799} \times USDinflation$$

$$C_{ENG} = 3112 \times (0.043 \times T_{MAX} + (2342.25 \times M_{MAX}) + 0.969 \times T_{turineinlet}) - 2228) \times USDinflation$$

$$\begin{aligned} AvionicCost(USD) &= C_{Avionics} \times Q \times USDInflation \\ AutonomyCost(USD) &= (C_F + C_D + H_T \times R_T + H_E \times R_E + AvionicCost) \times 0.3 \text{ RDTE} \\ FlyawayCost(USD) &= (C_F + C_D + C_M + AutonomyCost + HT \times RT + HE \times RE + HM \times RM + HQ \times RQ + AvionicCost \end{aligned}$$

$$\text{Cost per Aircraft} = (\text{RDTE} + \text{Flyaway Cost}) / Q$$

The program cost analysis results is presented in figure AJ.1.2 and more details can be found in:

Digital Appendix: AERO 490 > Report > Final report > Digital Appendix > Cost Analysis > \Cost Analysis .xlsx" > Sheet: Graphs

Total Cost (USD)	Quantity of aircraft produced	Cost per aircraft (Million USD)	Profit per aircraft (Million USD)
\$661,034,009	1	\$661	-\$640
\$911,104,197	5	\$182	-\$161
\$1,096,611,487	10	\$110	-\$89
\$1,237,157,717	15	\$82	-\$61
\$1,355,600,445	20	\$68	-\$47
\$1,460,301,121	25	\$58	-\$37
\$1,555,408,296	30	\$52	-\$31
\$1,643,331,547	35	\$47	-\$26
\$1,725,615,152	40	\$43	-\$22
\$1,877,204,377	50	\$38	-\$17
\$2,205,536,931	75	\$29	-\$8
\$2,488,531,922	100	\$25	-\$4
\$2,884,745,557	140	\$21	\$0
\$3,399,021,108	200	\$17	\$4
\$4,131,986,743	300	\$14	\$7
\$4,771,116,840.97	400	\$12	\$9
\$5,349,114,106.06	500	\$11	\$10

Table AJ.1.2: Program cost analysis results

A break even point is at 140 aircraft produced where the profit per aircraft sold is zero. The Arctic Fox will be sold at 21 million USD, at a competitive price when comparing to ATR 42-600, which is sold at 19.5 million USD [77].

References

- [1] “Canada’s northern food subsidy nutrition north canada: a comprehensive program evaluation,” 2016. [Online]. Available: <https://www.tandfonline.com/doi/full/10.1080/22423982.2017.1279451>
- [2] “2016-2017: Full fiscal year,” Government of Canada, Apr. 2018. [Online]. Available: <http://www.nutritionnorthcanada.gc.ca/eng/1524237277832/1524237310943>
- [3] “How nutrition north canada works,” 2018. [Online]. Available: <https://www.nutritionnorthcanada.gc.ca/eng/1415538638170/1415538670874>
- [4] “Nutrition north canada advisory board second report,” 2014. [Online]. Available: <https://www.nutritionnorthcanada.gc.ca/eng/1508938932551/1508938956924>
- [5] “Humanitarian airdrops: How do they work?” 2016. [Online]. Available: <https://www.cnn.com/2016/06/03/middleeast/airdrops-humanitarian-aid-syria/index.html>
- [6] M. Maurer, C. Gerdes, B. Lenz, and H. Winner, *Autonomous Driving Technical, Legal and Social Aspects*. Springer Open, 2016.
- [7] “Canadian aviation regulations,” Transport Canada. [Online]. Available: <https://laws-lois.justice.gc.ca/eng/regulations/SOR-96-433/FullText.html>
- [8] “Makivik corporation,” Makivik Corporation. [Online]. Available: <https://www.makivik.org/corporate/history/makivik-corporation/>
- [9] “Makivik mandate,” Makivik Corporation. [Online]. Available: <https://www.makivik.org/corporate/makivik-mandate/>
- [10] “Nunavik airlines report “solid returns,” give millions to makivik,” Nunatsiaq News, Oct. 2017. [Online]. Available: https://nunatsiaq.com/stories/article/65674makivik-airlines_report_solid_returns_return_5_million_dividends_to_nu/

- [11] “Nunavik to benefit from announcements at the first day of the katimajiit conference,” Makivik Corporation, Aug. 2007. [Online]. Available: <https://www.makivik.org/katimajiit-conference/>
- [12] J. George, “Stop cross-polar flights, reduce arctic warming, save money: study,” Nunatsiaq News, Dec. 2012. [Online]. Available: https://nunatsiaq.com/stories/article/65674stop_cross-polar_flights_reduce_arctic_warming_save_money_study/
- [13] “Marine transportation,” Government of Canada, 2011. [Online]. Available: <https://www.tc.gc.ca/eng/policy/anre-menu-3019.htm>
- [14] “The canadian transportation system,” Government of Canada, 2018. [Online]. Available: <https://www144.statcan.gc.ca/tdih-cdit/cts-rtc-eng.htm>
- [15] C. Pollon, “<https://www.thediscourse.ca/energy/what-will-take-get-canadas-arctic-off-diesel>,” The Discourse, Feb. 2017. [Online]. Available: <https://www.thediscourse.ca/energy/what-will-take-get-canadas-arctic-off-diesel>
- [16] A. Cutan, “Autonomous vehicles and the future of work in canada,” Information and communications technology council (ICTC), 2017. [Online]. Available: https://www.ictc-ctic.ca/wp-content/uploads/2018/01/ICTC_Autonomous_Vehicles_and_The_Future_of_Work_in_Canada_1-1.pdf
- [17] “Pilots could soon lose their jobs to robots,” 2016. [Online]. Available: <https://nypost.com/2016/10/18/pilots-could-soon-lose-their-jobs-to-robots/>
- [18] Mckinsey & Company, “A future that works: automation, employment, and productivity,” Mckinsey Global Institute, 2017. [Online]. Available: <https://www.mckinsey.com/~/media/mckinsey/featured%20insights/digital%20disruption/harnessing%20automation%20for%20a%20future%20that%20works/a-future-that-works-executive-summary-mgi-january-2017.ashx>

- [19] Mckinsey & Company, “The canadian population in 2011: Age and sex,” Statistics Canada, 2011. [Online]. Available: <https://www12.statcan.gc.ca/census-recensement/2011/as-sa/98-311-x/98-311-x2011001-eng.cfm>
- [20] J. Roskam, *Airplane Design*, 4th ed. DARcorporation, 2005.
- [21] M. Sadraey, *Aircraft design: A systems engineering approach*. John Wiley & sons, Ltd., 2013.
- [22] W. F. Phillips, *First Edition*. John Wiley & Sons, Inc, 2004.
- [23] *Part VI - General Operating and Flight Rules - Aircraft Requirements*, Transport Canada Canadian Aviation Regulations Chapter 605, 2019. [Online]. Available: <http://www.tc.gc.ca/en/transport-canada/corporate/acts-regulations/regulations/sor-96-433.html>
- [24] “Turboprop engine,” NASA, May 2015. [Online]. Available: <https://www.grc.nasa.gov/www/k-12/airplane/aturbp.html>
- [25] “Type certificate data sheet no. im.e.041,” European Aviation Safety Agency, Mar. 2018. [Online]. Available: <https://www.easa.europa.eu/sites/default/files/dfu/EASA%20IM.E.041%20TCDS%20Issue%204.pdf>
- [26] “Type certificate data sheet no. eh-2005t09,” Hamilton Sundstrand Corporation, Apr. 2005.
- [27] *Part VII - Commercial Air Services - Standard 724 - Commuter Operations - Aeroplanes*, Transport Canada Canadian Aviation Regulations Standard 724, 2019. [Online]. Available: <http://www.tc.gc.ca/eng/civilaviation/regserv/cars/part7-standards-standard724-aero-2169.htm>
- [28] *Part 25 - Airworthiness Standards: Transport Category Airplanes*, Federal Aviation Administration Federal Aviation Regulations Part 25, 2019. [Online]. Available: <https://www.ecfr.gov/cgi-bin/text-idx?node=14:1.0.1.3.11>

- [29] W. Blake, *Jet Transport Performance Methods*. The Boeing Company, Mar. 2009.
- [30] OpenVSP, October 2018. [Online]. Available: <http://openvsp.org/>
- [31] O. Majeed, “Parametric specific fuel consumption analysis of the pw120a turboprop engine,” Specific Range Solutions Ltd., July 2009. [Online]. Available: <http://www.srs.aero/wordpress/wp-content/uploads/2009/03/srs-tsd-002-rev-1-pw120a-sfc-analysis.pdf>
- [32] S. Gudmundsson, *General Aviation Aircraft Design: Applied Methods and Procedures*, 1st ed. Elsevier, 2014.
- [33] XinZhao, J. M. Guerrero, and X. Wu, “Review of aircraft electric power systems and architectures,” IEEE, 2014. [Online]. Available: <https://ieeexplore.ieee.org/document/6850540/references#references>
- [34] “An aviation services co.” Jan. 2019. [Online]. Available: <https://www.an-aviation.com/why-is-fuel-stored-in-the-wings-of-aircraft/>
- [35] D. P. Raymer, *Aircraft design: a conceptual approach*, 5th ed. AIAA, 2012.
- [36] E. F. Bruhn, *Analysis and Design of Flight Vehicle Structures*. Jacobs Publishing, Inc., 1973.
- [37] M. C.-Y. Niu, *Airframe structural design*. Hong Kong Commlit Press LTD., 1989.
- [38] “Forklift safety for ramps, slopes and inclines,” ProLift Equipment, 2017. [Online]. Available: <https://www.proliftequipment.com/blog/forklift-safety-ramps-slopes-and-inclines/>
- [39] “Guide for selecting continuous hinges,” Sierra Pacific Engineering and Products, August 2012. [Online]. Available: <https://www.spes.com/public/Webpictures/iStore/images/HingeGuide.pdf>

- [40] *Part V – Airworthiness Chapter 525 - Transport Category Aeroplanes*, Transport Canada Canadian Aviation Regulations Chapter 525, 2019. [Online]. Available: <http://www.tc.gc.ca/eng/civilaviation/regserv/cars/part5-standards-525-menu-1738.htm>
- [41] M. C.-Y. Niu, *Airframe stress analysis and sizing*, 2nd ed. Hong Kong Commilit Press LTD., 1999.
- [42] “What is convergence in finite element analysis,” Mar. 2019. [Online]. Available: <https://www.simscale.com/blog/2017/01/convergence-finite-element-analysis/>
- [43] E. Torenbeek, *Synthesis of Subsonic Airplane Design*, 1st ed. Kluwer Academic, 1982.
- [44] T. Heid, “The abc’s of engine mount inspection & repair,” Aviation Pros, 10 2000. [Online]. Available: <https://www.aviationpros.com/home/article/10388510>
- [45] “Engine mount analysis report,” Apollo Canard, 08 2003. [Online]. Available: http://www.apollocanard.com/index.htm_files/Engine%20Mount%20Analysis.pdf
- [46] P. Kabade and R. Lingannavar, “Design and analysis of landing gear lug attachment in an airframe,” Master’s thesis, MSSCET, 2013. [Online]. Available: <http://www.rroij.com/open-access/design-and-analysis-of-landing-gear-lug-attachment-in-an-airframe.pdf>
- [47] “Aluminum properties,” Experimental Aircraft Info. [Online]. Available: <https://www.experimentalaircraft.info/articles/aircraft-aluminum.php>
- [48] S. Liscouet-Hanke and K. Huynh, “A methodology for systems integration in aircraft conceptual design - estimation of required space,” *SAE International Journal of Aerospace*, 2013.
- [49] R. Seresinhe and C. Lawson, “Electrical load-sizing methodology to aid conceptual and preliminary design of large commercial aircraft,” *Journal of Aerospace Engineering*, 2015.

- [50] J. D. Anderson, *FUNDAMENTALS of AERODYNAMICS*, 2nd ed. McGraw-Hill, 1991.
- [51] I. Moir and A. Seabridge, *Aircraft Systems: Mechanical, electrical, and avionics subsystems integration*, 3rd ed. John Wiley & Sons, Ltd, 2008.
- [52] “Anti-ice and deice systems,” Flight Learnings. [Online]. Available: <http://www.flightlearnings.com/2010/04/15/anti-ice-and-deice-systems-part-one/>
- [53] S. W. Churchill and M. Bernstein, “A correlating equation for forced convection from gases and liquids to a circular cylinder in crossflow,” *The American Society of Mechanical Engineers*, vol. 99, no. 2, p. 7, May 1977. [Online]. Available: <http://heattransfer.asmedigitalcollection.asme.org/article.aspx?articleid=1436684>
- [54] Y. A. Cengel, *Heat and Mass Transfer: Fundamentals and Applications*, 5th ed. McGraw-Hill Education, Apr. 2014.
- [55] “Agard advisory report no. 127: Aircraft icing,” Advisory Report, Advisory Group For Aerospace Research And Development, Jan. 1979. [Online]. Available: <https://apps.dtic.mil/dtic/tr/fulltext/u2/a063794.pdf>
- [56] C. Müller and D. Scholz, “The vapor compression cycle in aircraft air-conditioning systems,” Master’s thesis, Hamburg University of Applied Sciences, Apr. 2017.
- [57] M. Bahrami, “Steady conduction heat transfer,” SFU. [Online]. Available: <https://www.sfu.ca/~mbahrami/ENSC%20388/Notes/Steady%20Conduction%20Heat%20Transfer.pdf>
- [58] V. Stetsyuk, K. J. Kubiak, L. Liu, and J. C. Chai, “An alternative approach to evaluate the average nusselt number for mixed boundary layer conditions in parallel flow over an isothermal flat plate,” *International Journal of Mechanical*

- Engineering Education*, vol. 46, no. 3, pp. 241–251, 2017. [Online]. Available: <https://journals-sagepub-com.lib-ezproxy.concordia.ca/doi/pdf/10.1177/0306419017743214>
- [59] “Airbus technical notes.” [Online]. Available: <https://hursts.org.uk/airbus-technical/notes.pdf>
- [60] S. D. A. Fletcher, P. Norman, S. Galloway, and G. Burt, “Impact of engine certification standards on the design requirements of more-electric engine electrical system architectures,” *SAE International Journal of Aerospace*, vol. 7, no. 1, 2014.
- [61] B. Zhang, “Applying reliability analysis to design electric power systems for more-electric aircraft,” Master’s thesis, University of Maryland, College Park, 2014.
- [62] *System safety analysis and assessment for part 23 airplanes*, Federal Aviation Administration Advisory Circular, 2011.
- [63] F. Pranoto, A. Wirawan, and D. Purnamasari, “Electrical power budgeting analysis for lsa-02 uav technology demonstrator,” *IOP Conf. Series: Materials Science and Engineering*, 2016.
- [64] *Part V – Airworthiness Chapter 551 - Aircraft Equipment and Installation*, Transport Canada Canadian Aviation Regulations Chapter 551, 2019. [Online]. Available: <http://www.tc.gc.ca/eng/civilaviation/regserv/cars/part5-standards-chapter551-258.htm>
- [65] *14 CFR 23.1337 - Powerplant instruments installation.*, Federal Aviation Administration Std., 2019. [Online]. Available: <https://www.law.cornell.edu/cfr/text/14/23.1337>
- [66] J. Bennett, “Boeing and japan’s space agency are testing lidar on aircraft,” Aug. 2017. [Online]. Available: <https://www.popularmechanics.com/flight/news/a27595/boeing-japan-space-agency-develop-lidar-planes/>

- [67] "How lidar is revolutionizing mapping and geospatial data," DJI Enterprise. [Online]. Available: <https://enterprise.dji.com/news/detail/how-lidar-is-revolutionizing-mapping-and-geospatial-data>
- [68] L. Huang, J. H. Jiang, Z. Wang, H. Su, M. Deng, and S. Massie, "Climatology of cloud water content associated with different cloud types observed by a train satellites," Specific Range Solutions Ltd., Apr. 2015. [Online]. Available: <https://agupubs.onlinelibrary.wiley.com/doi/full/10.1002/2014JD022779>
- [69] F. Stability and A. Control, *Second Edition*. McGraw - Hill, 1998.
- [70] D. Performance, Stability and C. of Airplanes, *Second Edition*. AIAA Education Series, 2004.
- [71] J. Patel, "Module 5 - takeoff performance," Lecture Notes in AERO 446, Concordia University, Montreal, Canada, Feb. 2018.
- [72] "Flight test guide for certification of transport category airplanes," AC 25-7D, U.S Department of Transportation Federal Aviation Administration, p. 449, Apr. 2018. [Online]. Available: https://www.faa.gov/documentLibrary/media/Advisory_Circular/AC_25-7D.pdf
- [73] B. Haines, "Hackers + airplanes: No good can come of this," Lecture Notes in Hackers + Airplanes: No Good Can Come Of This, Renderlab.net, Krakow, Poland, May 2012.
- [74] "Atr 42-500 operating costs," PriJet LLC, 2018. [Online]. Available: <https://prijet.com/operating-costs/ATR%2042-500>
- [75] "Bombardier dash 8-q300 operating costs," PriJet LLC, 2018. [Online]. Available: <https://prijet.com/operating-costs/Bombardier%20Dash%208-Q300>
- [76] "Bombardier q300," Bombardier Aerospace, June 2006. [Online]. Available: https://www2.bombardier.com/Used_Aircraft/pdf/Q300_EN.pdf

- [77] “Atr 42-500 unrivalled performance,” ATR Aircraft, Sep. 2014. [Online]. Available: http://www.atraircraft.com/datas/download_center/34/fiches_500_septembre2014_34.pdf
- [78] “Cargo rates,” Air North, 2019. [Online]. Available: <https://www.flyairnorth.com/Cargo/CargoRates.aspx>
- [79] “Air cargo rates,” Air North, Feb. 2019. [Online]. Available: <https://www.airtindi.com/app/media/2423>
- [80] K. Wilcox, “Cost analysis,” Lecture Notes in 16.885 Aircraft Systems Engineering, MIT Aerospace Computational Design Lab, Boston, USA, September 2004.
- [81] J. Patel, “Module 7 - engine out enroute performance & landing performance,” Lecture Notes in AERO 446, Concordia University, Montreal, Canada, Feb. 2018.
- [82] D. P. Wells, B. L. Horvath, and L. A. McCullers, “The flight optimization system weights estimation method,” National Aeronautics and Space Administration, Tech. Rep. TM-2017-219627, 2017.
- [83] “Flight control actuation system,” Nov. 2018. [Online]. Available: <https://patents.google.com/patent/US6776376B2/en?oq=US+6776376+B2>.
- [84] A. Fayyad, “Cfd analysis of propeller effects on jetstream-31,” Master’s thesis, Cranfield University, Aug. 2016, thesis.